METAL FLOW AND TOOL DESIGN IN FLASHLESS FORGING OF ALUMINUM ALLOYS:
Semi-Solid Forging (SSF) of Round Parts and Tool Design for Forging of a Connecting Rod

A Thesis

Presented in Partial Fulfillment of the Requirements for
the Degree Master of Science in
the Graduate School of the Ohio State University
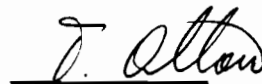
by

Muammer Koç, B.S.M.E.

* * * * *

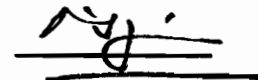The Ohio State University
1995

Master's Examination Committee: Approved by:

Taylan Altan

J. Altan
Adviser

Rajiv Shivpuri

Co-adviser

Department of Mechanical Engineering

ACKNOWLEDGMENTS

VITA

April 5, 1968.. Born - Kutahya, Turkiye

1991... Bachelor of Science, Mechanical

Engineering, Middle East Technical

University, G.Antep, Turkiye

1991-1992.. Instructor, Anadolu University, Bilecik,

Turkiye

1992-1995 .... Research Assistant at Dumlupinar

University, Kutahya, Turkiye

1994-Present .... Graduate Research Associate, ERC for

Net Shape Manufacturing, The Ohio

State University, Columbus, Ohio

FIELDS OF STUDY

Major Field: Mechanical Engineering

Studies in Manufacturing Processes, Industrial Engineering,

Metal Forming, Process Modeling, CAD/CAM,

TABLE OF CONTENTS

LIST OF TABLES

LIST OF FIGURES

ix

xv

Chapter I

INTRODUCTION

In order to be economically competitive, net-shape or near net-shape manufacturing (NNSM) becomes an ultimate goal of automotive and other manufacturers. In NNSM, the final shape of a part is obtained by forming materials in solid, liquid or semi-solid state using a die or mold. The objective is to eliminate or reduce machining.

Forging, one of the imported NNSM processes, produces parts with good mechanical properties, long service life, great structural integrity, homogeneous microstructure (free from porosity and inclusions) and optimum grain-flow orientation[Knoerr, et al., 1989]. Due to its excellent characteristics, the forging process undergoes many developments to obtain high performance and cost efficient products.

The main goals of the developments in this process are, first, to have high performance parts with long service life, and second, to reduce the weight of the parts. These goals would contribute to the economics of the

1

forging industry both in the short and the long terms. In order to achieve these goals, several issues in forging are investigated. These are the use of new materials, and techniques and a combination of both.

In terms of using new materials, replacement of steel parts with aluminum alloys may be given as an example. Moreover, introduction of Metal Matrix Composites (MMC), Semi-Solid materials and combination of them (i.e. semi-solid Al-MMCs) may contribute to the economic and performance capabilities of the forging process since it offers lighter parts with good mechanical properties. Powder metallurgy forging (P/M forging) and warm forging are also techniques used to produce net- or near net-shape parts. Finally, developments in die design and investigations on prevention of die failure would contribute greatly for achieving low cost/benefit ratio.

Pursuing these considerations, in this study, investigations are performed on (a) Semi-Solid Forging (SSF) and (b) Design of Shrink Rings to Prevent Premature Failure of Forging Dies.

1.1 Research Objectives

a) Metal Flow Simulations for Semi-Solid A356 Aluminum Alloys

SSF process, which promises cost efficient components, is a hybrid combination of conventional casting and forging processes. It depends

essentially on the use of semi-solid materials which are basically produced by stirring a metal during its solidification from molten state. Semi-solid materials have round grains rather than dendritic microstructure obtained from conventional solidification. Globular structure of semi-solid materials provides thixotropy state that enables metals to behave like a fluid under deformation forces while standing free without any pressure on them. The SSF presents net-shape, porosity free, uniform and sound products. SSF parts have mechanical properties as good as conventional forgings. Research on SSF process is summarized in Chapters 2 through 4.

Briefly, the objectives of this study on Semi-Solid Forging are (a) to evaluate the applicability of DEFORM FE code to simulate SSF process, and (b) to predict the metal flow and die filling in SSF

b) Stress Analysis of Connecting Rod Dies

It was found in a study performed in Germany that 25 % of the die failures occur due to mechanical cracking [Knoerr, et al., 1992]. Mechanical cracks are mainly due to the stresses induced in the areas where forging and die are in contact. Contact stresses result in a multiaxial stress state in the die [Knoerr, et al., 1989]. Design of shrink rings to counteract those contact stresses can reduce the induced tensile stresses which cause die failure. Shrink rings or Pressure fitting has been used for many years. However, often calculations for interference, thickness and shape of the shrink rings were carried out by simplified analyses. A finite element solution can

present a better technique than the conventional methods. Determination of high contact stress areas, calculation of interference between die and shrink ring and optimization of shape of the shrink rings for non-axisymmetric parts can be achieved by finite element modeling techniques. Chapter 5 and 6 discuss the effect of different designs of the shrink ring for a non-axisymmetric part, i.e. connecting rod.

Research objectives of the study on Shrink Ring Tool Design are:

1. Investigation of the current design methods and industrial applications

2. Simplification of the non-axisymmetric tooling design into axisymmetric sections, and performing 2-D Elastic-Plastic stress analysis of the simplified sections to verify the design to be used in the next steps

3. Performing three dimensional FE Elastic-Plastic stress analysis of die and shrink ring for different designs based on results from phase two.

4. Optimization of the tool design and development of a methodology to design shrink ring tooling for non-axisymmetric dies

1.2 Thesis Outline

Chapters 1 through 4 are about the Semi-Solid Forging process. Chapter 1 presents a brief introduction to both SSF and Shrink Ring design topics. It presents the research objectives of both parts.

In Chapter Two, after an introduction to semi-solid materials, different production methods for semi-solid alloys are discussed. Characteristics and properties of semi-solid alloys are presented.

Chapter three emphasizes on the Semi-Solid Forging process, its characteristics and advantages. It also gives information on SSF applications and their mechanical properties.

FEM simulations results for SSF of A356 alloy are presented in Chapter four. First, a brief introduction on the flow stress curves of semi-solid A356 alloy is given. After presenting the process condition, results from simulation are discussed. Future recommended work and conclusions are also in this chapter.

In Chapter Five, first, design of axisymmetric shrink rings by design guidelines are given. Next, simplification of the non-axisymmetric connecting rod die into two axisymmetric designs is presented. Approximate calculations using Lamé equations and design guidelines for axisymmetric designs are performed. Verification of these designs by 2-D elastic-plastic FE stress analysis simulations is then illustrated. Conclusion and future work on Design of Shrink Ring Tooling for Non-axisymmetric Dies are also available in Chapter Five.

Chapter II

SEMI-SOLID METAL FORMING: PRODUCTION OF SEMI-SOLID MATERIALS AND THEIR CHARACTERISTICS

2.1 Introduction to Semi-Solid Metal Forming

There is a constant need to develop new, low-cost and high-performance processes to replace conventional manufacturing processes. Production problems, such as porosity and shrinkage in casting, high-loads and poor filling in forging, as well as poor mechanical properties of final parts provide a motivation for investigating new promising processes such as the Semi-Solid Metal Forming (SSMF). It includes:

1. Semi-Solid Forging (SSF) or Thixoforging
2. Semi-Solid Casting (SSC) or Thixocasting

These processes are in their development stage, and incorporate elements of both casting and forging for manufacturing of the net-shape or near-net-shape parts. SSMF processes take the advantage of the thixotropy state of semi-solid (SS) materials. The viscosity of a thixotropic material strongly decreases with

an increasing shear rate. A semi-solid material behaves like a fluid when a shear force is applied. Stirring a material mechanically or electromechanically during solidification in a controlled temperature environment gives a nondendritic microstructure that is essential for SSMF. This nondendritic structure allows SSMF processes to use lower deformation loads than solid forming processes. SSMF processes can often fill much more complicated die cavity shapes, often resulting in good mechanical properties. In addition, SS metals can be handled and manipulated as if they were completely solid, which allows easy handling of the material, Figure 2.1.

The principles of this technology have been known and investigated since the early 1970s when David Spencer, a Ph.D. student of Professor M.C. Flemings at Massachusetts Institute of Technology (MIT), discovered low apparent viscosity in solidifying alloys by continuous stirring while cooling them into the solid-liquid range (see Figure 2.2). However, the commercialization of the parts produced by SSMF is still limited due to the lack of the information about this technology, scarse raw materials, inability to model the process, and finally unknowns in the material properties and process specifications. In spite of the limitations indicated above, companies and researchers from different countries are highly interested in the SSMF process, and are actively developing it to a degree such that it can be successfully applied to manufacturing specific commercial components.

Figure 2.1:   A semi-solid material, being cut with a saw blade while standing free [Endabmesssungsnahe Fertigung-Ur/Umformtechnik (EFU) brochures, 1994].
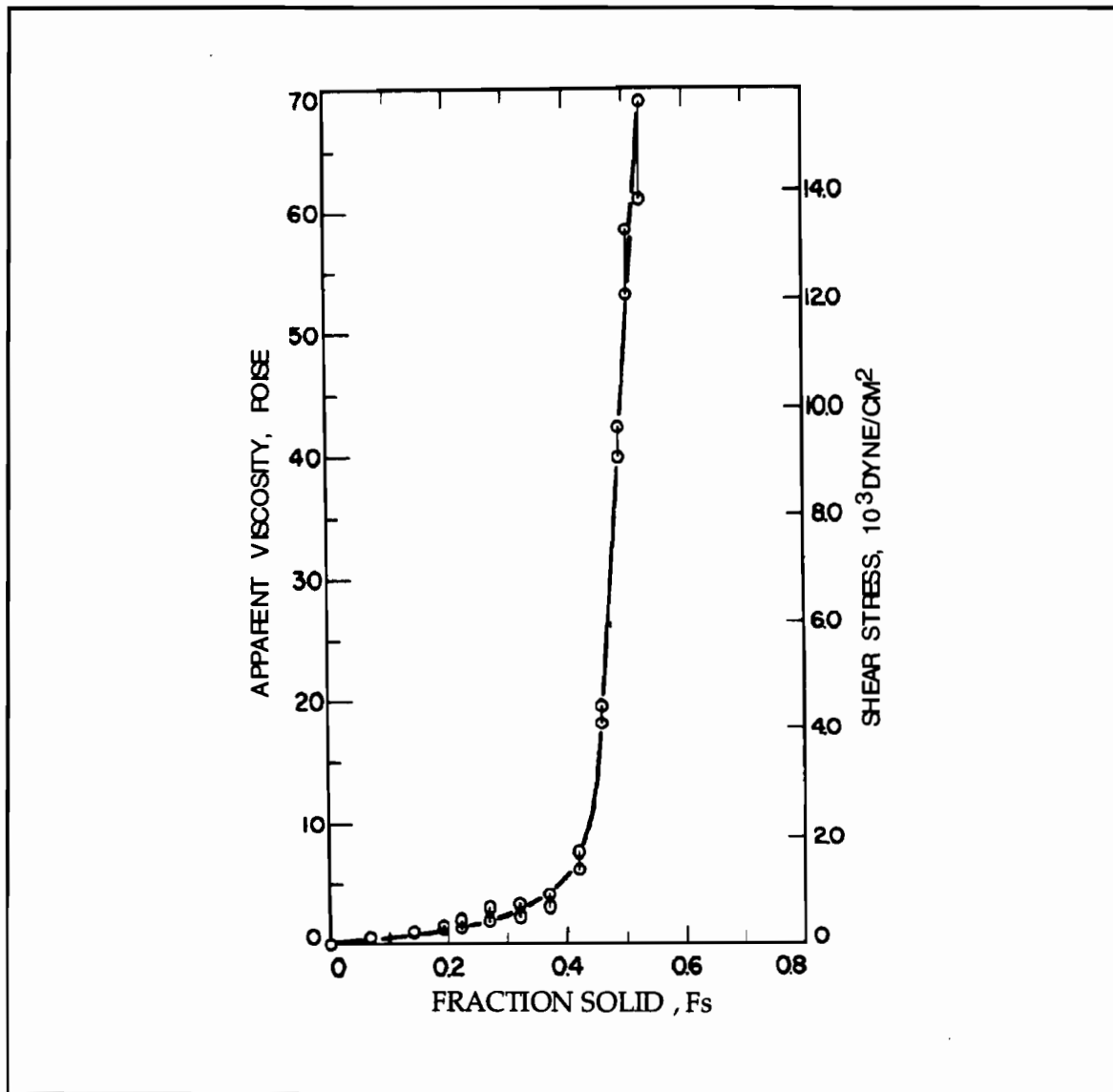
Figure 2.2: Shear stress and apparent viscosity vs. fraction solid, fs, in the Sn-15%Pb alloy in its semi-solid state [Flemings, et al., 1973].

The major commercial SSMF activity is in the semi-solid forging (SSF) of a variety of aluminum alloy parts for different military, aerospace and automotive applications.

2.3 Background

During his experiments, Spencer obtained surprising results with the Sn-15%Pb alloy [Spencer, D.B., et al., 1972]. He noticed that when he began shearing the material above the liquidus and then slowly cooled it into the solidification range while shearing, the shear stress increased slowly. The shear stress measured at a given temperature below the liquidus was lower in five orders of magnitude than when the samples were cooled to that temperature before shear (Figure 2.2). The grain structure obtained at the end of these experiments was nondendritic, Figure 2.3, and the material was behaving liquid like so that even an apparent viscosity equal to or less than that of olive oil could be assigned [Flemings, 1991]. Metals with this nondendritic structure can be directly cast in their partially solidified state up to solid fractions of 50%. This process is known as **"rheocasting"**.

Another SSMF process, known as **"compocasting"** is used for the production of Metal Matrix Composites (MMC). The viscous nature of the semi-solid metals can provide the possibility for incorporation of non-metallic particles or short fibers, even if they are not necessarily wetted by the

metal matrix alloy. The presence of the primary solid phase in the viscous semi-solid metal prevents the non-metallic from settling, floating or agglomerating. With continuous stirring , the non-metallics may eventually interact with the matrix alloy, and thus promote bonding and a homogeneous distribution of the reinforcing phase over the MMCs [Kiuchi, et al, 1992] [Flemings, 1991].
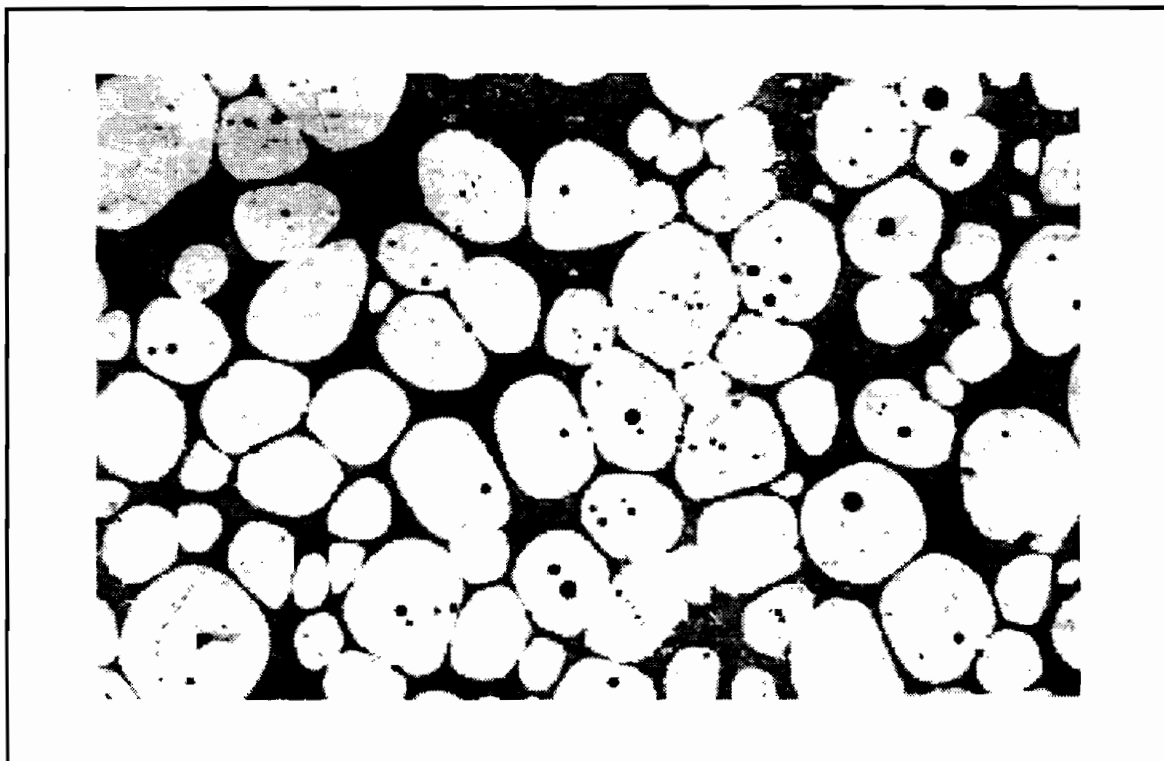
Figure 2.3: Non-dendritic microstructure of AlSi7Mg alloy [EFU brochures, 1994].

In the past two decades, many researchers from different parts of the world have conducted studies on fundamental and engineering aspects of these processes, which were earlier called rheocasting, later grouped under the term **"Semi-Solid Metal Forming"**. Numerous companies are now able to produce various parts using SS metals.

2.4 Definition of Semi- Solid State in Metals

Until recent years, there has not been any general recognized terminology about semi-solid metals and their forming processes. In the early literature, several expressions, i.e. **semi-solid, mushy-state, doughy-state** for the material state, and **rheocasting, thixoforming** and **squeeze casting** for the forming processes have been used by particular researchers.

According to the method of preparation and the processing route followed, the metals used in the semi-solid forming processes can be divided into three categories; semi-solid slurry, semi-solid slug and liquid molten metal. The *semi-solid slurry* refers to the state when the material is between the solidus and liquidus line in the phase diagram and can be stirred by different means to generate spheroidal grains. A phase diagram showing conventional casting range and rheocasting range is shown in Figure 2.4. Parts can be directly formed from the semi-solid slurry state. This process is called as rheocasting. When this semi-solid slurry is cast into ingots, and these ingots are cut into pieces or short slugs for eventual processing by

reheating into a particular temperature range and then feeding into either die casting or forging process, *semi-solid slug* state is obtained. Finally, the *liquid metal* state is that when the molten metal is heated to some degree of superheat over the alloy's liquidus temperature [Chu, et al, 1994].

In rheocasting, the slurry is cast directly into a shape, whereas in thixocasting the liquid-solid mixture is forced to behave like a solid until it is sheared (as in the die casting); then, it behaves as a slurry and flows to fill the die cavity [Flemings, 1973].
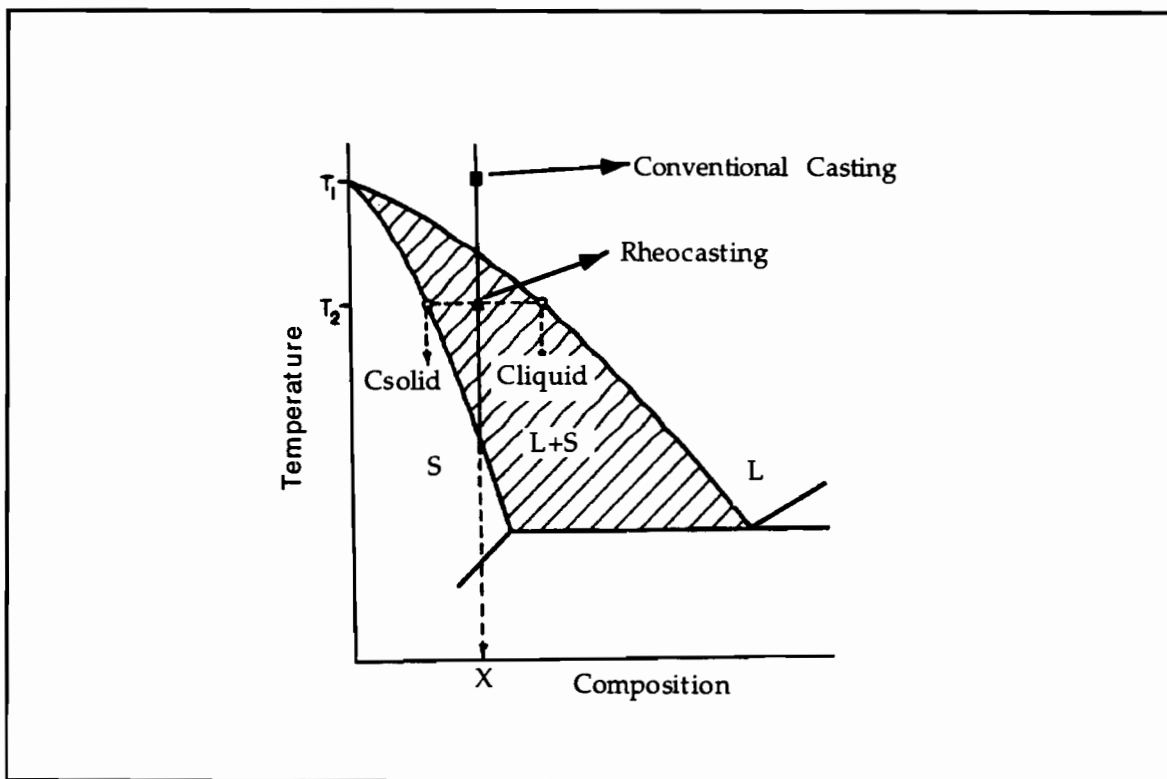
Figure 2.4: Phase diagram showing conventional casting at T_1 and rheocasting at T_2 [Cheng, et al., 1986].

2.5 Production of Semi-Solid Metals (SSM)

A variety of processing methods are available for producing semi-solid slurries. The objective is to obtain equiaxed, rounded particles that provide the characteristic SSM behavior. The basic way is to agitate the alloy vigorously during its solidification process. This shearing process breaks down the dendritic network, yields individual or combined spheroidal particles and lowers the viscosity [Brown, et al., 1993] [Kattamis, et al., 1991]. The most common processes used to obtain non-dendritic structure in semi-solid metals are *Mechanical Stirring, Electromagnetic Stirring, Strain Induced-Melt Activated (SIMA) process and Gircast.*

2.5.1 Mechanical Stirring Processes

Mechanical stirring can be classified into two methods as; *batch rheocasting* and *continuous rheocasting processes*. It was used during early MIT research and later in exploratory studies by others [Flemings, M.C. 1991].

Batch Rheocaster Process

This process consists of a crucible in which the molten liquid being cooled is mechanically mixed. Through the mechanical stirring action, the dendritic structure formed due to cooling will crush into small solid particles and disperse in the remaining molten metal. This process has been

incorporated in vacuum or inert atmosphere chambers to produce semi-solid metal of high melting point alloys and to reduce air entrapment [Kenney, et al., 1988].

Continuous Rheocasting Process

This process uses a liquid metal reservoir, and a mixing and cooling chamber formed by a single piece crucible (Figure 2.5). The mixing rotor is a hollow tube of high purity alumina, and it can be raised or lowered while rotating to control the flow of the existing slurry, and to minimize the air entrapment. Generally, induction heating is used [Flemings, 1976] [Joly, et al., 1976].
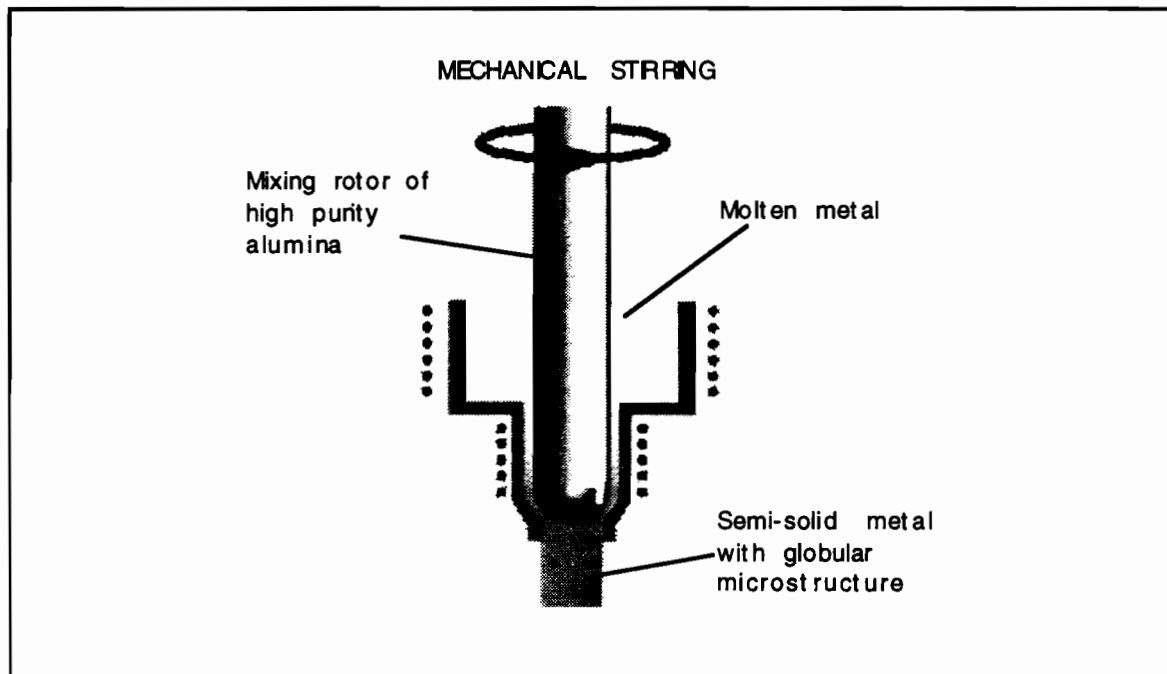
Figure 2.5: Continuous rheocasting (mechanical stirring) process [EFU brochures, 1994].

Electromagnetic Stirring Process
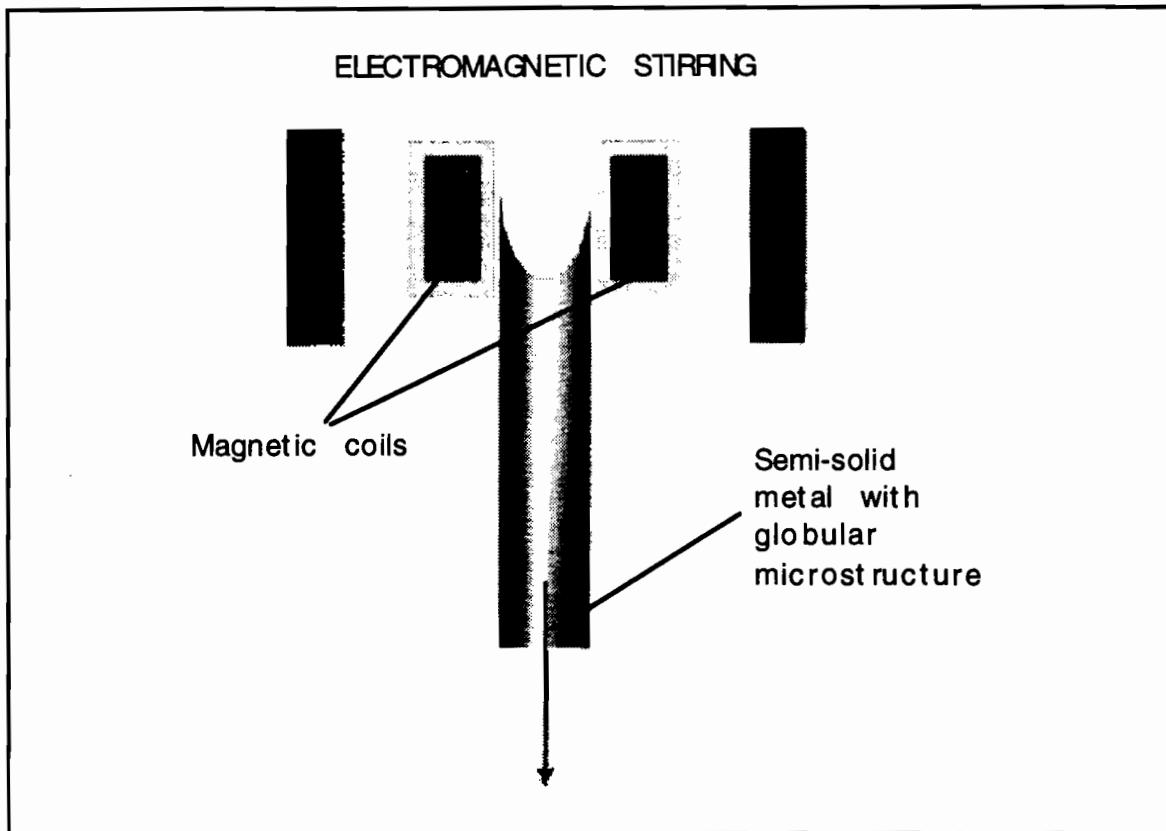
Figure 2.6:   Electromagnetic stirring process [EFU brochures, 1994].

Electromagnetic stirring of continuous cast ingots is also known as "Magnetohydrodynamic (MHD)" process. MHD is used to produce SSM of large diameters. This process permits production of large tonnages, and it is applicable to high temperature metals such as steel [Flemings, 1991]. The development of this technology recognized the need for the exclusion of gases, oxides and nonmetallic inclusions and avoided other discontinuities. The design of the MHD casting system incorporates the feed of filtered and

degassed metal into the direct chill mold. The metal near the freezing point in the mold, is vigorously stirred by a dynamic electromagnetic field, which creates the necessary shearing action. At the same time, the metal is cooled by the water jacket, Figure 2.6. Therefore, MHD process provides the ability to control precisely the shearing action and the rate of heat removal and thus delivers the desired solidified microstructure with a grain size that is normally about 30μm [Kenney, et al., 1988].

Today, MHD casting systems are installed both vertically and horizontally in a company plant to produce a variety of fine-grain semi-solid metalworking aluminum alloys from 38 mm to 152 mm in diameter [Kenney, et al., 1988]. Furthermore, various European companies such as Alusuisse (Switzerland), EFU GmbH (Germany), Pechiney, and Alures have used this method along with the thixocasting or thixoforging processes to produce commercial parts [Hirt et al., 1993]. A modified electromagnetic rheocaster method, used to produce thixotropic aluminum alloy slurries, has been presented by Vives. Rotating permanent magnets are used, which permit intense stirring in solidifying alloys [Vives, 1992].

2.5.2 Strain Induced-Melt Activated (SIMA) Process

Since small diameter materials (less than 38 mm) and some wrought alloys are difficult and/or expensive to cast. A number of researchers have

studied the possibilities of solid-state processing. For example, method named Strain Induced-Melt Activated (SIMA) process was developed by Young in 1981 [Kenney, et al., 1988]. In this process, an alloy billet or bar with small cross-section is cold worked to a critical amount such that reheating up to the liquid-solid zone provides the desired spheroidal structure.
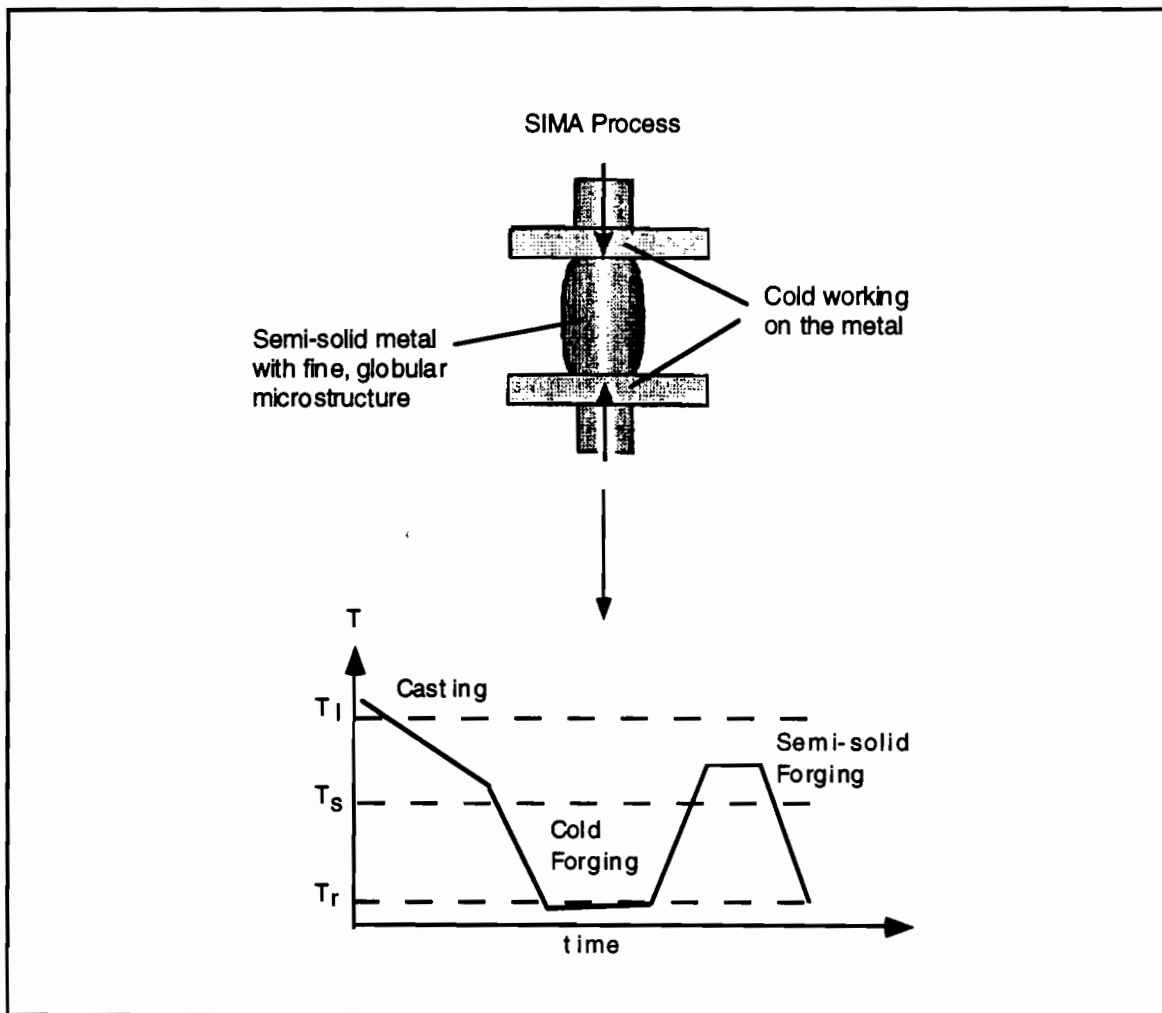
Figure 2.7: Schematic of SIMA process and its time vs. temperature diagram showing process sequence [EFU brochures, 1992].
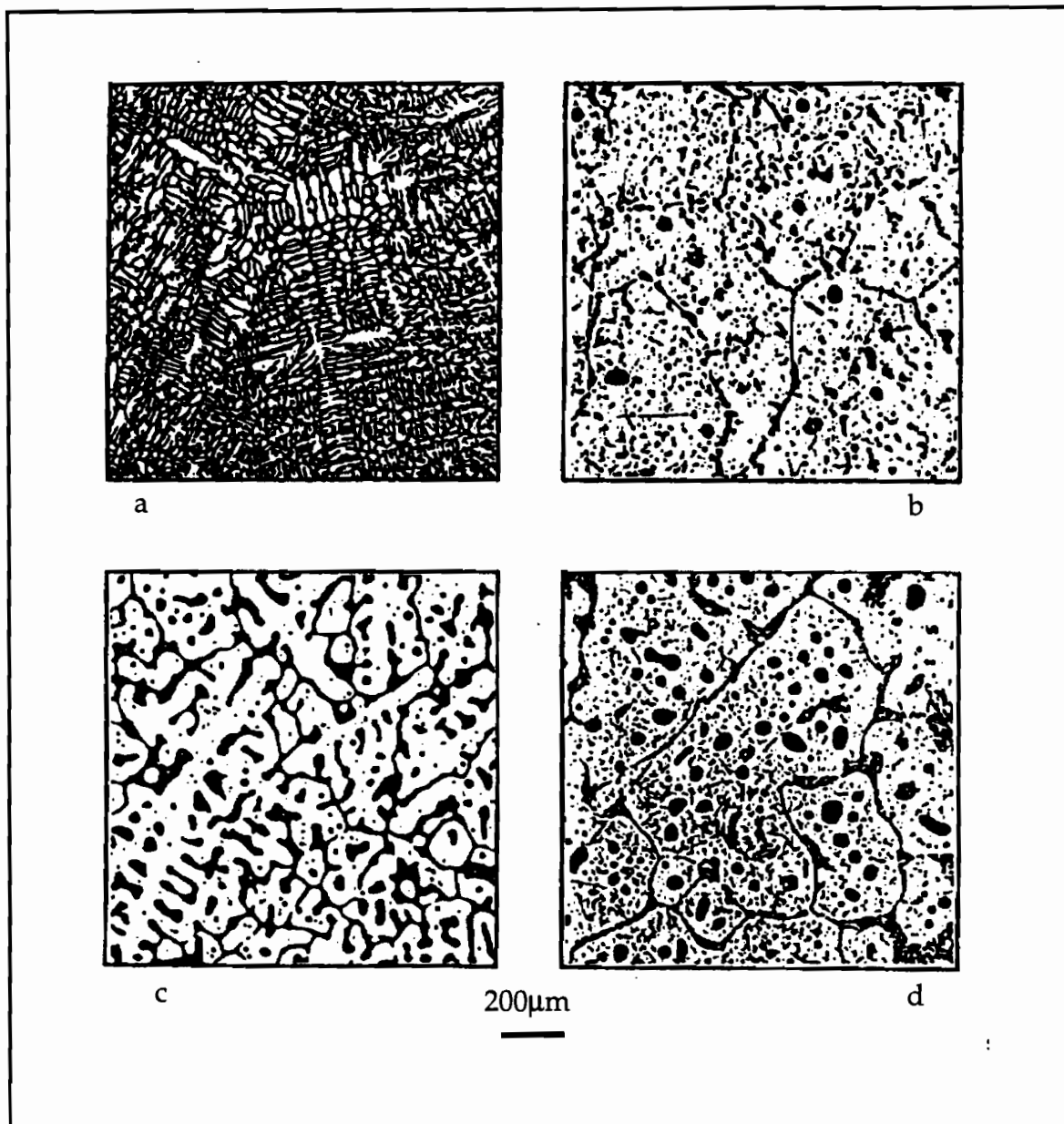
Figure 2.8:   Microstructure of DC cast 356 alloy with time at 580 ºC: a) initial structure, b) 1 min, c) 5 min, d) 30 min [NCEMT, 1994].

The schematic of the SIMA process is illustrated in Figure 2.7. A typical SIMA operation starts with conventional cast billets. These billets are extruded and cold worked prior to heating up to the semi-solid temperature range. During the final heating stage, material first recrystallizes, and then, melting initiates, grain boundary generation occurs, which isolates the discrete particles within a liquid matrix. This results in extremely fine, uniform, nondendritic spherical microstructure [NCEMT, 1994]. In Figure 2.8, the influence of cold work on microstructure of 356 Aluminum alloy produced by SIMA is shown. This process offers a cost-effective and readily available source of small-diameter aluminum, magnesium and copper billets [Kenney, et al., 1988].

2.5.3 Other Processes

GIRCAST Process

The GIRCAST process was developed at CEMEF in France. Stirring is applied when the crucible and its counterweight are in the vertical position. Liquid nitrogen is then sprayed over the crucible while the crucible is rotated for three minutes. The quenched ingot, usually 60 mm in diameter, exhibits a thixotropic structure [Collot, et al., 1992].

Shearing / Cooling Rolling (SCR) Process

A new process named SCR (Shearing/Cooling/Rolling) was developed in Japan. It consists of a rotating shearing/cooling roll, a shoe which is fixed

to a supporting block and a stripper. The molten metal is poured into the roll-shoe gap, then is drawn into the gap by the frictional force of the rotating roll. At the gap, it is cooled and stirred by the rotating roll and shoe. The dendritic structure is crushed into small solid particles by the shearing force created by the rotating roll and the fixed shoe producing semi-solid metal [Kiuchi, M., 1991].

2.6 Characteristics of Semi- Solid Metals

Alloys with dendritic microstructure possess rheological properties in the semi-solid state. They behave thixotropically (behave more fluid like as the applied force is increased), and viscosity can be varied over a wide range, depending on processing conditions. The metal structure and rheological properties are retained after solidification and partial remelting [Flemings, 1991].

2.6.1 Flow Behavior of Semi-Solid Metals

Structure and flow behavior of non-dendritic materials are shown in Figure 2.9. For a non-dendritic material with a fraction solid of 0.4, the maximum shear stress is 0.2 kPa which is three times less than for a dendritic material with the same fraction solid. Figure 2.10 illustrates the change of apparent viscosity and microstructure with respect to shear rate.
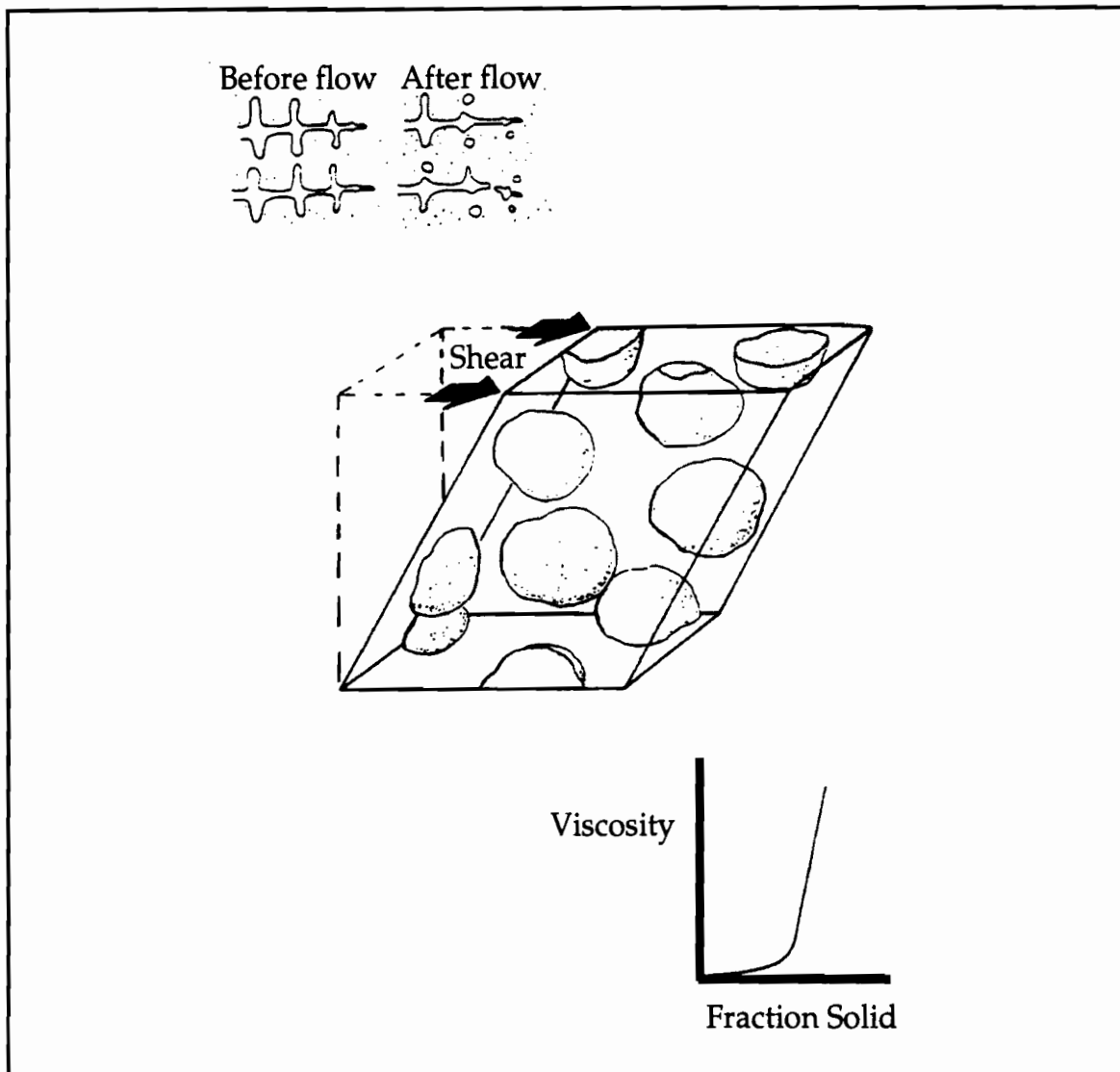
Figure 2.9: Fundamentals of semi-solid forming: top left, breaking of dendrite by shear, center: rheological behavior of a volume element of semisolid nondendritic material, bottom right: viscosity vs. fraction solid [Flemings, 1991].
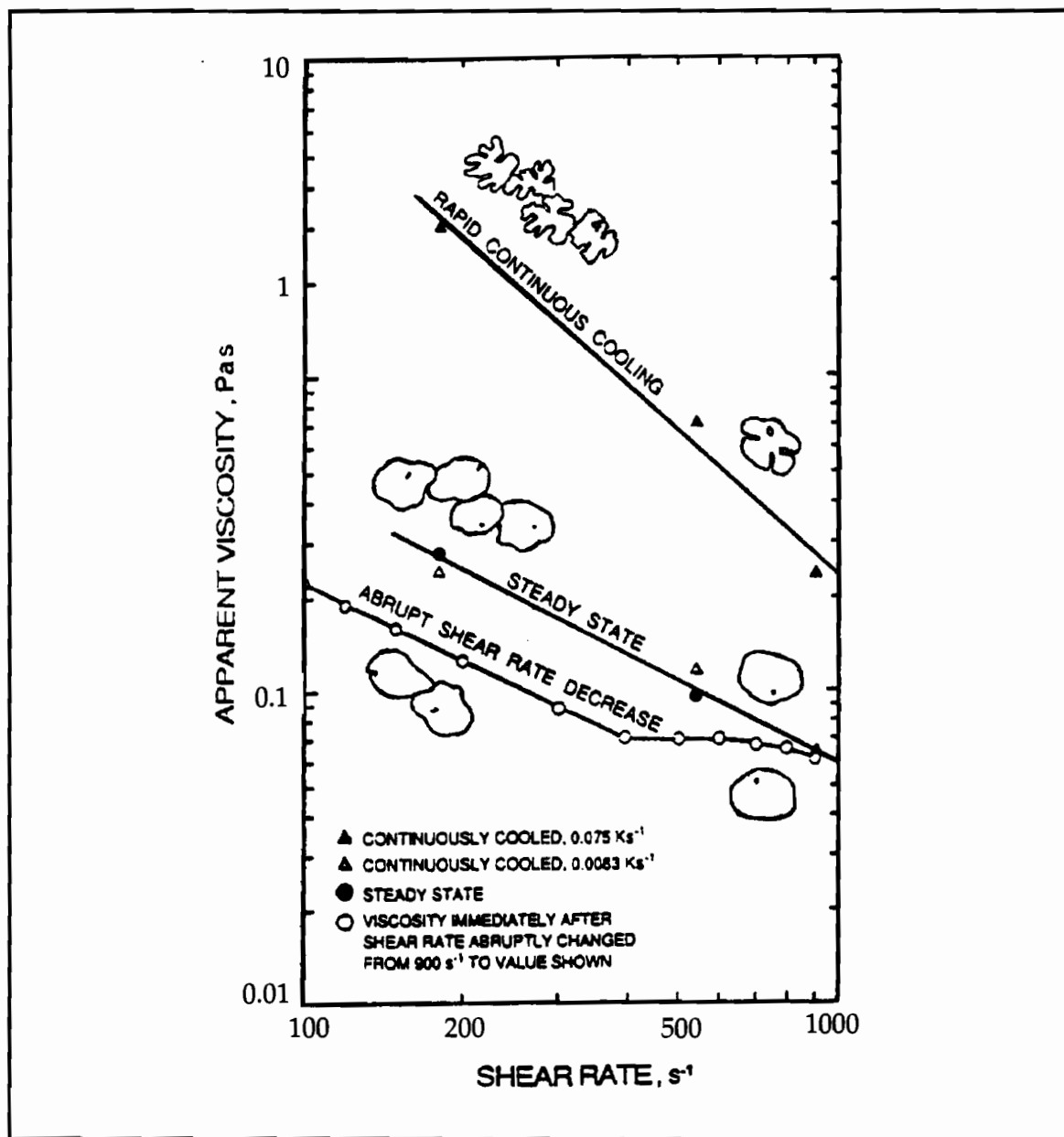
Figure 2.10: Viscosity vs. shear rate for Al-5.5% Si alloys at 0.4 fraction solid, and corresponding microstructure evolution [Flemings, 1991].

The constitutive flow behavior of semi-solid materials is highly non-linear, and even in slurries with relatively small solid fractions, i.e. less than 0.1, flow behavior is influenced by the interaction of the solid particles. The most important factors that dominate the flow behavior of the semi-solid metal are temperature, shear rate history and characteristics of the slurry [Kumar, et al., 1992]. As sketched in Figure 2.10, viscosity is high at low shear rates due to two reasons: first, grains are somehow still in dendritic form; second, these grains agglomerate As shear rates increases, the agglomeration decreases, and the grains become more rosette like. The grains are more dense and rounded, and they have more agglomeration at the lower shear rates. Viscosity decreases with this spheroidal grain structure at steady-state as compared with the material that is rapidly and continuously cooled.

Viscosity of a semi-solid metal slurry is found to be a strong function of shear rate ($\dot{\gamma}$), cooling rate (E) and temperature (volume fraction solid, f_s) when it is continuously cooled. Figure 2.11 (a) shows that at a given cooling rate E, the viscosity decreases with increasing initial shear rate $\dot{\gamma}$. Figure 2.11 (b) shows that at a given initial shear rate, the viscosity decreases as the cooling rate decreases. Generally, viscosity increases with increasing volume fraction solid, increasing cooling rate, and decreasing initial shear rate. [Joly, 1976].
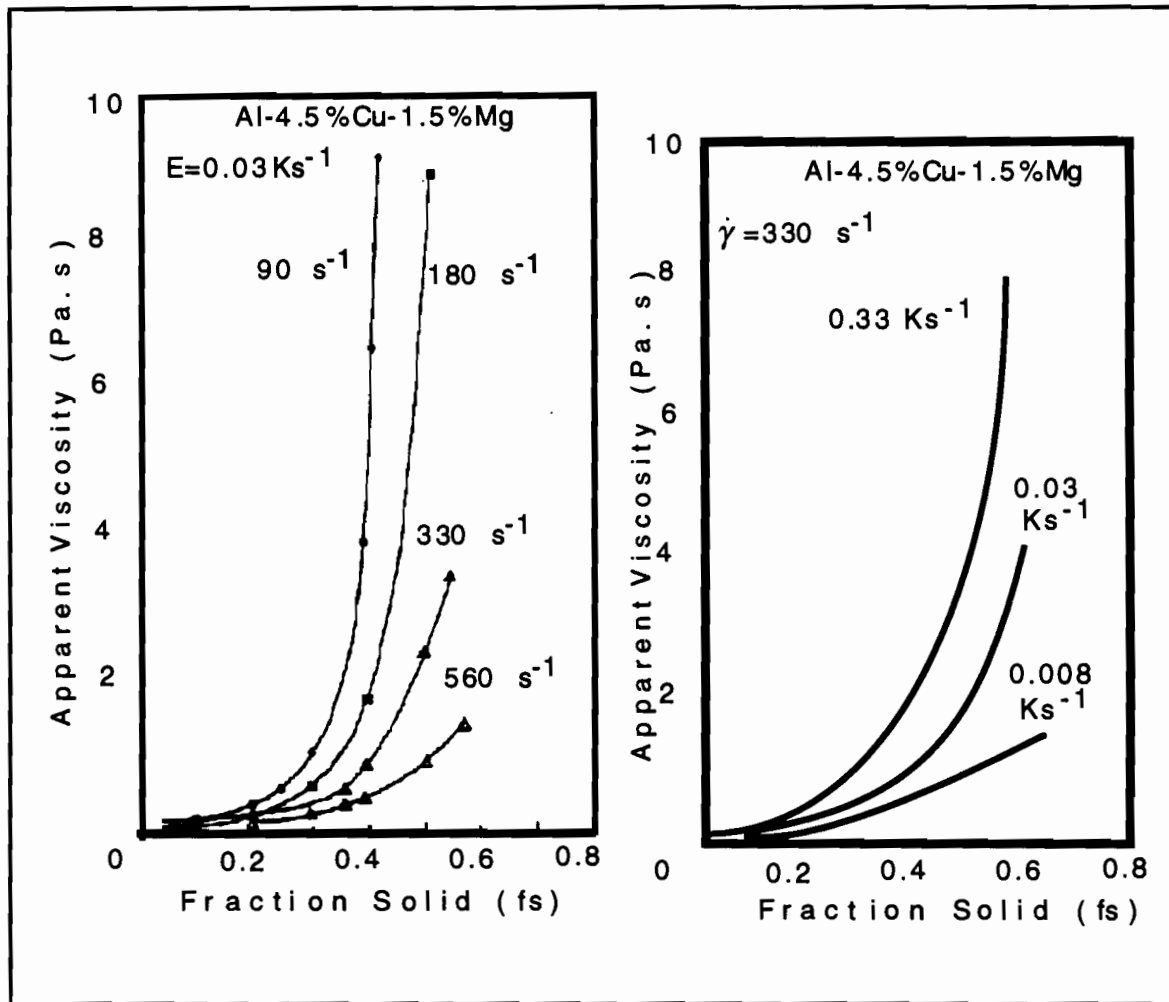
Figure 2.11: Effect of a) shear rate and b) cooling rate on apparent viscosity of semi-solid alloy: Al-4.5%Cu-1.5%Mg (E= cooling rate, $\dot{\gamma}$ = shear rate) [Flemings,1991].

Structure

Both increasing shear rate and decreasing cooling rate result in denser and more round particles [Flemings, 1991]. The size of the primary solid particles in the slurry decreases with increasing cooling rate. The primary solid particles have the same average size; however, there is less entrapped liquid within the particles that have experienced the higher shear rate. The amount of entrapped liquid at slow cooling rates is less than that at the higher cooling rates [Joly, et al., 1976]. As the final volume fraction solid in the slurry decreases, it becomes more difficult to distinguish the primary solid particles from the quenched liquid matrix. As a result, at the lower cooling rate the primary solid particles are larger, smother, more uniform in size, and have less entrapped liquid, and the amount of entrapped liquid within the particles decreases as final volume fraction solid increases.

2.7 Comparison with Conventional Materials and Processes

Comparison of semi-solid metals with other metals can give us some important understanding of their properties, particularly by comparing them with well known materials such as water, steel, oil, etc. One of the properties that can be easily compared is the viscosity. In this case, viscosities of semi-solid materials at 40 to 50% fraction solid are in the range of 0.1 to 10 Pa.s, which is two or four orders of magnitude higher than the viscosities of water or fully liquid metal respectively and is in the range of olive oil, glycerol and honey. Table 2.1 illustrates this comparison.

Semi-solid materials, with the viscosities in the range given above, can be easily handled as if they were fully solids. Flemings gives a sample calculation to demonstrate the easiness of their manipulation. A 50-mm cube of semi-solid aluminum is assumed to be held between two parallel plates. Gravity produces a shear force. Required viscosity is estimated as the shear force divided by shear rate ($\eta = Fs/\dot{\gamma}$). The result is a calculated viscosity of approximately 10^6 Pa.s. Semi-solid thixocast alloys at 40 to 50% easily reach this viscosity [Flemings, 1991]. Moreover, "K" (consistency) and "n" (power-law index) values used in the empirical "power law ($\eta = K \dot{\gamma}^{n-1}$) to describe pseudoplastic behavior of fluids can be compared. The smaller the power-law index, the greater the shear thinning effect (viscosity decreases with increasing shear rate). Table 2.2 shows some typical values of K and n for familiar materials and for semi-solids. Table 2.3 lists shear rates of familiar processes and compares them with semi-solid metal working process.

Table 2.1: Typical viscosities for different materials [after Flemings, 1991].

10 E7	
10 E6	
10 E5	GLASS WORKING RANGE
10 E4	
10 E3	MOLASSES
10 E2	TOOTH PASTE, SHEAR RATE = 5 (1/S)
10 E1	HONEY
10 E0	GLYCEROL
10 E-1	OLIVE OIL
10 E-2	BICYCLE OIL
10 E-3	WATER, LIQUID METALS
10 E-4	

VISCOSITY (Pa.s)

SEMI SOLID ALLOYS at solid fraction, $f_s = 0.4$
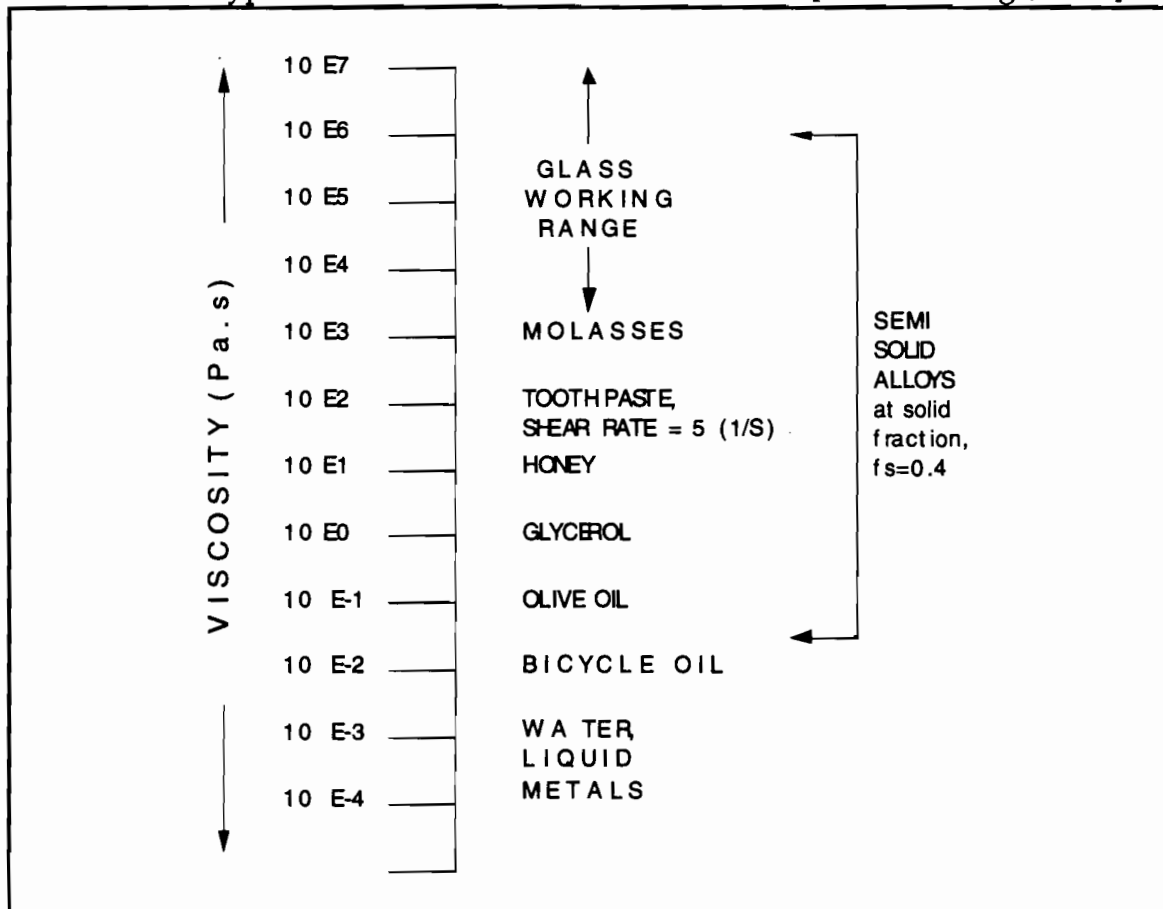
Table 2.2: Materials of comparable shear thinning behavior, $\eta^* = K\,\dot{\gamma}^{n-1}$ [Flemings, 1991].

MATERIAL	η^*	VISCOSITY, η, Pa.s, at $\gamma = 200\ s^{-1}$
Lubricating grease	0.1	9
Skin cream	0.1	2
Rheocast (steady state, fs=0.4)	0.1	0.3
Yogurt	0.1	0.3

Table 2.3:   Shear rates of conventional processes [after Flemings, 1991].

SHEAR RATE 1/s		
10 E6		
10 E5	ENGINE LUBRICATION	
10 E4	EXPLOSIVE FORMING PRESSURE DIE CASTING	
10 E3		SEMI SOLID METAL FORMING
10 E2	STAMPING, COLD FORMING, GRAVITY CASTING	
10 E1	STIRRING, SWALLOWING	
10 E0		
10 E-1		
10 E-2	ISOTHERMAL FORGING	
10 E-3	SUPERPLASTIC FORMING	
10 E-4		
10 E-5		
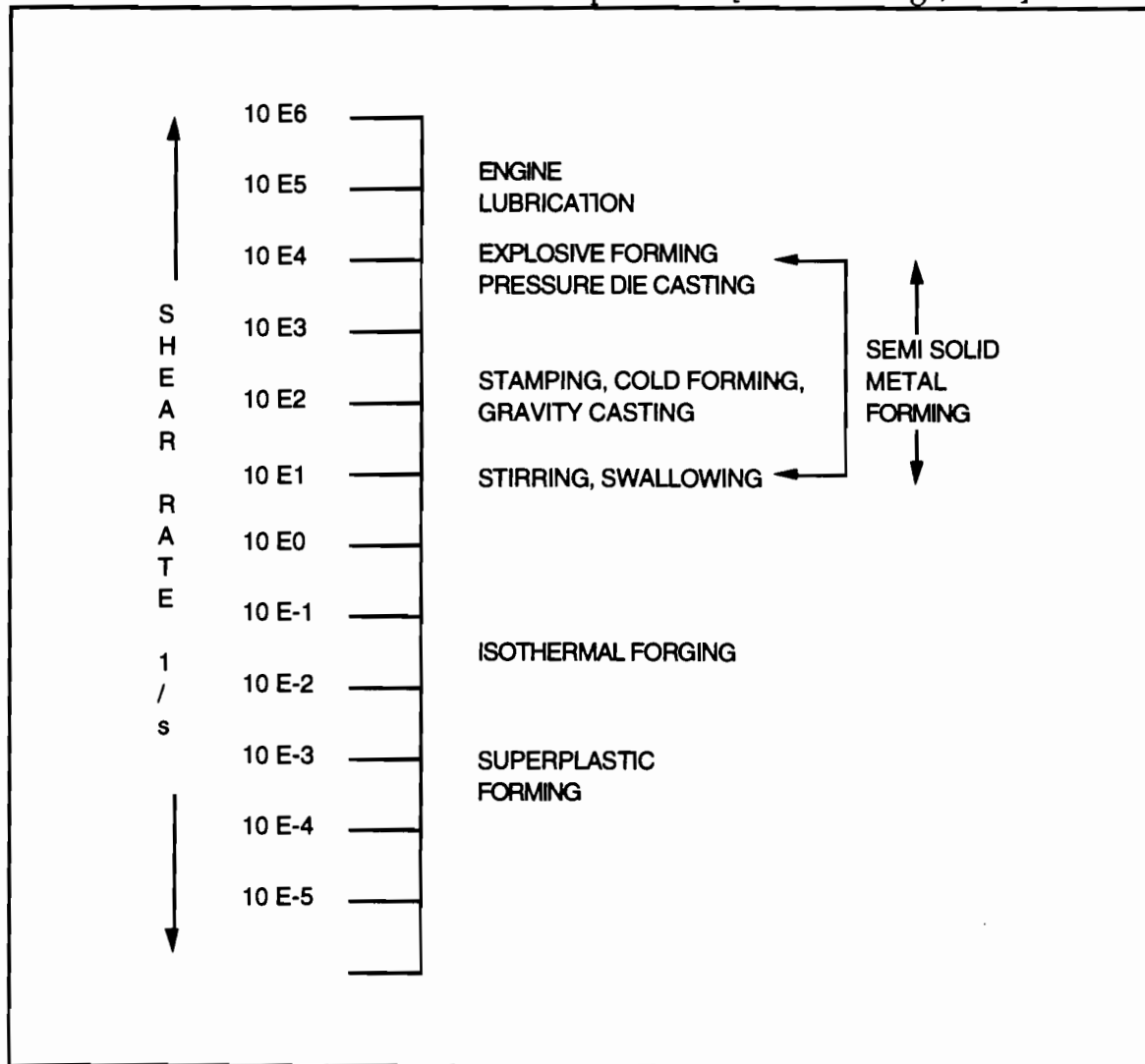
Chapter III

SEMI-SOLID FORGING (SSF), ITS CHARACTERISTICS AND OTHER SEMI-SOLID METAL FORMING (SSMF) PROCESSES

SSMF processes can be classified as follows:

    1.   Thixoforming

                a. Semi-Solid Forging (SSF) or Thixoforging

                b. Semi-Solid Casting (SSC) or Thixocasting

    2.   Compoforming: Forging of Metal Matrix Composites (MMCs)

3.1 Thixoforming

Figure 3.1 illustrates the Thixoforming processes, Thixoforging and Thixocasting basically. Today, thixoforming processes are highly automated as shown in Figure 3.1. Billets are reheated under computer control and then transported by robot arms to the forming operation for again shaping and removing from die automatically.

3.2 Compoforming

Semi-solid forging gives many advantages for the production of composite materials. The blending of second-phase particles into the alloy becomes easy, particularly if the particles are not wetted easily by the liquid phase. A schematic diagram of manufacturing processes for metal matrix composites (or particle reinforced metals-PRM) by utilizing semi-solid state processing is shown in Figure 3.2. The process can be outlined as follows:

1) Until the desired solid fraction is reached, the metal matrix is heated up, and second-phase particles such as ceramics are added to it. Then, this mixture is stirred and a homogeneous distribution of particulates is obtained.

2) The uniform mixture of primary metal and reinforcing particles can be either directly transferred to the forming machines, such as die cavities, extrusion press, forging press or rolling mill; or it can be cooled, solidified and cut into the billets. The billets are reheated to the semi-solid region and supplied to the following SSM processes:

3) The compoformed billets are made into bars, wires, tubes, sheets or machine parts by semi-solid metal working processes such as forging, rolling and extrusion.

4) Instead of the procedure above, the mixture of metal powder and reinforcing particles can be supplied to the same SSM processes after heating [Kiuchi, 1993].
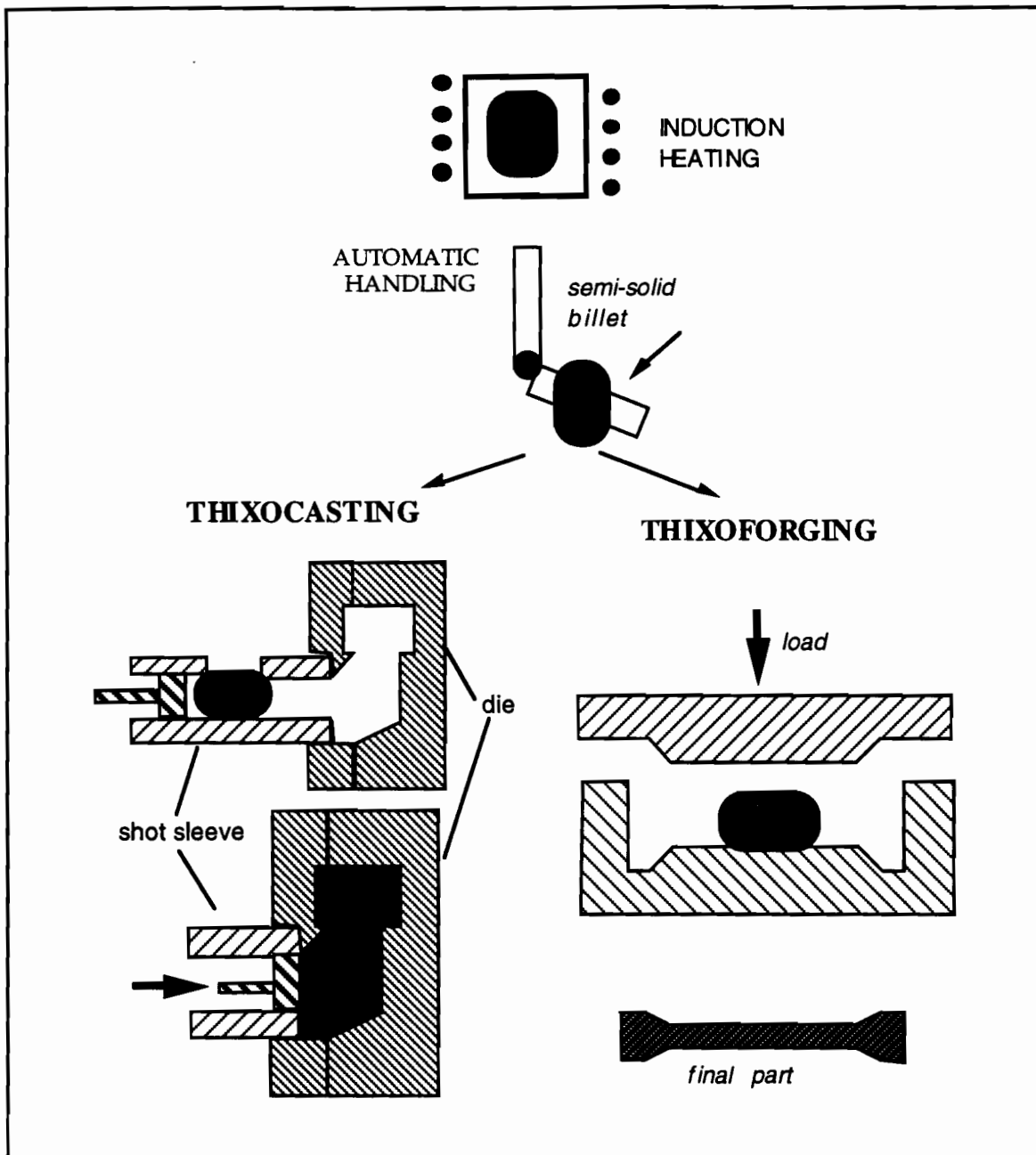
Figure 3.1: A simple illustration of thixoforming processes: metal is induction-heated until it reaches the semi-solid temperature range, then it is either thixocast or thixoforged [after Hirt, et al., 1994].

Many researchers found that the composites, with or without partial metal solidification, exhibit thixotropic behavior similar to that of partially solidified fully metallic slurries. Also, the fraction of primary solid alloy particles is reduced when the composite is reheated. The added second-phase particles can lower the flow resistance of semi-solid slurries. The second-phase particles prevent contact of the primary particles reducing this interaction because they are normally smaller than the primary particles and remain between them in the liquid matrix, Figure 3.2. Compoforging process has the potential of producing a variety of composite materials for improved wear resistance, improved strength and for low-friction applications.
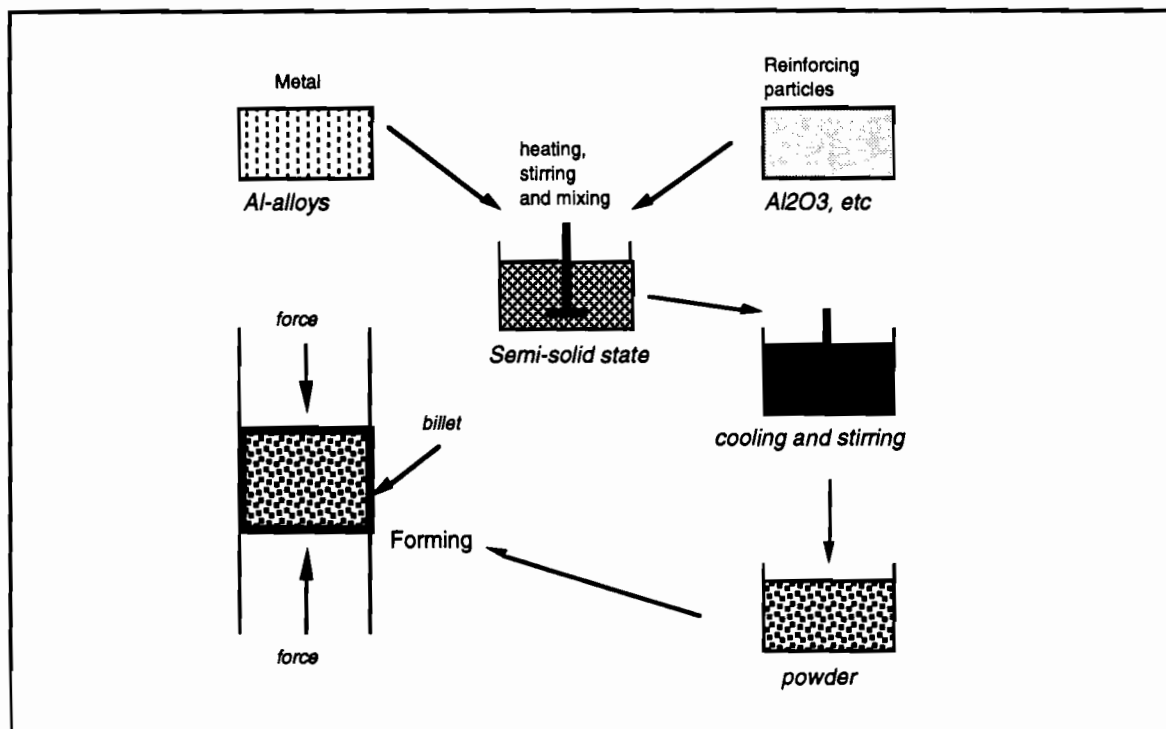
Figure 3.2: Semi-solid forging for manufacturing of particle reinforced metals [after Kiuchi, 1993].

3.3 Characteristics of Semi-Solid Forging (SSF) Process

SSF process is suitable for manufacturing complex parts with dependable mechanical properties using low machine loads at tolerable costs. Nondendritic alloys with 0.8 fraction solid can be deformed homogeneously without cracking to very large strains. For instance, thixoforging loads of a semi-solid metal with fraction solid less than 0.55 are 7 kPA to 70 kPa and those of a semi-solid metal with 0.60 solid fraction are 172.5 kPa to 207 kPa to achieve a 50% compression ratio. For a dendritic alloy, to achieve a 10% compression ratio, 80 kPa is required at a solid fraction of 0.36 [Laxmanan, et al, 1980].

In addition, SSF permits the production of high quality heat-treatable and oxide-free components. SSF has a distinct advantage because of that a partially solidified semi-solid charge metal is inclined to homogeneous deformation. Therefore, more sound products can be obtained with several other good mechanical properties.

Semi-Solid Forging (SSF) offers numerous advantages over conventional casting and forging processes, namely:

1. Production of porosity-free and heat treatable parts
2. Good mechanical properties as in conventional forging
2. Good surface finish

3.   High metal utilization

5.   Lower deformation loads

5.   Automation in the process

7.   Single-step, simple and easy operations

Table 3.1 and 3.2 compare the advantages of semi-solid forging with permanent mold casting and machining, respectively.

Semi-solid alloy slurries have a much higher viscosity than fully liquid alloys; therefore, flow becomes laminar and a die fills more evenly during deformation.   Furthermore, less gas is entrapped during filling of a die, resulting in less center-line porosity, improved soundness, and an increased forming speed. Apparent viscosity of semi-solids can be tailored for different die geometries by controlling the stirring and temperature before processing; hence, an improved surface finish is obtained.

Metal forming processes including forging, extrusion, rolling and strip casting can be applied for semi-solids with a high solid fraction. Since they are not fully solid, much lower machine loads will be enough to achieve deformation, and much more intricate parts can be filled without any difficulty. (Figure 3.3.) Lower flow stress in SSF causes high performance production with a reduction in cost of components because smaller machine tools are required when compared with machines used in conventional forging. Figure 3.4 depicts the energy savings obtained using SSF process.

A very important advantage that comes with SSF is the availability of automation; semi-solids can be handled and manipulated easily although their deformation resistance is much lower than that of fully solids materials. Up to certain percentages of liquid phase, i.e. usually 60%, small reheated semi-solid billets can be picked up and moved without any deformation in their shape.

Table 3.1: Comparison of SSF with mold casting in terms of part mass and production rate for a master brake cylinder [Kenney, et al., 1988].

Process	Al-Alloy	Mass as formed, g	Finished part mass, g	Machine loss, %	Production rate, pcs/mold/ hour
SSF	357 - T5	450	390	13	150
Permanent mold cast	356 - T6	760	450	40	24

Table 3.2: Comparison of SSF with machining for an electrical connector [Kenney, et al., 1988].

Process	Al-Alloy	Raw material mass, g	Finished part mass, g	Machine loss, %	Production rate, pcs/hour/ (primary operation)
SSF	6262- T6	25	23	8	300
Machining	6262 - T9	245	23	81	200
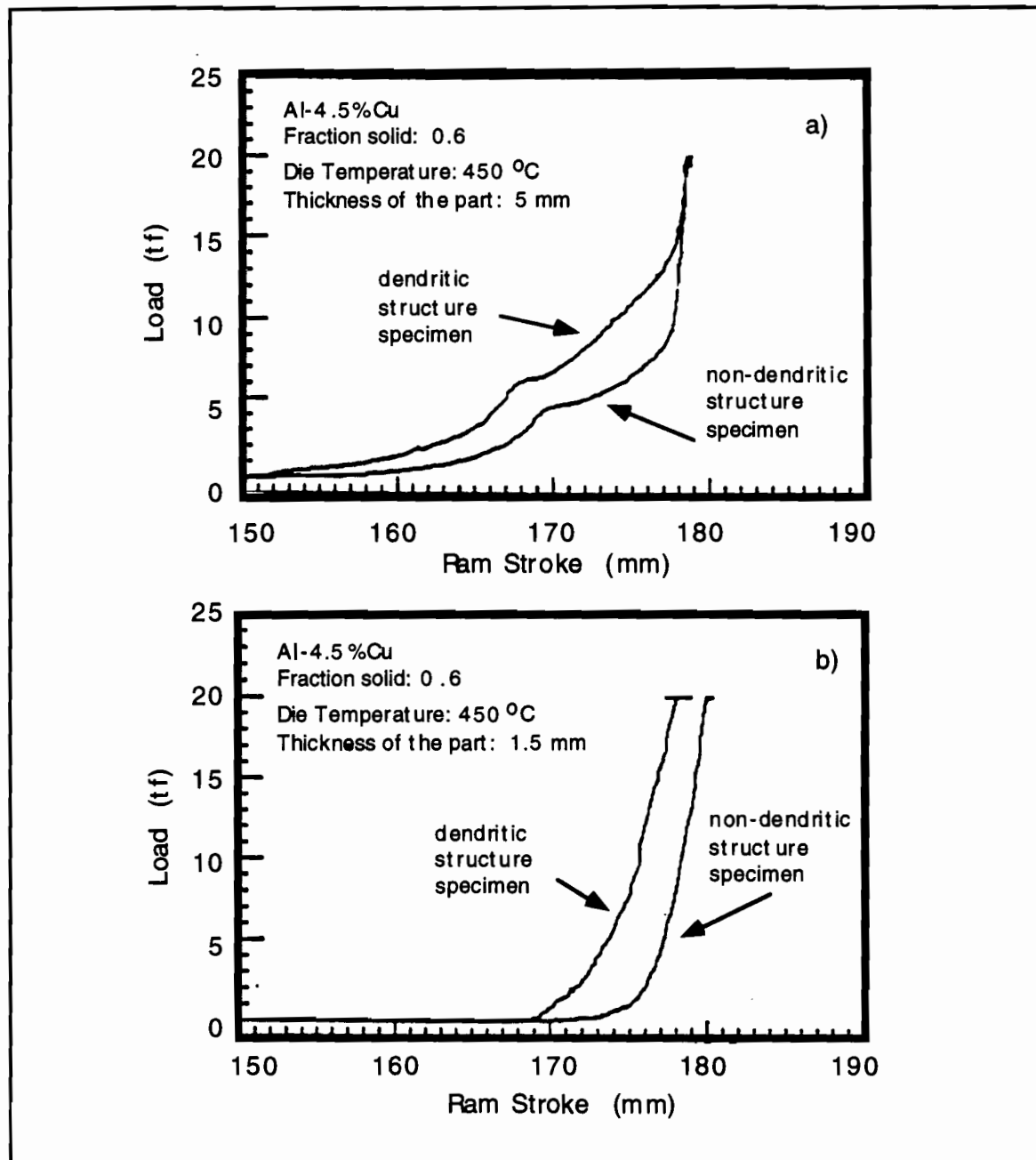
Figure 3.3: Load vs. stroke during SS Forging of Al-3.5% Cu alloy, comparison between loads in dendritic and nondendritic cases [after Yoshida, et al., 1992].
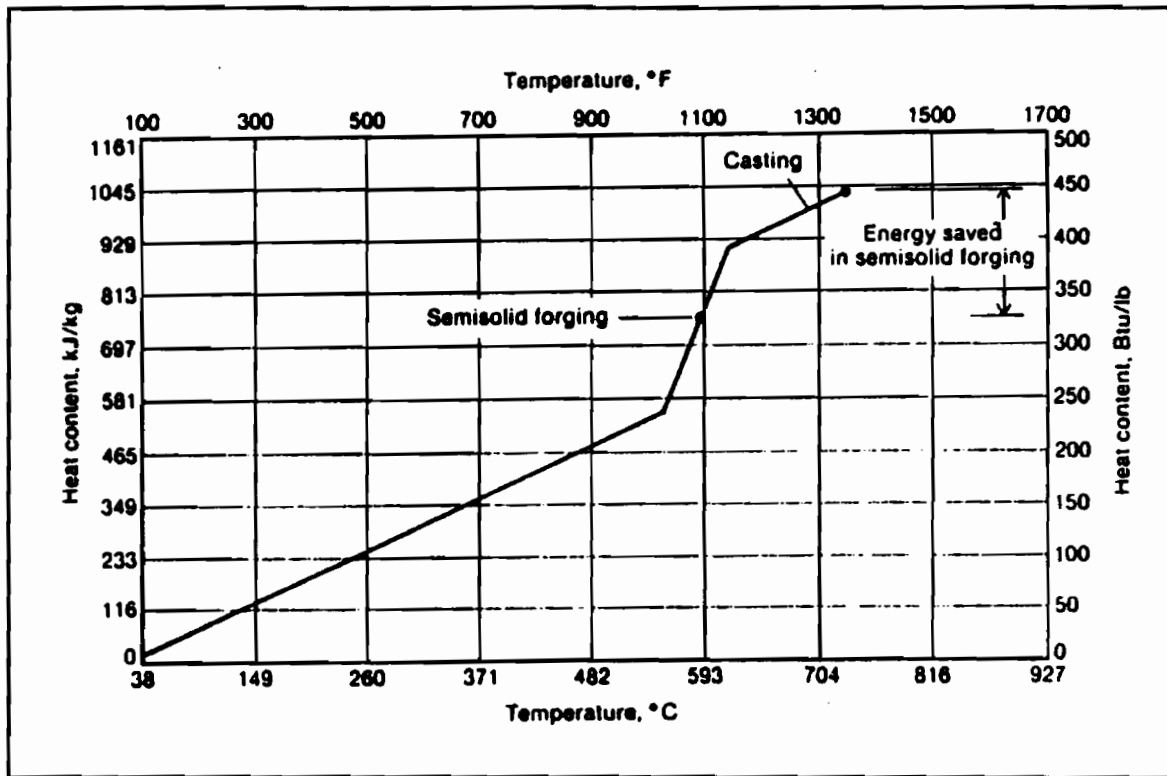
Figure 3.4:   Heating curves showing energy saving in SSF vs. casting of 357 Al alloy [Kenney, et al., 1988].

Finally, since SSF provides improvement in blending of second-phase particles into the alloys, metal matrix composites can be bulk formed even though the particles are not easily wetted by the liquid phase. On the other hand, the limitations for the semi-solid forging are as follows:

• Specially prepared raw material is required: conventional metals can not be used in these processes. Materials having non-dendritic microstructure are necessary

- Expensive raw material: for the production of semi-solids, the equipment used is more expensive and the time spent is longer than for conventionally cast metals

- Few sources of raw material: only a limited number of alloy systems are practically used in SSF processes

- Expensive tooling and equipment of special design is required either at the production stage of semi-solids or at the forming stage, special designed equipment is required to obtain the desired properties from the final products [Kenney, et al., 1988]

3.4 Steps in Semi-Solid Forging (Thixoforging) Process

Semi-solid slugs that were rheocast, solidified and sectioned can be forged using conventional equipment with much smaller machine loads than are required with fully solid forgings. Semi-solid billets with solid fractions from 0.5 to 0.9 can be forged and extruded without any difficulty. It has been found experimentally that forging rates must be relatively high to prevent separation of liquid and solid phases [Loué, et al., 1993]. Cracking of free surfaces can also occur if the state of stress at those surfaces involves large tensile components.

Figure 3.5 illustrates the basic steps in SSF process. SSF can be accomplished in a three-step process. First, the billet is cut to the required weight. Second, the billet is heated usually via induction heating because

uniform temperature distribution can be obtained in a short time. Figure 3.6 shows liquid fraction vs. temperature diagram for three different alloys. These diagrams were obtained during the reheating for thixoforging process at EFU GmbH, Germany [Hirt, et al., 1994].
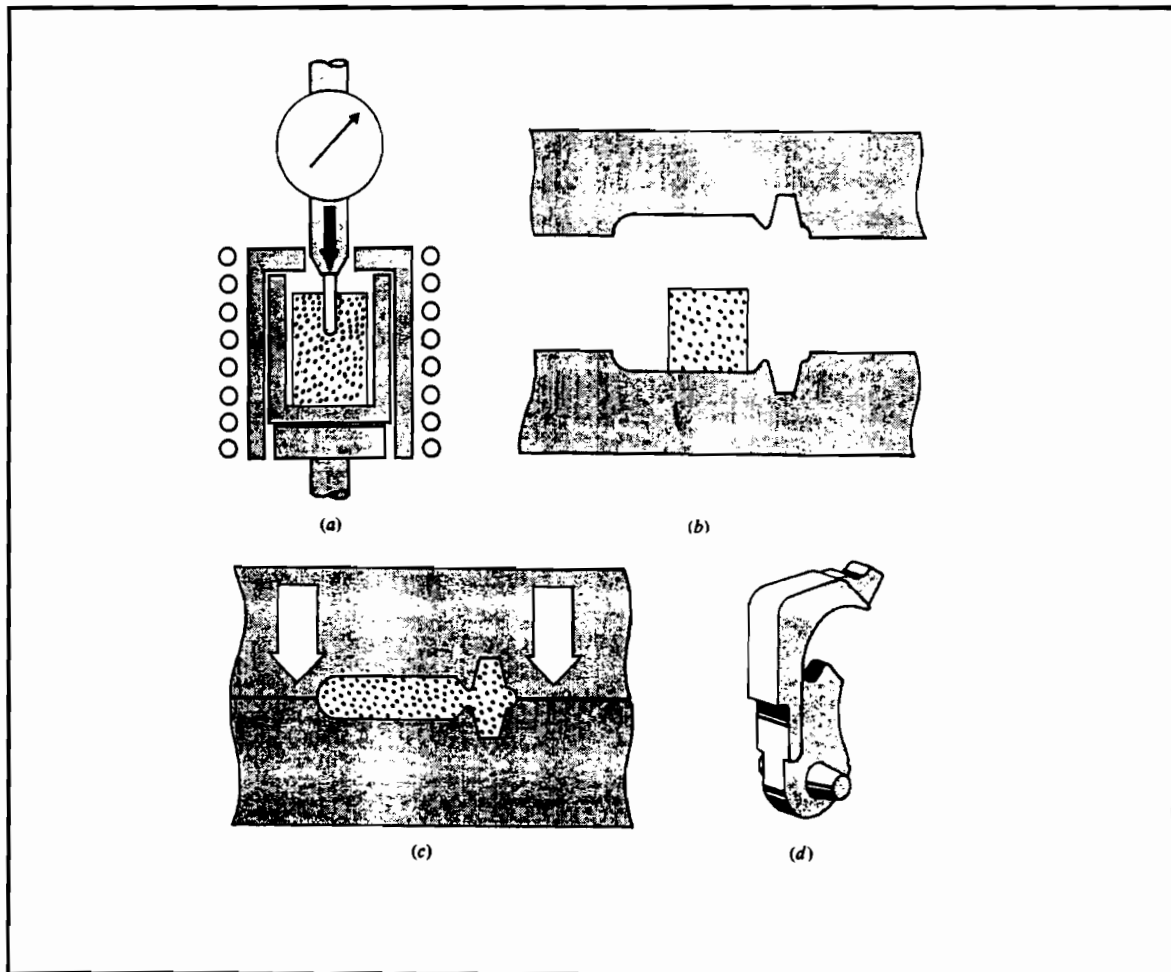
Figure 3.5: Schematic of steps in SSF process: billets are: a) reheated until they reach the required SS state, b) placed into the die and c) forged with small loads, d) final product having equal or even better mechanical properties than the conventionally forged parts [Flemings, 1991].
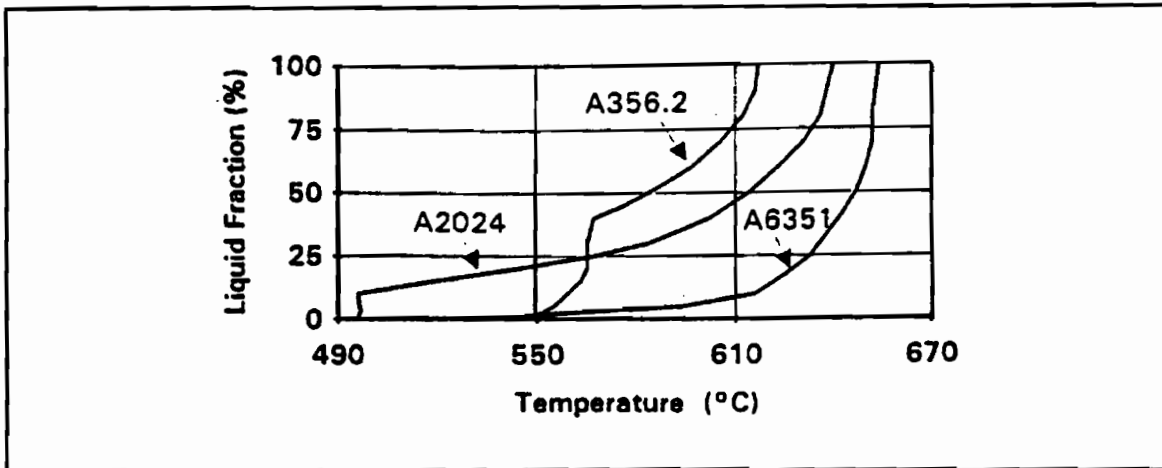
Figure 3.6: Liquid fraction as a function of temperature for different alloys [Hirt, 1994].
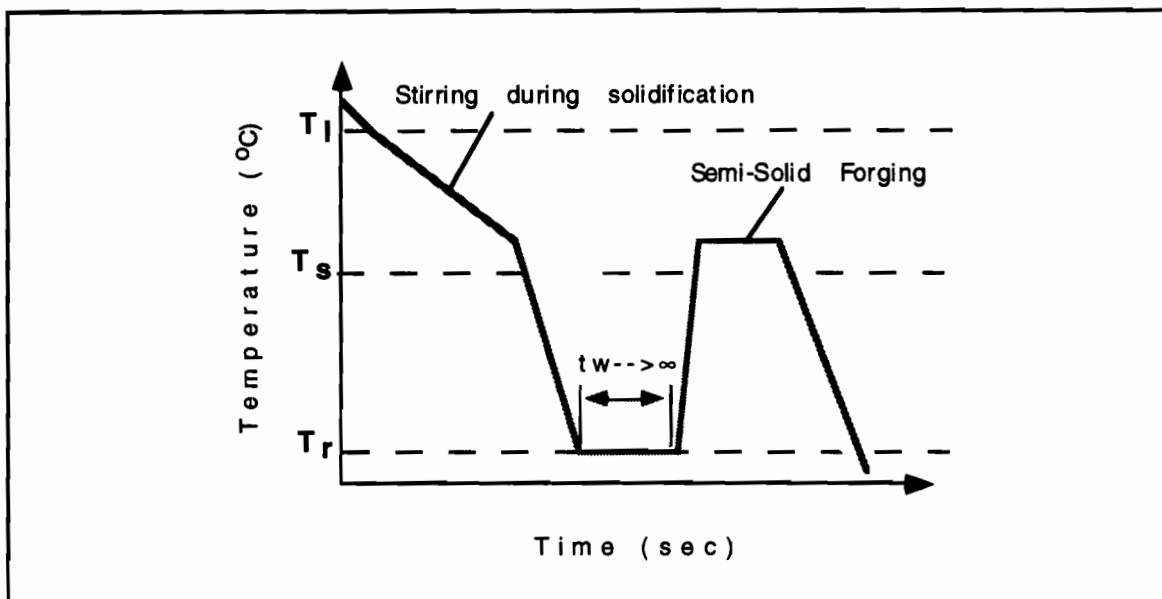
Figure 3.7: Temperature vs. time diagram of thixoforging process: alloys are stirred between solidus and liquidus temperatures (e.g. T_l and T_S), cooled to room temperature, T_r. When required, they are reheated to the SS temperature range and forged [After EFU brochures].

Finally, after the desired solid fraction is reached the billet is transferred to the forging press and forged. Figure 3.7 shows temperature vs. time diagram during SSF process.

The thixotropic nature of the semi-solid metal allows the slug to flow into the die cavity uniformly at very low pressures. Only at the end of the forming stroke the pressure increases to the selected level to form the fully dense component. For sound parts, a dwell time under a predefined pressure is required, too. The mold pressure is from a few hundred pounds per square inch to 140 MPa depending on the geometry and size of the components to be produced [Young, et al., 1988].

If the solid fraction of the billet is between 0.35 and 0.85, and if the die speed is rather low, then the liquid component tends to flow separately from the solid component. In many cases, the liquid component moves to the surface layers, and it sometimes flows out of the billet at initial stages of deformation, as shown schematically in Figure 3.8. As the billets fills up the die cavity, the liquid component that penetrated out is cooled by the dies, solidifies and becomes the outer layer of product. The internal structure of the product obtained in this way is heterogeneous. The inner portion mainly consists of the initial solid grains and the outer portion is mainly made up of the solidified liquid phase. However, this heterogeneous structure of the products can be improved and modified by an appropriate heat treatment method, such as T5 and T6 temper [Kenney, et al., 1988].

In order to prevent separation of liquid and solid phases, high speed forging is preferable. It is assumed that flow speed of solid particles is increased at the same rate as that of the liquid in the high speed forging, Figures 3.8 and 3.9. Additional information on the optimum forging conditions for SSM Al-Alloys are available [Kapranos, et al., 1994] [Yoshida, et al., 1992] [Hirt, et al., 1994].
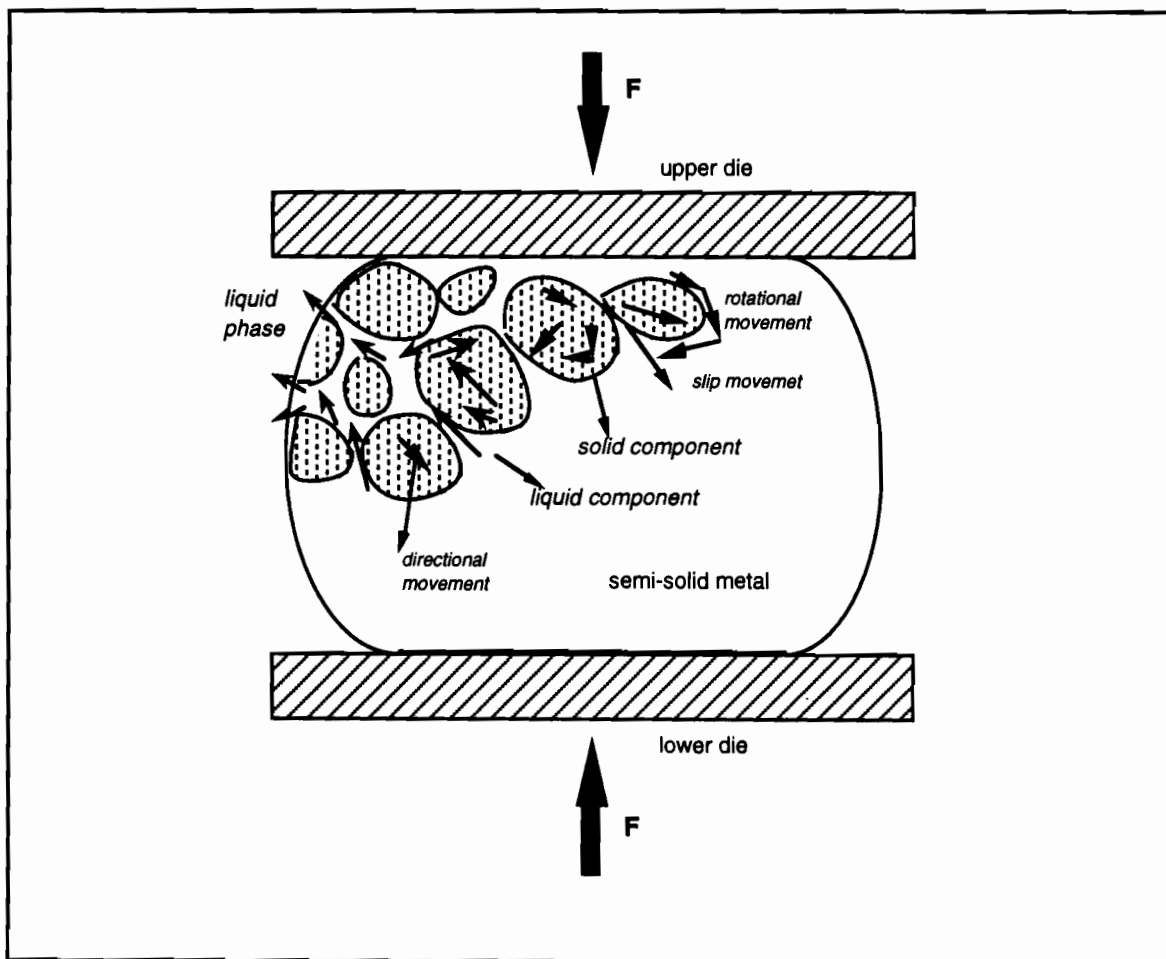
Figure 3.8: Schematic of flow deformation of a semi-solid metal during SSF [After Kiuchi, 1993].

upper die

liquid | solid

liquid

solid

liquid

solid

lower die

a) semi-solid metal standing free in die

b) semi-solid forging

c) finished part
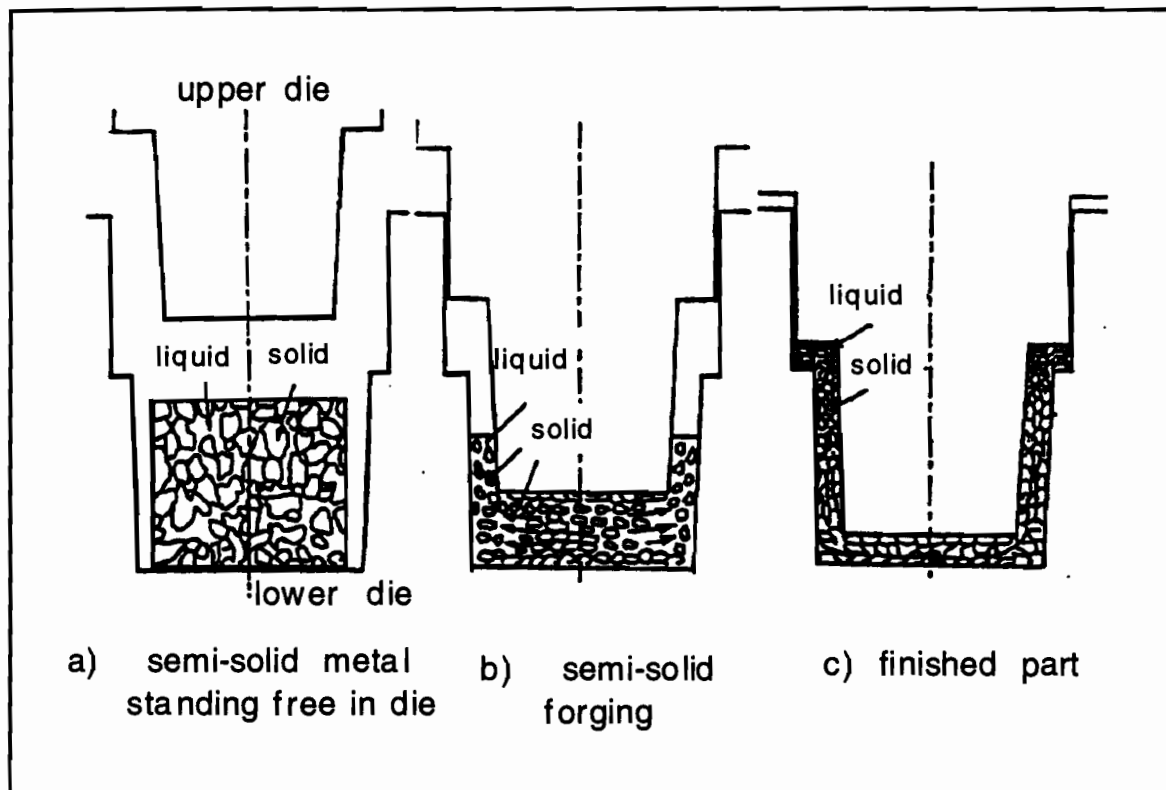
Figure 3.9: Behavior of solid and liquid phases during SSF [Yoshida, et al., 1992].

3.5 Structure and Mechanical Properties of Semi-Solid Forged Parts:

Metallographic examination of the parts produced by SSF shows no porosity or insignificant oxide entrapment, Figure 3.10. In addition, a very fine microstructure, very small grain sizes (5-10 μm for aluminum alloys) and good mechanical properties obtained [Hirt, et al., 1994].
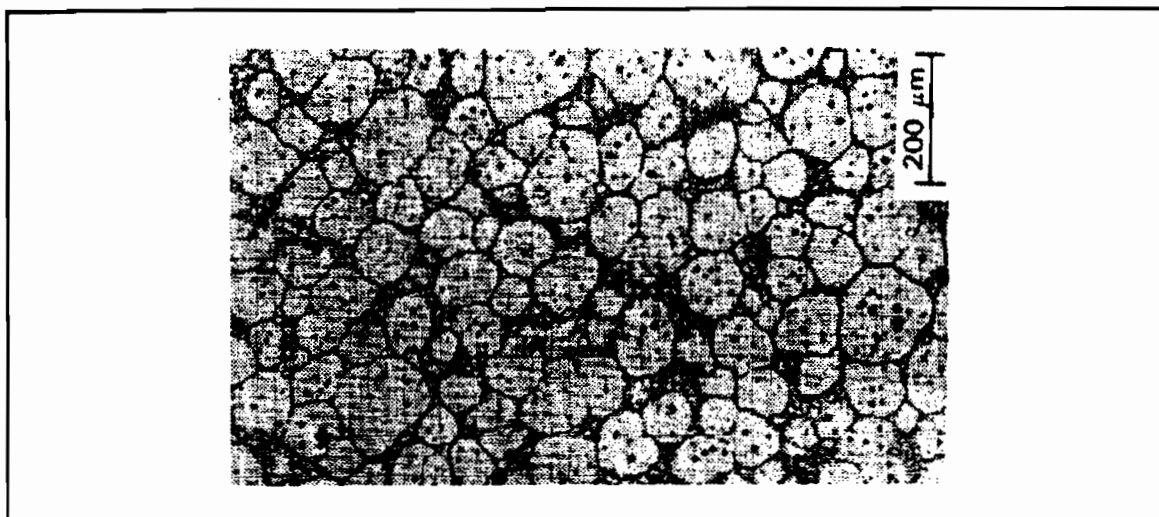
Figure 3.10: Microstructure of thixoforged alloy 2024 [Hirt, 1994].

Table 3.3: Mechanical properties SSF aluminum parts [Kenney, et al., 1988].

Al-Alloy	Temper	UTS MPa	Yield S. MPa	Elongation %	Hardness HB
206	T7	386	317	5.0	103
2017	T4	386	276	8.8	89
2219	T8	352	310	5.0	89
6061	T6	330	290	8.2	104
6262	T6	365	330	10.0	82
7075	T6	496	421	7.0	135
356	T5	234	172	11.0	89
356	T6	296	193	12.0	90
357	T5	296	207	11.0	90
357	T6	358	290	10.0	90

Mechanical properties of thixoforged aluminum alloys are shown in Table 3.3 [Kenney, et al., 1988]. It is seen that, the properties of SSF parts are almost the same with the conventionally forged parts.

3.6 Detection of Solid Fraction

During reheating of the semi-solid metals, it is very important to know the degree of the slug softness, especially in Thixoforming. The following methods are used for determination of the fraction solid:

- Pulsed high power lasers can be used to generate broad band ultrasound and laser interferometers can also be used as detectors. Interferometric detectors generally require a good surface finish although rough surface interferometers are now being developed [Edwards, et al., 1992].

- Whetstone bridge set up was used to measure fraction solid of the semi-solid materials during reheating by Kiuchi [Kiuchi, et al., 1991]. Any change in the resistance of the reheated semi-solid specimen results in a voltage difference affecting the equilibrium of the circuit. This can be monitored on a digital or an analog display.

3.7 Semi-Solid Forging Applications

Applications of SSF technology are usually in the production of aluminum automotive components, and automotive industry seems to be the largest market for SSF aluminum parts. It is indicated that the average U.S. automobile uses about 180 pound of SSF aluminum parts today [Courtois, et al., 1994].

Although cost of the raw material used in SSF is higher than the conventional processes, it becomes cost-effective on the total part cost basis for many applications. SSF process results in near-net or net shape parts reducing scrap rate, further machining time, cost and labor. In addition, it lowers the weight to strength ratio and eliminates the impregnation. Since the production rate is higher than the conventional forging, SSF becomes feasible and competitive in terms of cost. Additional information on specific SSF appilications are available [Koç, et al., 1994] [Kenney, et al. 1988] [Hirt, et al., 1995] [EFU brochures, 1994].

Chapter IV

FE SIMULATIONS FOR THE SEMI-SOLID FORGING OF A356 ALUMINUM ALLOY

One of the major factors affecting the results of FE simulations of semi-solid forging is the flow stress behavior. Since the flow stress of semi-solid alloys depends on the temperature, flow stress curves for semi-solid alloys need to be determined with reasonable accuracy to obtain accurate simulation results.

Flow Stress of semi-solid alloys can be defined as a function of temperature in the form of

$$\sigma = f(T, \dot{\varepsilon}) \tag{1}$$

$$\sigma = C(T)\dot{\varepsilon}^{m(T)} \tag{2}$$

where   T = Temperature ($^\circ$C)

                 C= Strength coefficient (MPa)

                 m= Strain-rate-sensitivity exponent

                 σ= Flow Stress (MPa)

                 $\dot{\varepsilon}$ = strain Rate

A second way to express the flow stress of semi-solid alloys is as follows: Throughout a large range of shear rate (10^{-3} sec^{-1} $<\dot{\gamma}_{w}<$ 10^{3} sec^{-1}) the rheological behavior of the semi-solid alloys can be expressed by pseudoplastic type of behavior as [Levaillant, C., 1993] [Loué, R., et al., 1993]:

$$\eta = k\dot{\gamma}^{m-1} \tag{3}$$

$$\tau = k\dot{\gamma}^{m} \tag{4}$$

$$\overline{\sigma} = k' \dot{\overline{\varepsilon}}^{m} \tag{5}$$

If the Von Misses effective stress and strain rate are assumed for a state of pure shear, the relation between k and k' can be found as [Hosford, W., et al., 1993]

$$k' = k\sqrt{3}^{m+1} \tag{6}$$

because

$$\overline{\sigma} = \sqrt{3}\tau \tag{7}$$

$$\dot{\overline{\varepsilon}} = \dot{\gamma} / \sqrt{3} \tag{8}$$

Then, the flow stress of semi-solid alloys can be described as below by substituting equations (6), (7) and (8) into (5):

$$\overline{\sigma} = \sqrt{3}^{m+1} k \dot{\overline{\varepsilon}}^m \tag{9}$$

where k is a constant and is defined as:

$$k = k_\circ \exp(mQ/RT) \tag{10}$$

k, k', k_0 :	strength coefficient (MPa)
m :	strain-rate-sensitivity exponent
τ :	shear stress
$\overline{\sigma}$:	effective stress
$\dot{\gamma}$:	shear rate
$\dot{\overline{\varepsilon}}$:	strain rate
$\dot{\eta}$:	viscosity of semi-solid alloys
Q :	activation energy of the alloy
R :	universal gas constant
T :	temperature (K)

The available flow stress data for semi-solid alloys is limited either to some specific alloys, i.e. Aluminum MMC [Witulski, et al., 1994], or to some specific experimental parameters, i.e., low strain and strain rates [Loué, et al., 1993]. In this research, however, A356 (AlSi7Mg) aluminum alloy was used. The average strain rates obtained during the preliminary simulations were higher than the values available in the literature. In order to perform reliable FE simulations, extrapolation of these flow stress values had to be done. Using the information for semi-solid alloys given by Loué and Witulski, and the information for solid AlSiMg alloys given in the Atlas of Hot Working Properties of Non-Ferrous Metals [German Society of Materials Science], first, the flow stress values for the strain rates under 0.1 sec^{-1} were linearly extrapolated to the flow stress values at strain rates up to 100 sec^{-1}. Second, for the temperatures lower than 580 ^{o}C, linear extrapolation was performed. Figures 4.1, 4.2 and 4.3 show the approximate flow stress curves at temperatures 565 ^{o}C, 575 ^{o}C and 580 ^{o}C.

Equations (3) through (10) could be used to obtain flow stress of A356 alloys, but available experimental data was not sufficient to construct the flow stress curves. Therefore, the approximation of flow stress curves was preferred.

In FE simulations of the metal flow in the semi-solid forging, DEFORM 2-D was used. The geometry of the final part is a disk of 201 mm in diameter. The die and initial billet configuration is presented in Figure 4.4.

Axisymmetric conditions were assumed in all simulations.

The DEFORM FE simulations were performed on an IBM Risk 6000. In order to obtain complete cavity filling and to check for the presence of defects in the closed-die forging operation, isothermal and non-isothermal metal flow simulations for two different disk shaped geometries were run (see Figure 4.5). The deformation behavior as a function of temperature was investigated in the non-isothermal simulations. Flow stress values for A356 alloy at 580 °C were used in the isothermal simulations. For each type of disk geometry, two different thickness values were simulated. The thickness values were 3.6 mm and 7 mm. The geometry of the final part for disk 1 and disk 2 are shown in Figure 4.4. Figure 4.6 and Figure 4.7 show the FE models used, for disk 1 and disk 2 respectively.

The disks were forged at an initial billet temperature of 580 °C, which is between the solidus and liquidus temperatures of A 356 (AlSi7Mg) alloy system. The dies were modeled as rigid bodies, but they were discretized to perform a heat transfer analysis in non-isothermal simulations. The initial temperature of the die was 250 °C in these cases. A constant shear friction factor (m=0.2) was assumed to represent the friction condition between the aluminum workpiece and the steel dies in a hot working condition [Altan, et al., 1983]. Since the heat transfer capacity of DIN 1.2312 tool steel, which was used in the experiments in EFU, Germany, was not found in the literature, the heat capacity values for H13 were used instead.
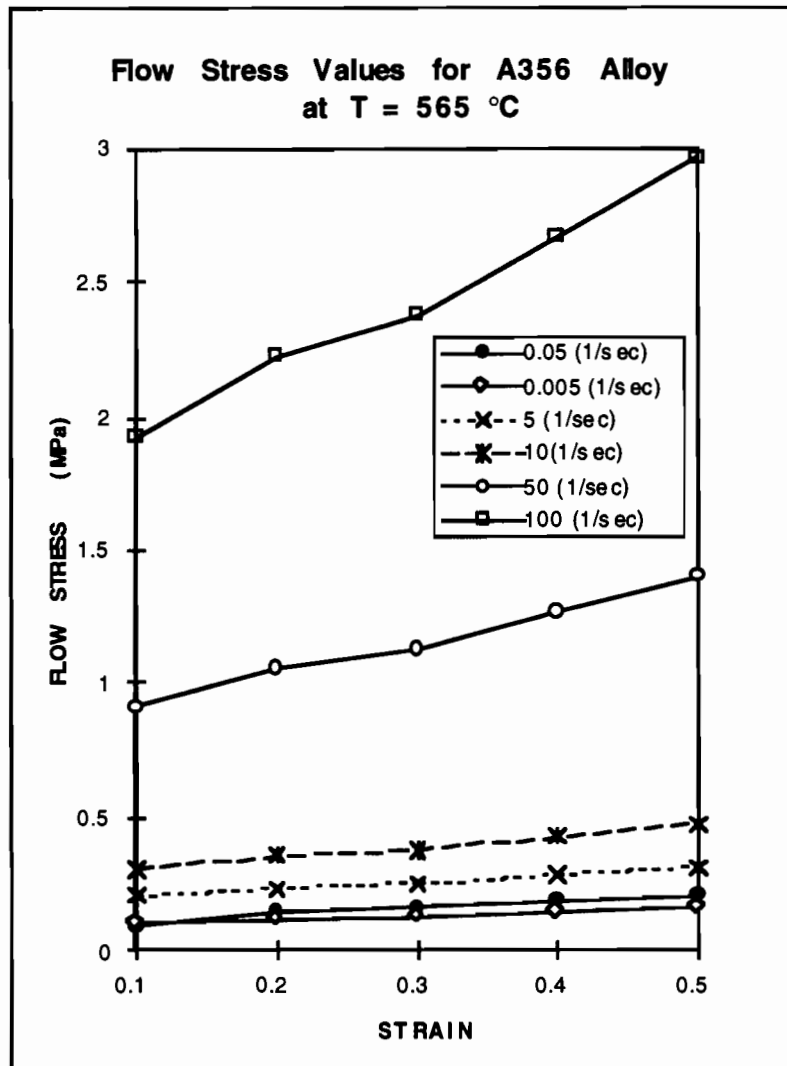
Figure 4.1:   Approximated flow stress curves for A356 alloy at T=565 °C at different strain rates as a function of strain (extrapolated from [Witulski, et al. 1994], [Loué, et al., 1993] and [Atlas of Hot Working Properties of Non-Ferrous Metals, German Society of Materials Science])
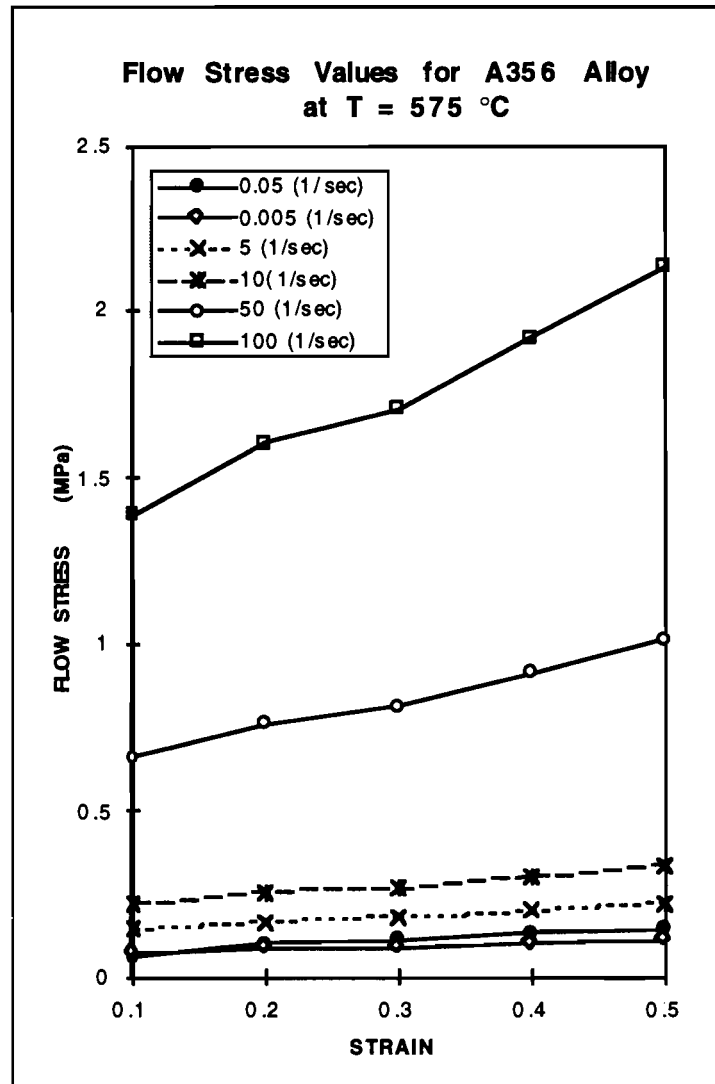
Figure 4.2: Approximated flow stress curves for A356 alloy at T=575 °C at

different strain rates as a function of strain (extrapolated from [Witulski, et al.

1994], [Loué, et al., 1993] and [Atlas of Hot Working Properties of Non-Ferrous

Metals, German Society of Materials Science])
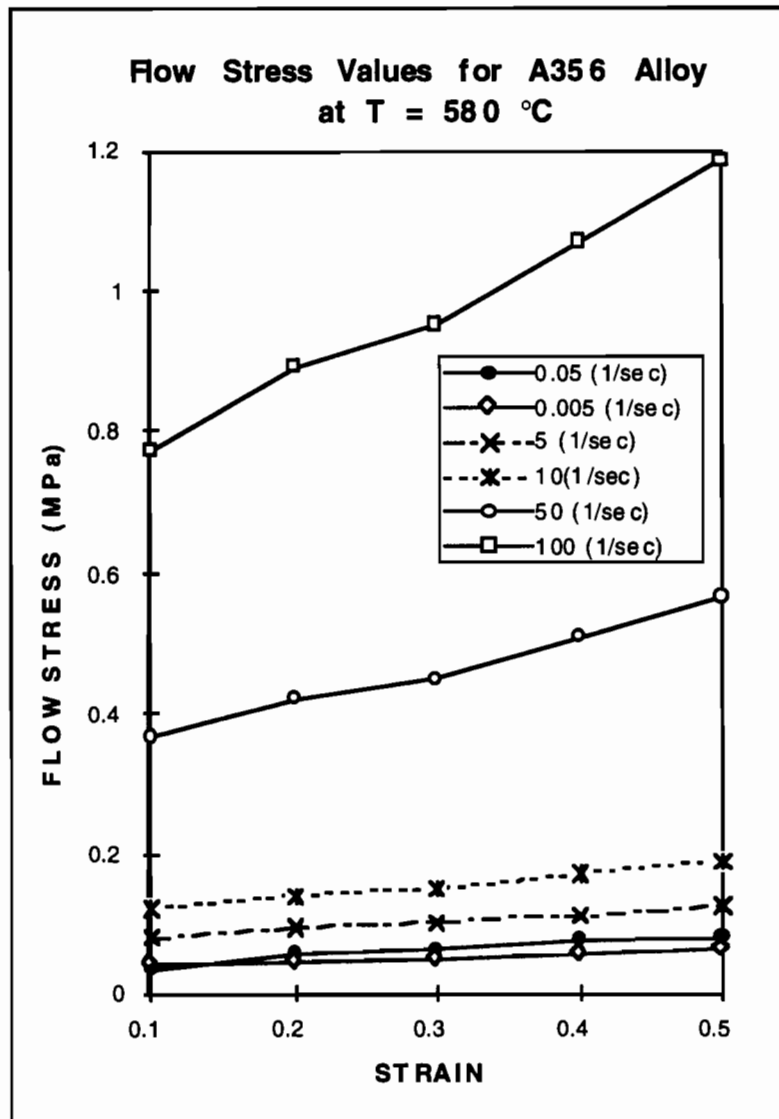
Figure 4.3: Approximated flow stress curves for A356 alloy at T=580 ºC at different strain rates as a function of strain (extrapolated from [Witulski, et al. 1994], [Loué, et al., 1993] and [Atlas of Hot Working Properties of Non-Ferrous Metals, German Society of Materials Science])
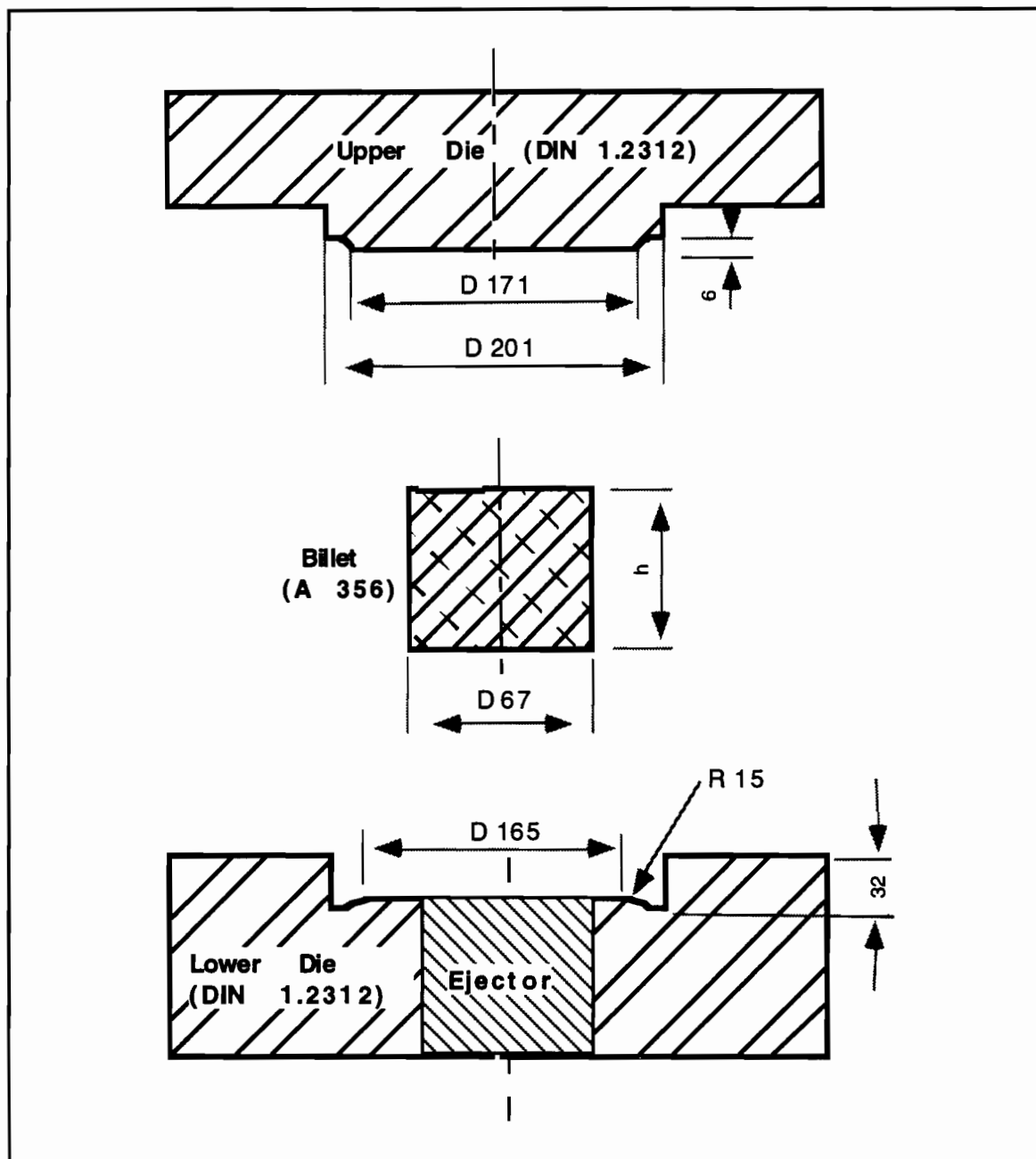
Figure 4.4: Die and initial billet configuration (provided by EFU), dimensions in mm
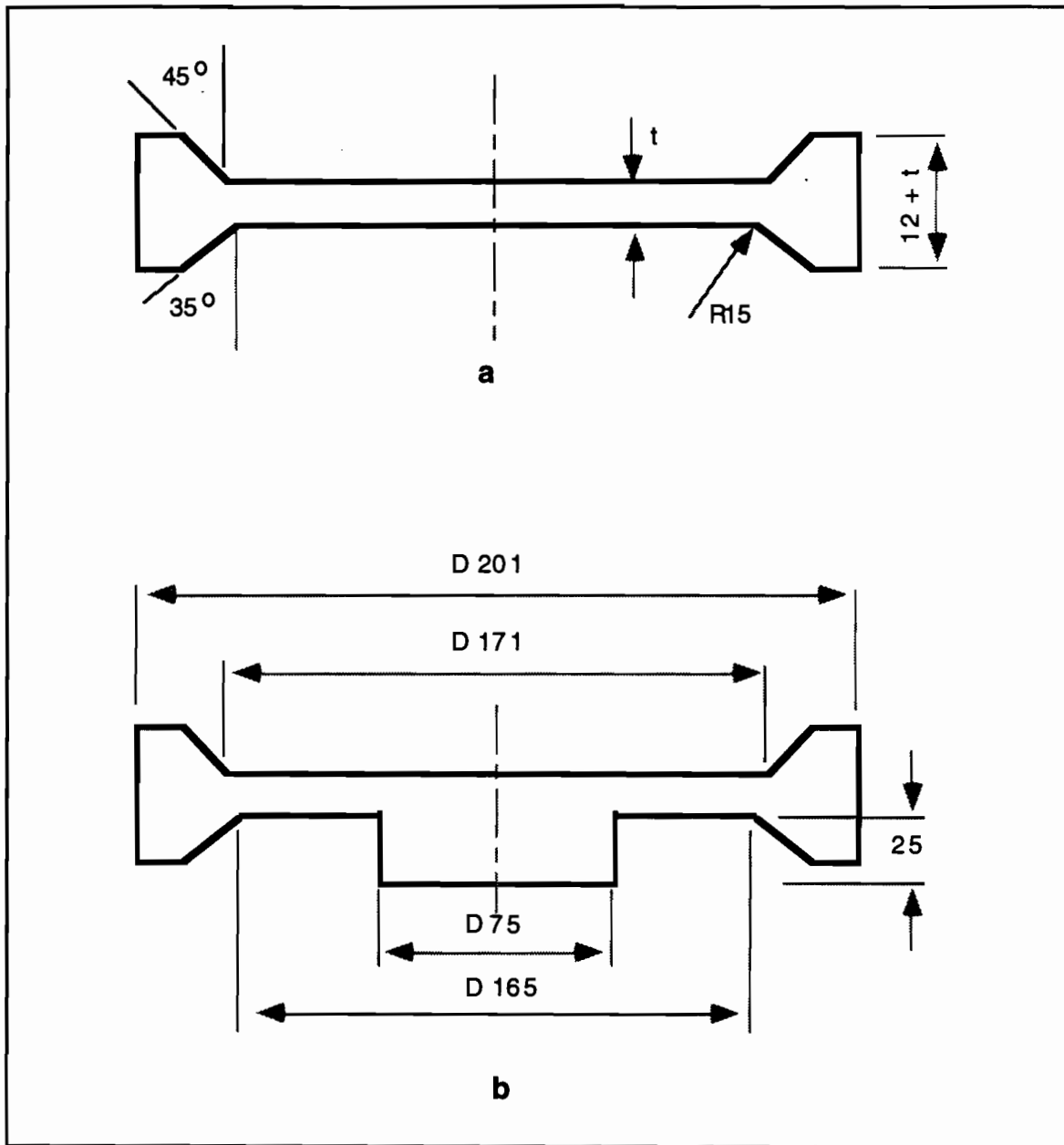
Figure 4.5: Final configuration of the disk shaped part, a) Disk 1, b) Disk 2, dimensions in mm
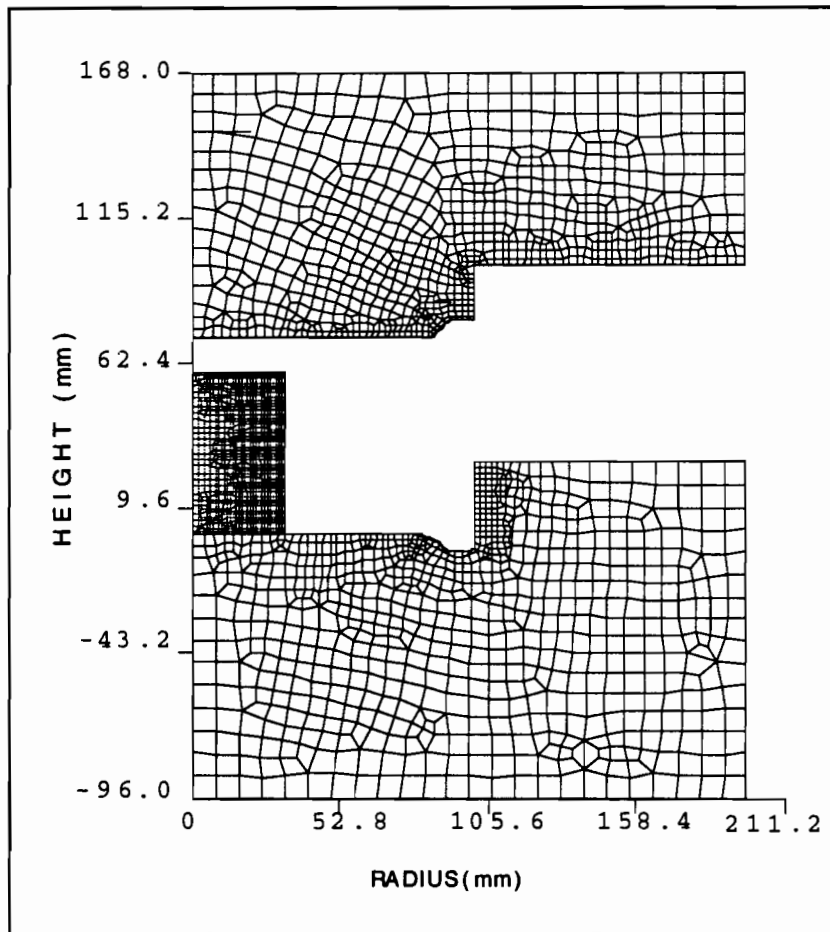
Figure 4.6: FE model for Disk 1 case with a 3.6 mm final web thickness
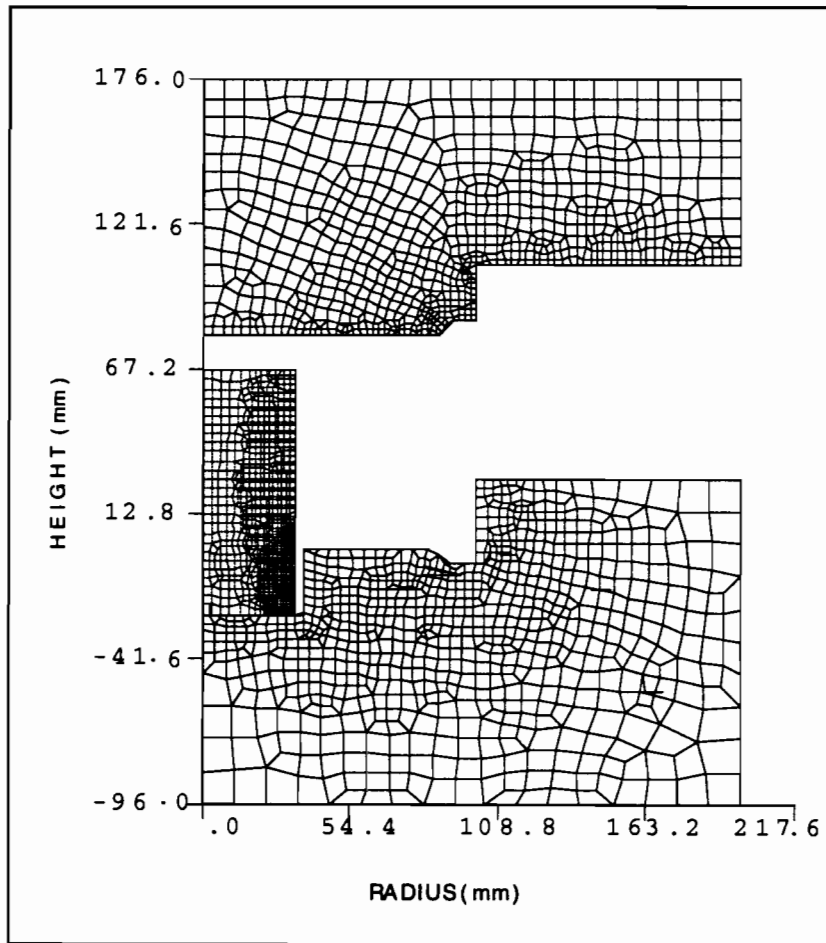
Figure 4.7: FE model for Disk 2 case with a 3.6 mm final web thickness

4.1 Welding of Folding Defects in Semi-Solid Forging of Aluminum Alloys

In Semi-Solid Forging (SSF), the workpiece is at a temperature range between solidus and liquidus. Any laps or flow defects that may form during forging usually weld together during deformation. More information about welding during forming of Aluminum alloys is given by Laue [Laue, K., 1981]. "During hot hollow extrusion of aluminum, welding is used for production of complicated parts. The internal shape of the tube or hollow section is formed by a short mandrel supported on two or more arms by the die and its support tooling. The metal is divided by the arms into several strands of large cross section and, as deformation continues, these enter the inlets, flow around the arms and are rewelded in the welding chamber to form the section". The purpose of the welding chamber is to supply heat to the metal in that region so that it reaches the welding temperature, i.e. usually the temperature range is above 500 $^{\circ}$C for aluminum and Al alloys. Figure 4.8 shows the construction of dies for the welding chamber process used for aluminum. It is also indicated by Laue that AlSiMg alloys have good welding properties.

Therefore, due to the temperature at which SSF is performed, any fold that forms is expected to reweld. However, if the compaction of the forging, i.e. the deformation during process, is not enough there may be some remaining pores or holes at the welding zone.
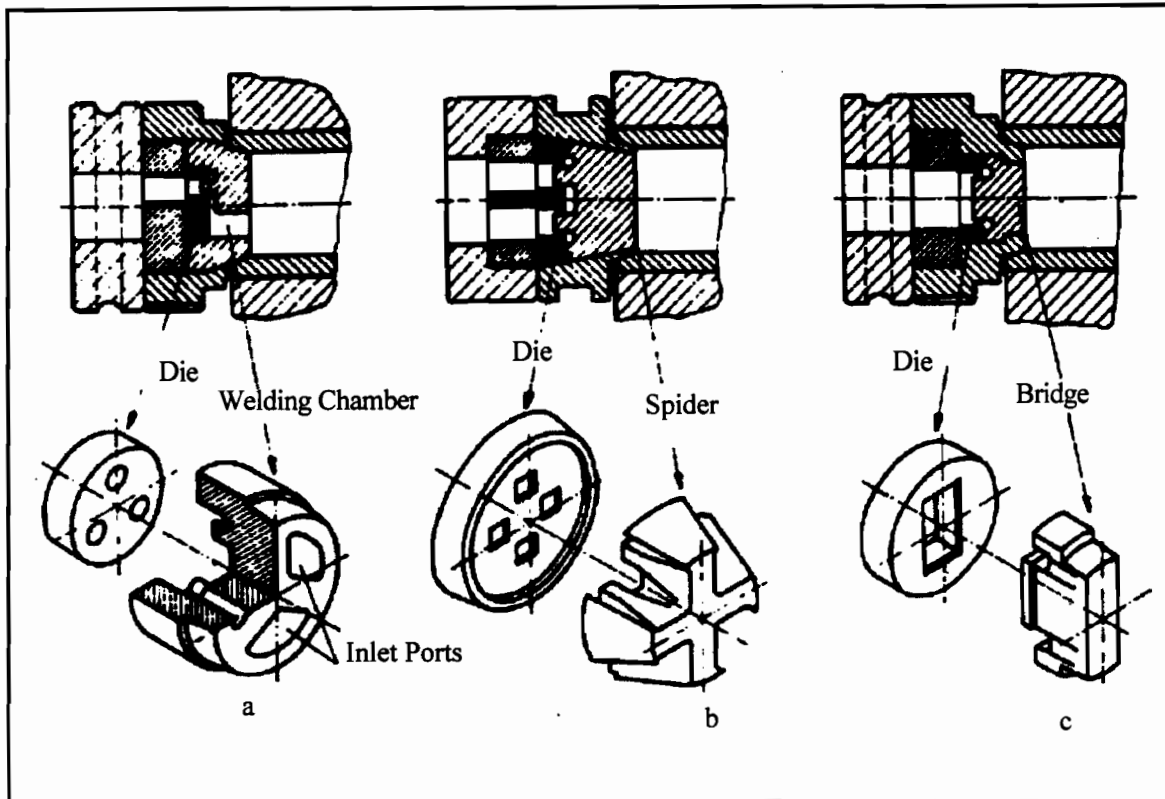
Figure 4.8: Construction of extrusion dies for the welding chamber process used for aluminum, a) multihole porthole die, b) multihole spider die, c) bridge die [Laue, K., et al., 1981].

4.2 Finite Element Analysis in SSF

For the simulation of semi-solid deformation processes, the FE code must be able to predict accurately the final shape of the billet. This requirement was satisfied by the code DEFORM. In addition, DEFORM code is able to create interaction conditions not only between objects (i.e. die and forging) but also within an object (i.e. billet). This provides us with a model to simulate the rewelding of the folds during forging.

FE code DEFORM

DEFORM (Design Environment for FORMing) was developed at the Battelle Columbus Laboratories using the background of the code ALPID, also developed at Battelle with Air Force funding. The code is now supported by Scientific Forming Technologies Corporation, and has been commercially available since 1989. It is a two- and three-dimensional FEM code with the capability of simulating a large class of forming processes including: rigid, plastic, porous and elastic materials, viscoplastic behavior, and plastic analysis under isothermal or non-isothermal conditions.

FEM simulations of forming operations require remeshing when a considerable amount of plastic deformation occurs. In conventional remeshing procedures, the user regenerates a mesh and continues the simulation, which is usually time consuming. The DEFORM system, by

means of the AMG (Automatic Mesh Generation), achieves the following tasks without user intervention :

- determine the need for remeshing,
- determine the optimum mesh density based on the geometric shape and prior solution behavior,
- construct the mesh based on the optimum mesh density,
- transfer information from the old mesh to the new mesh,
- continue the simulation to the next remeshing step or to the end.

The automatic meshing and remeshing procedure increases simulation productivity considerably by eliminating the time consuming conventional mesh generation. DEFORM has the capability to determine the mesh density and provides a better mesh system than the one generated by an experienced user. The pre-processing phase is realized with a menu driven program module that assists the user in entering all necessary simulation data. The input data is stored in the KEYWORD file.

The post processor is used to display results of the simulation in graphical or alphanumerical form. The available graphic representations include FEM mesh, contour plots of strain, strain rate, temperature and damage factor, the velocity vectors and the load-stroke curves.

4.3 Input Data

Semi-Solid A356 (Al Si7 Mg or DIN 3.2315) aluminum alloy system was used in experiments conducted at EFU in Germany. Thus, the same material was used in the simulations. The liquidus temperature of this alloy is 615°C, solidus temperature is 555°C [ASM Specialty Handbook]. Thermal conductivity and heat capacity of the billet material are presented in Figure 4.9 and Figure 4.10, respectively. The tables A.1 and A.2 in Appendix A display the values used to construct these figures .

4.3.1 Dies

DIN 1.2312 tool steel was used in the experiments at EFU, Germany. The only information provided about die material was its thermal conductivity. Therefore, the heat capacity of H13 tool steel was used, assuming that H13's thermal properties are close to that of DIN 1.2314. 40 Cr Mn Mo S 1 6 is equivalent of DIN 1.2312 [EFU, 1994]. The composition of DIN 1.2312 is given in Table 4.4. Since the heat capacity of H13 is assumed, its composition is presented in Table 4.4.

Table 4.1: Composition of DIN 1.2312 tool steel [Stahlschluessel]

	C	Si	Mn	P	S	Cr	Mo
%	0.35-0.40	0.30-0.50	1.4-1.6	≤0.03	≤0.05-0.10	1.8-1.0	0.15-0.25

Table 4.2:   Composition of H13 tool steel [Handbook of Comparative World
Steel Standards, 1990]

	C	Si	Mn	P	S	Cr	Mo	Ni	V
%	0.32-0.45	0.8-1.2	0.2-0.5	0.03	0.03	4.75-5.5	1.1-1.25	0.3	0.8-1.2
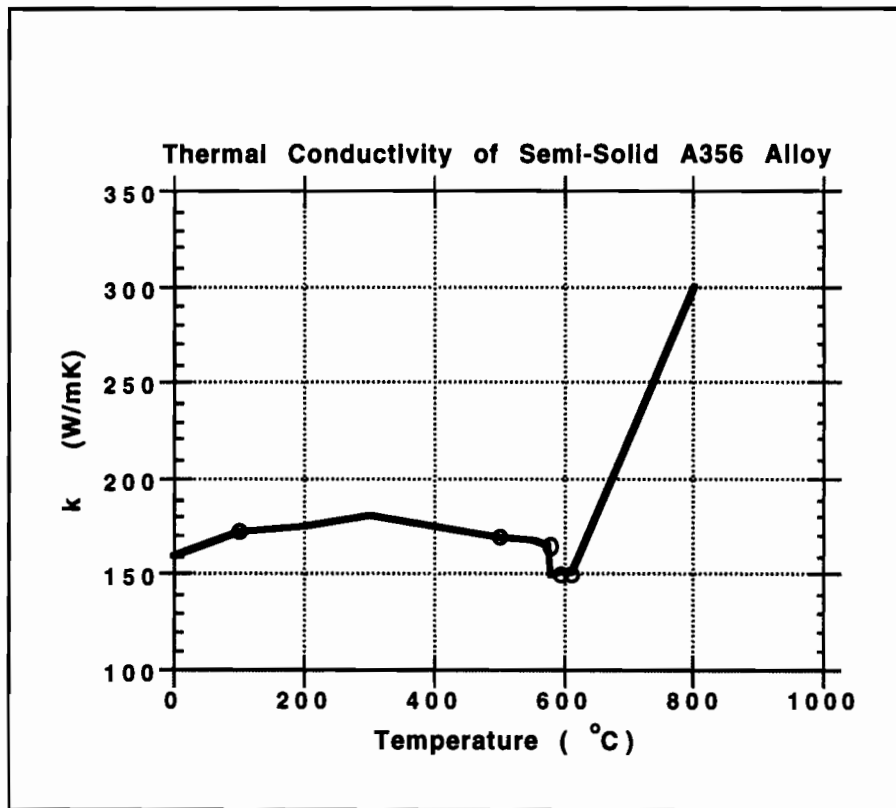
Figure 4.9:   Thermal conductivity of A356 semi-solid alloy vs. temperature
[EFU, 1994].
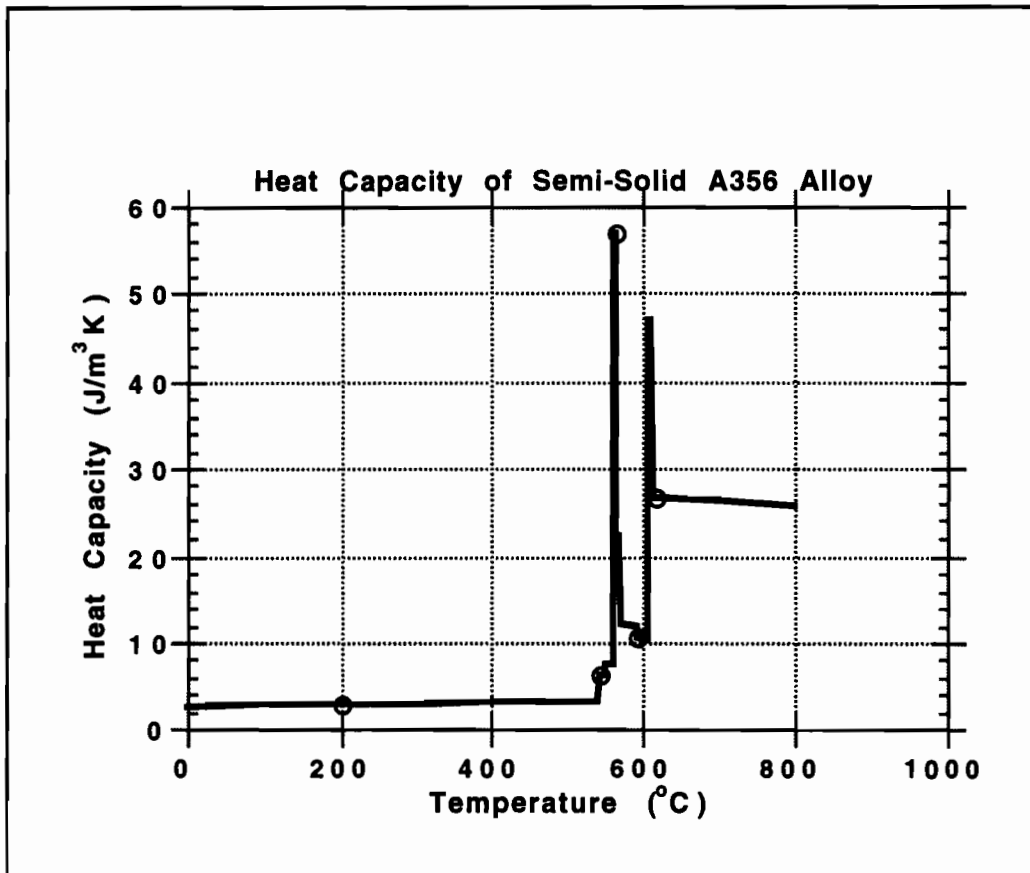
Figure 4.10: Heat capacity (specific heat X density) of A356 semi-solid alloy (including latent heat) [EFU, 1994].
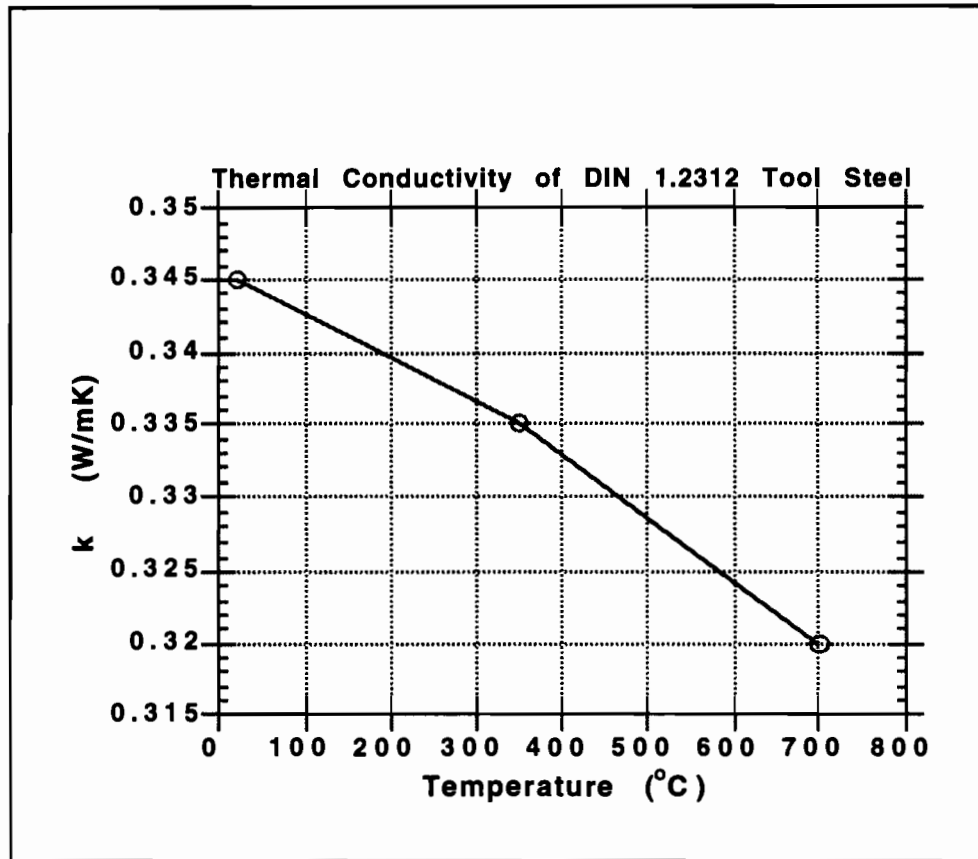
Figure 4.11: Thermal conductivity of DIN 1.2312 tool steel [EFU, 1994]
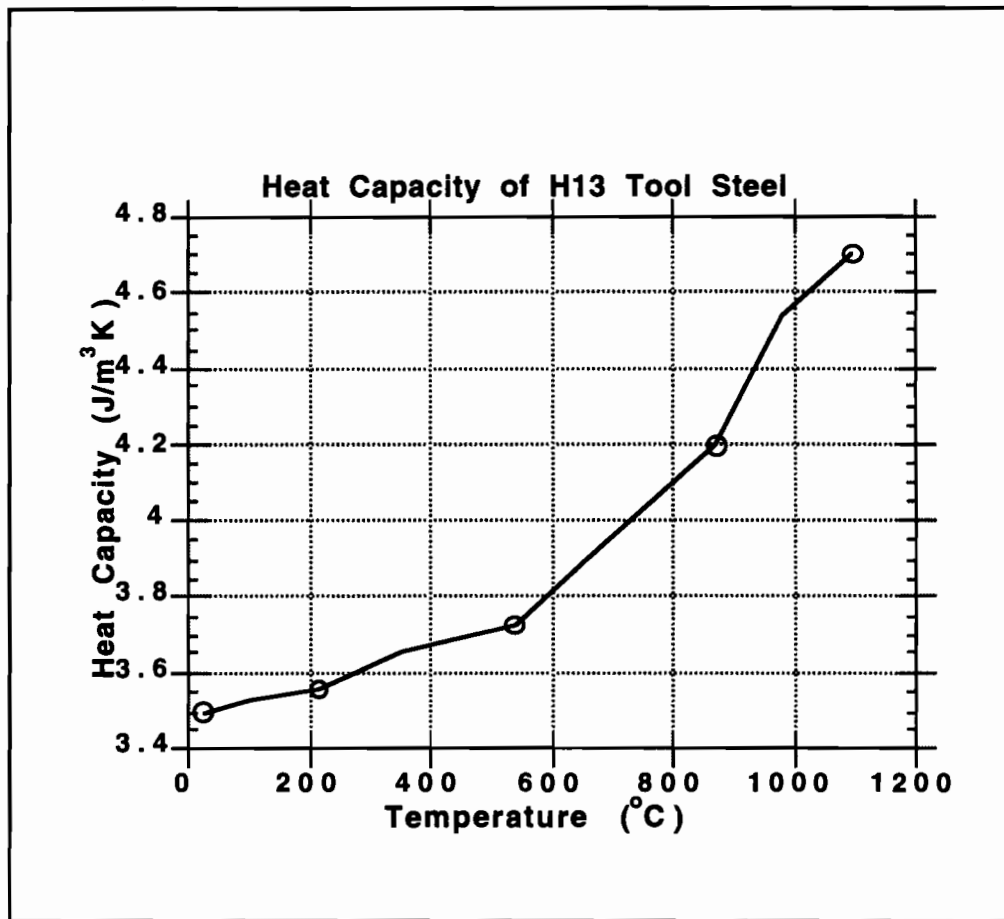
Figure 4.12: Heat capacity (specific heat X density) of H13 tool steel [Burte, P., 1989] [Im, Y.T., 1989]

4.3.2 Process and Initial Conditions

Table 4.3 shows the input values that were used for the FE simulations.

Table 4.3:   Process and initial conditions of the simulations [EFU, 1995] [ASM Handbook] [Burte, P., et al., 1989] [ASM Specialty Handbook-Aluminum and Al alloys].

Input	Value	Units
Initial Billet Temperature	580	^oC
Initial Die Temperature	250	^oC
Punch Velocity, constant	200	m/sec
Stroke	55.4 to 83.5	mm
Billet Diameter	67	mm
Billet Height	59.5 to 123	mm
Emissivity of A356	0.1	
Emissivity of H13	0.6	
Heat Convection Coefficient	35	kW/m^2K
Heat Transfer Coefficient	0.007	kW/m^2K
Constant Shear Friction Factor, m	0.2	
Press type used	Hydraulic	

4.4 Simulation Results

A total of eight simulations were performed. Four simulations were run for each type of disk. Isothermal and non-isothermal conditions were applied for each disk type. Figures 4.6 and 4.7 illustrate the FE models used.

During the experiments with Disk 1 the ejector was closed completely, and the reheated billet was placed on the lower die. Since the billet has a small volume, the heat losses into the die and the environment before the operation started were too high. To prevent this, during the experiments with Disk 2, the billet was placed on the ejector while it was below the lower die level. Just before the forming started, the piston was brought up to 25 mm below its upper position. Then the upper die was moved down, as shown in Figure 4.4.

Table 4.4: Initial height (h_o), stroke (S) and final disk thicknesses used in FE simulations

Geometry		Disk 1		Disk 2	
Final Thickness (mm)		3.6	7	3.6	7
	h_o (mm)	59	90.5	91.6	123
Non-isothermal	S (mm)	55.4	83.5	63	91
	h_o (mm)	59	90.5	91.6	123
Isothermal	S (mm)	55.4	83.5	63	91

In each case, either a final thickness of 3.6 mm or 7 mm was aimed for. For each thickness case, initial volume of the billet was calculated. Since the diameter of the billet was kept as 67 mm for all cases, the billet height was adjusted for each case. Table 4.4 illustrates these cases briefly.

4.4.1 Isothermal Simulations

As a preliminary study, isothermal simulations were performed with the aim of determining relevant characteristics of the material flow during SSF. Temperature is assumed to be constant at 580°C during an isothermal forming process. Four isothermal simulations with different final thickness and geometry were performed to investigate the effect of flow stress and geometry on the load and the deformation behavior.

Table 4.5: Isothermal simulation conditions and resulting loads.

	Disk 1		Disk 2	
Final Web Thickness (mm)	3.6	7	3.6	7
Calculated load at 99.5% stroke (kN/Klb)	340/49.3	130/18.9	300/43.5	130/18.9

In the preliminary isothermal simulations, a volume loss of 2-4 % was detected due to the remeshing steps needed to simulate the SSF process. After this volume was added to the initial billets, complete filling of the cavity was obtained. Only for Disk 1 case with a final thickness of 3.6 mm, 1.8 % underfilling was encountered (Figure 4.13).

Figure 4.13 illustrates that the isothermal deformation of semi-solid A356 alloy is similar to hot deformation of conventional aluminum alloys under similar conditions.

In the semi-solid temperature range, solid particles are suspended in a liquid matrix. During the deformation of the semi-solid materials, there is no grain deformation. The main plastic deformation mechanism is the movement of grains along the liquid grain boundaries. The movement may be rotational, directional or both. Slip between grains also contributes to deformation [Kiuchi, et al., 1993] [Avitzur, B., 1984]. Therefore, during the semi-solid forging, there will be no strain accumulation [Hirt, 1995]. Table 4.5 and Figures 4.14, 4.15, 4.16 and 4.17 present the loads obtained at the end of isothermal simulations. Complete filling of the die cavity was obtained at lower loads than the loads obtained at the end of the stroke. The load required to deform the semi-solid alloy developed at very end of the stroke. Until, approximately, 99 % of the stroke is reached, the load values stays at low values, i.e. less than 500 kN.
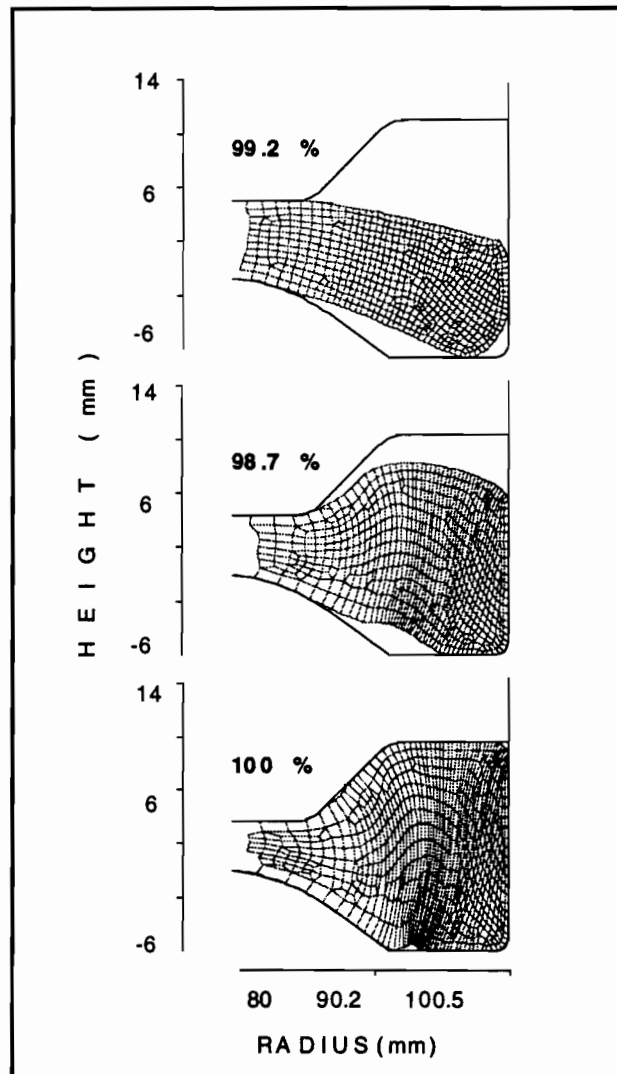
Figure 4.13: Deformation sequence of semi-solid billet for Disk 1 case under isothermal conditions with a final web thickness of 3.6 mm (dimensions in mm)
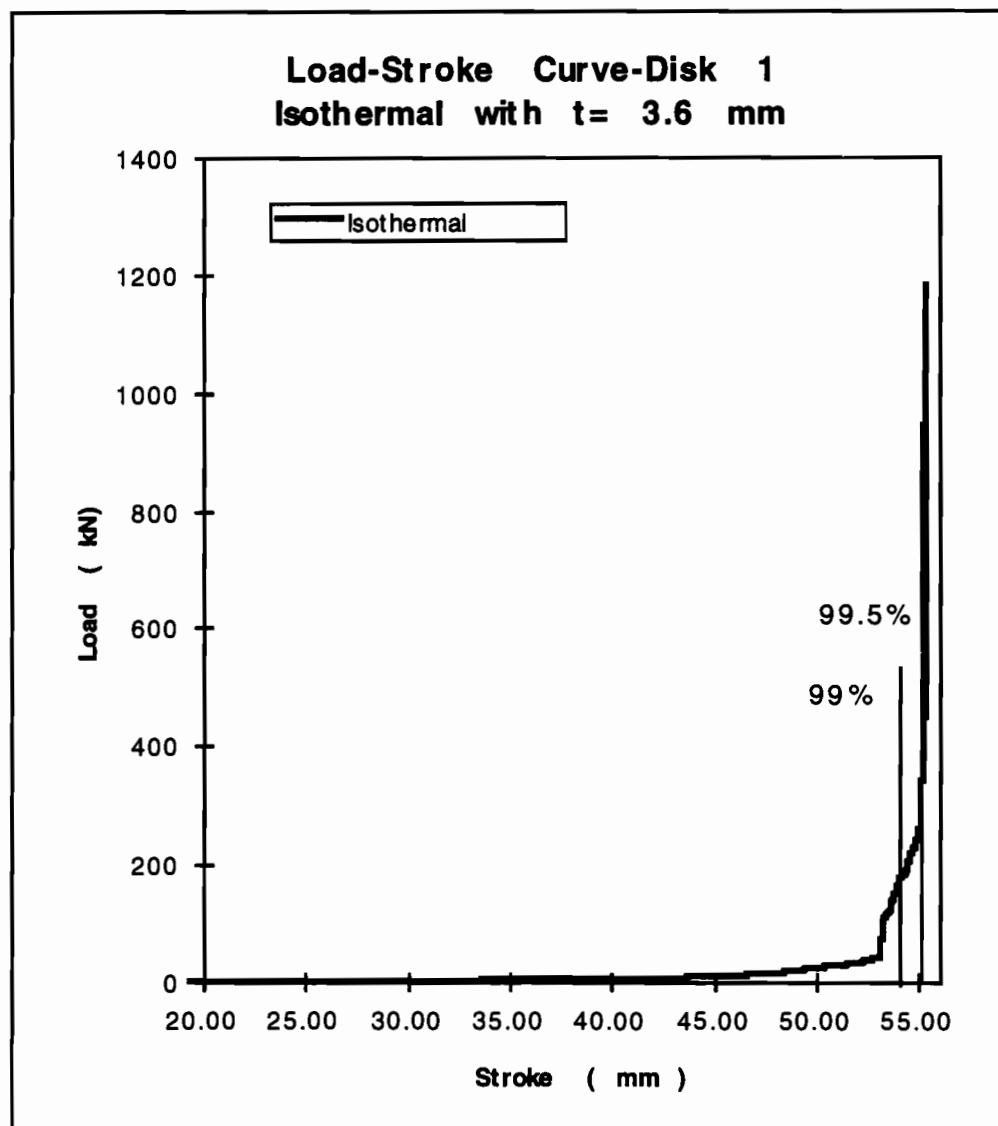
Figure 4.14: Estimated load-stroke curve for Disk 1 case with 3.6 mm final thickness under isothermal simulation
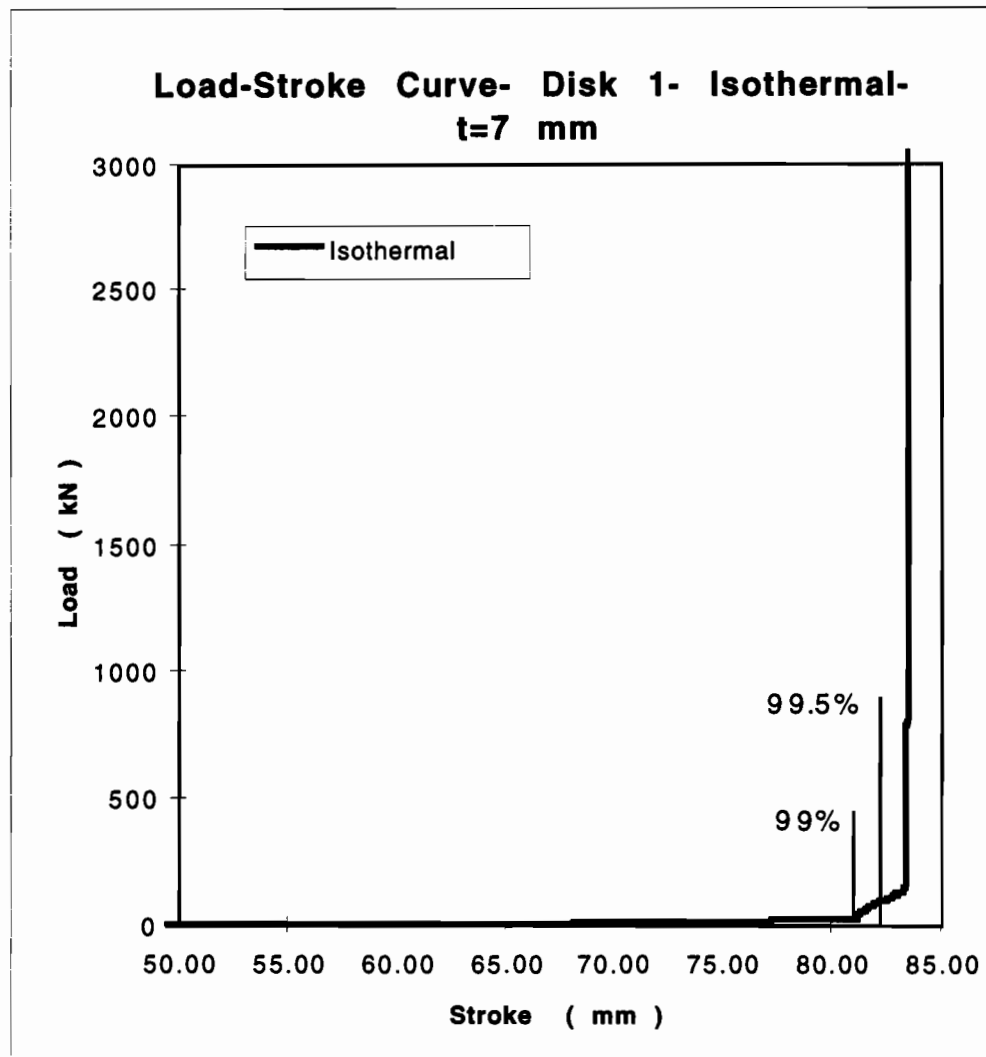
Figure 4.15: Estimated load-stroke curve for Disk 1 case with 7 mm final thickness under isothermal simulations, note that complete filling is obtained at a low forging load

Load-Stroke Curve- Disk 2- Isothermal- t= 3.6 mm
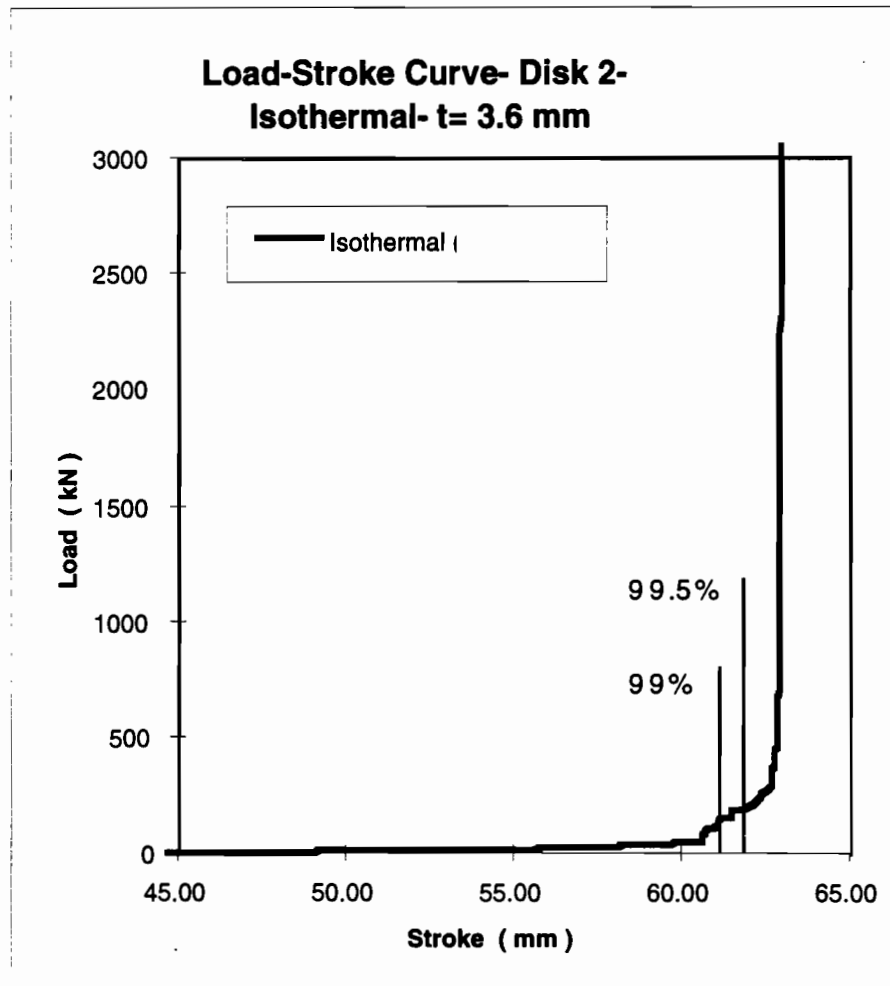
Figure 4.16: Estimated load-stroke curve for Disk 2 case with 3.6 mm final thickness under isothermal conditions
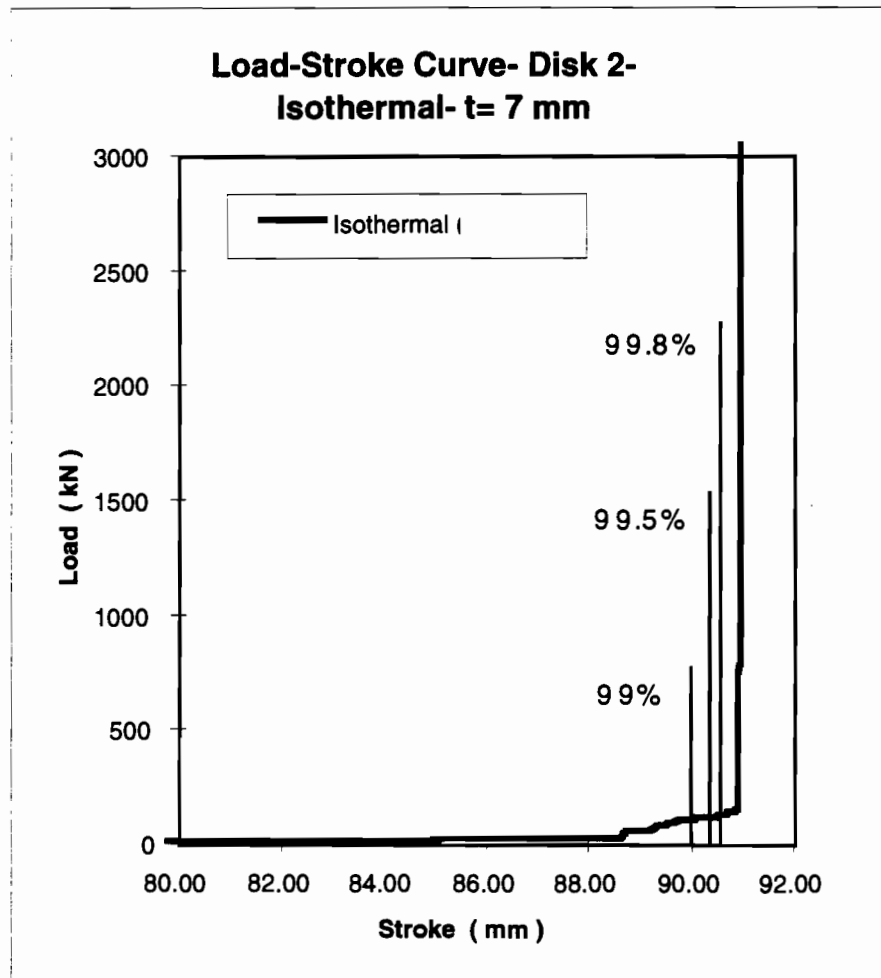
Figure 4.17: Estimated load-stroke curve for Disk 2 case with 7 mm final thickness under isothermal conditions

4.4.2 Non-isothermal Simulations

In reality, it is difficult to heat the dies to the semi-solid temperature range of aluminum alloys (580 $^\circ$C) to obtain isothermal conditions. Therefore, isothermal simulations would not predict the actual phenomena happening during forging of the semi-solid alloys.

In order to perform a more accurate analysis of SSF process non-isothermal simulations were necessary. These simulations involved the effect of temperature variation. Thus, they were expected to be more accurate in estimating the flow behavior and load requirement of the SSF process than the isothermal simulations.

In non-isothermal simulations, the billet was reheated at 580 $^\circ$C, and was placed on the die preheated at 250 $^\circ$C. The heat transfer conditions between billet and dies and the environment were considered. The heat transfer data is presented in Table 4.3.

Four non-isothermal simulations were performed. 2.5 % extra billet volume was added initially to compensate the volume losses occurred during the remeshing steps. Deformation sequences, at various strokes are illustrated in Figure 4.18 for Disk 1 case with 3.6 mm final thickness, in Figure 4.24 for 7 mm final thickness case, Figure 4.27 for Disk 2 case with 3.6 mm final thickness , and in Figure 4.34 for 7 mm final thickness.

The non-isothermal simulations predicted the formation of folds. Formation and rewelding of the folds are shown in Figures 4.19. 4.21, 4.27 and 4.29. Rewelding of the folds was also encountered during the experiments at EFU [Witulski, et al. 1995]. Rewelding could be observed only in 3.6 mm final-thickness cases. This is due to the fact that, in the 7 mm cases, there is no space for folding in the flange region. It is estimated that up to a critical thickness between 3.6 and 7 mm, there will be folding and rewelding of the billet in that region. But no simulations were performed to investigate the critical thickness.

Table 4. 6: Non-isothermal conditions and resulting forging loads

	Disk 1	
Final Web Thickness (mm)	3.6	7
Calculated load at **95%** stroke (kN/Klb)	100/14.5	50/7.25
Experimental load at 95% **stroke (kN/klb)**	1500/217.6	66/7.5
Calculated load at **99%** stroke (kN/Klb)	400/58	200/29
Experimental load at 99% **stroke (kN/klb)**	2720/395	704/102
Calculated load at **99.5%** stroke (kN/Klb)	925/134.2	210/30.5
Experimental load at 99.5% **stroke (kN/klb)**	2882/418	1628/236

As mentioned before, rewelding can be obtained under certain circumstances. When the temperature plots (Figures 4.20, 4.22, Figure 4.28, and 4.30) and deformation plots (Figures 4.18 and 4.26) are reviewed, it is observed that, first, there is enough space to allow folding, and second, the temperature, at the beginning of the rewelding and later on, is high enough for welding, i.e. around 520 $^{\circ}$C which satisfies the welding condition proposed and examined by Laue [Laue, 1981].

A brief explanation about all non-isothermal cases and their load-stroke information is provided in Table 4.4. As it is presented in Table 4.6, loads at which complete filling is obtained are higher than those obtained in isothermal simulations.

The load-stroke curves for each case simulated under non-isothermal conditions are shown in Figures 4.23, 4.25, 4.32 and 4.34.
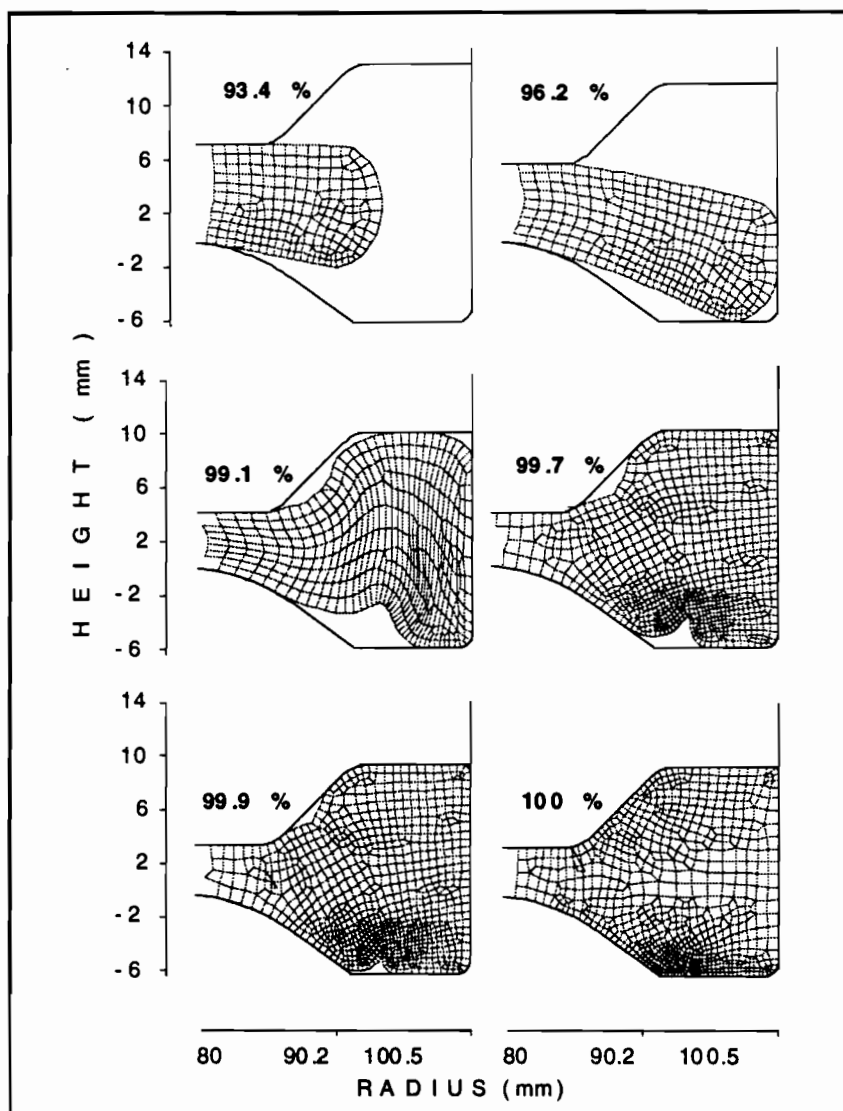
Figure 4.18: Deformation sequence of semi-solid billet for Disk 1 case under non-isothermal conditions with a final thickness of 3.6 mm (dimensions in mm)

99.9 % Stroke

Welding   Condition

A

a

A

HEIGHT (mm)

-1.0
-2.0
-3.0
-4.0
-5.0
-6.0

90.0   91.0   92.0   93.0   94.0   95.0

RADIUS (mm)

b
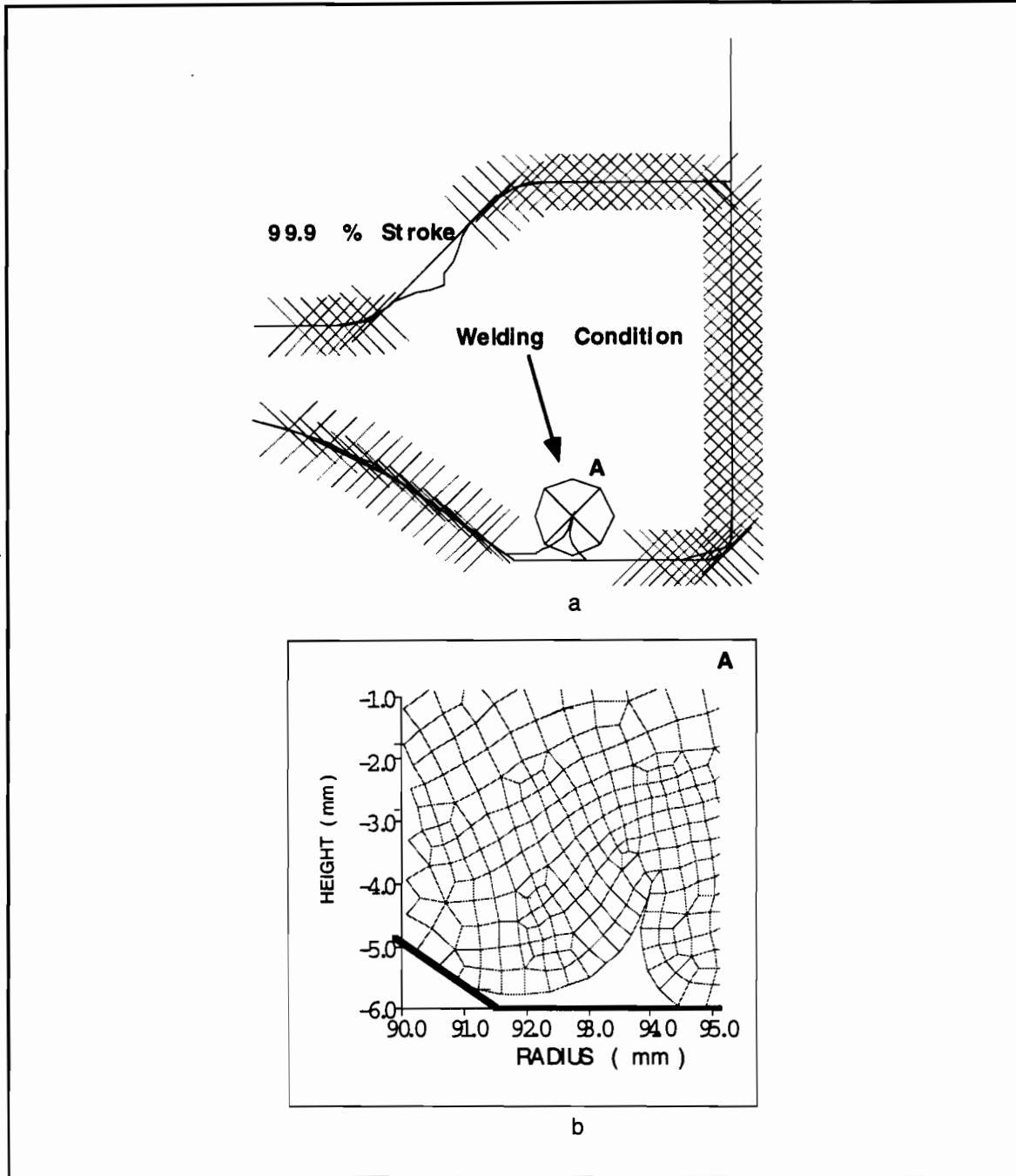
Figure 4.19:   For Disk 1 case with 3.6 mm final thickness, a) Beginning of rewelding process at 99.9 % stroke, b) detailed view of the section A
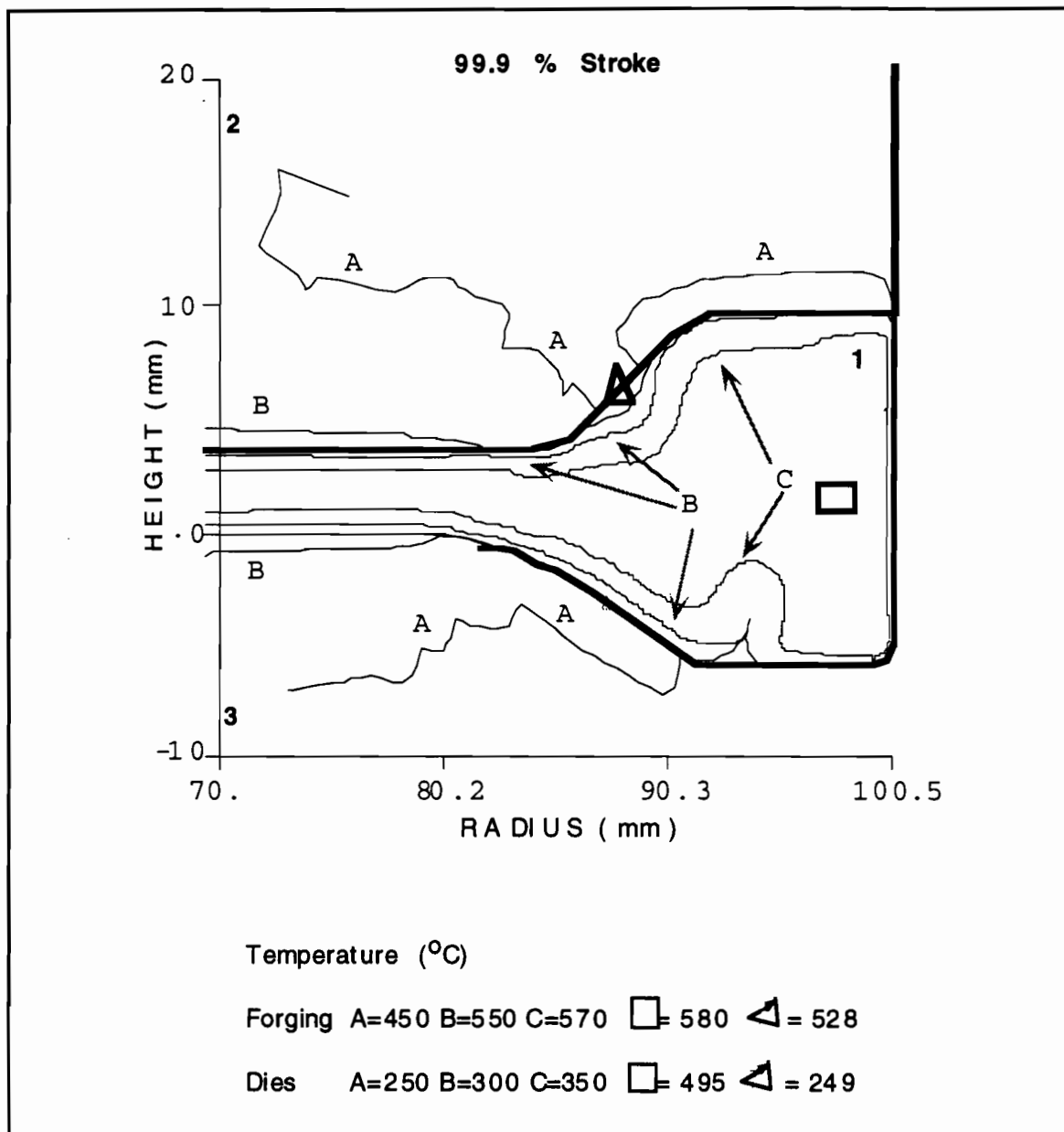
Figure 4.20: Temperature distribution (in °C) at the beginning of rewelding, notice that billet temperature is above 500 °C (for Disk 1 case with 3.6 mm final thickness)
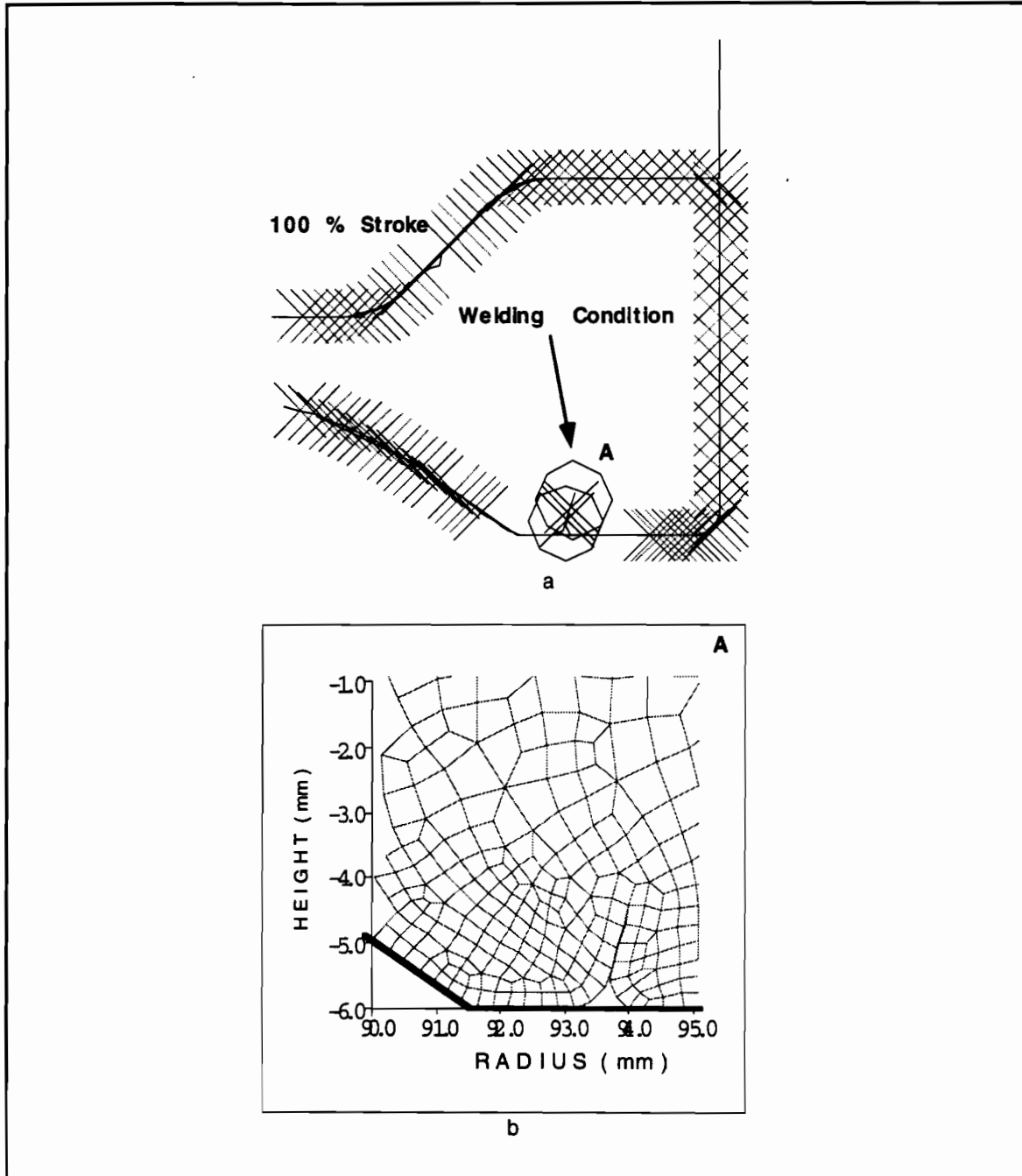
Figure 4.21: For Disk 1 case with 3.6 mm final thickness, a) End of the rewelding process at 100% stroke, b) detailed view of the section A
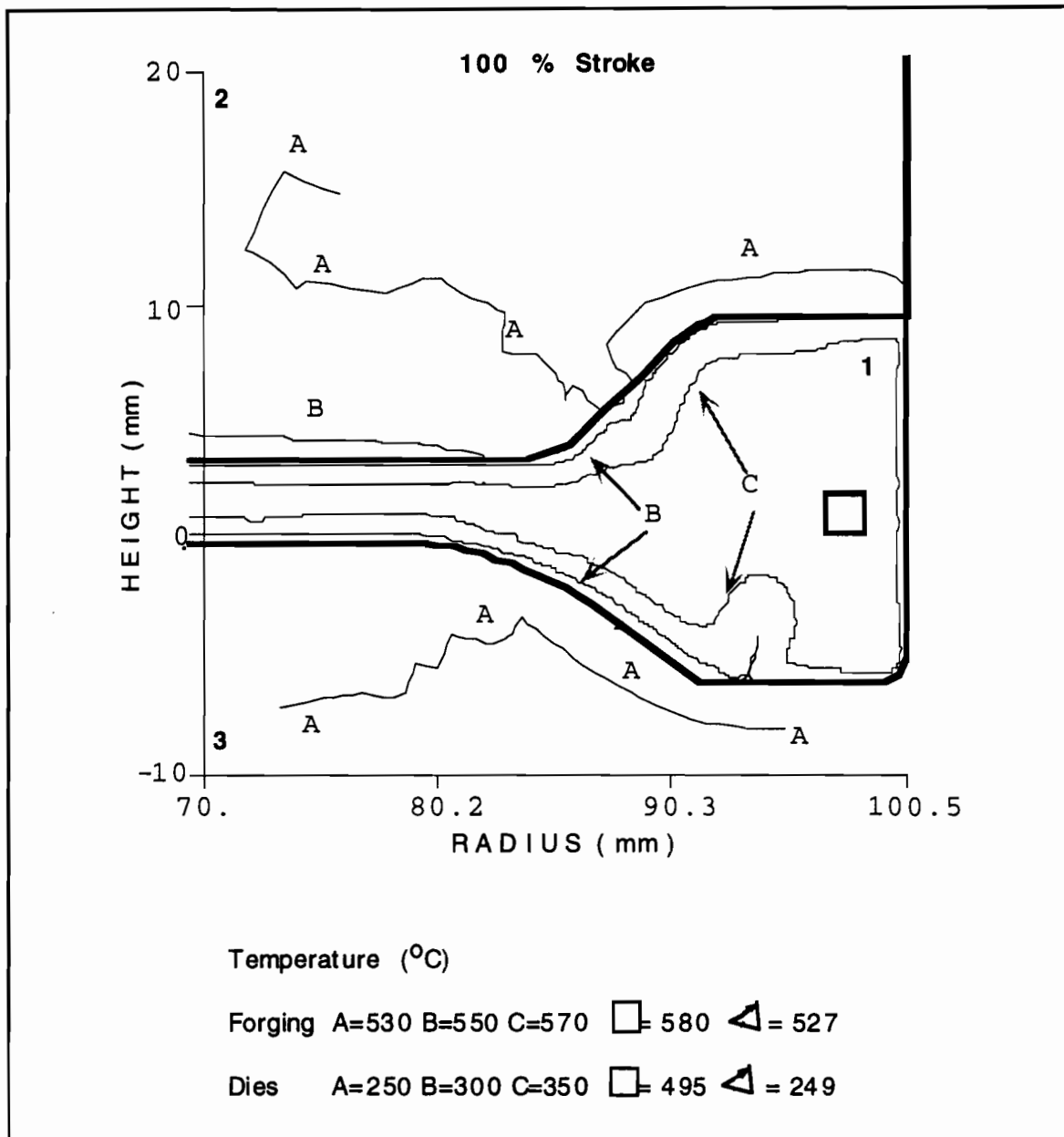
Figure 4.22: Temperature distribution (in °C) at the end of rewelding, notice that billet temperature is above 500 °C (for Disk 1 case with 3.6 mm final thickness)
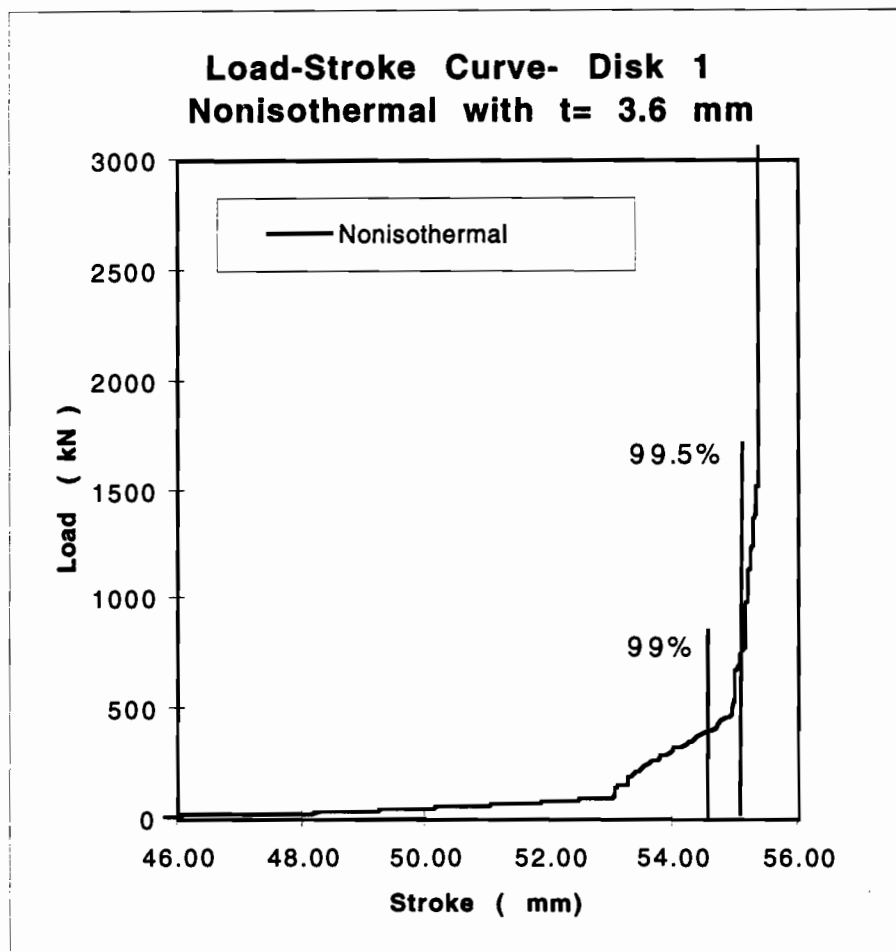
Figure 4.23: Load-stroke curve for Disk 1 case with 3.6 mm final thickness under non-isothermal conditions
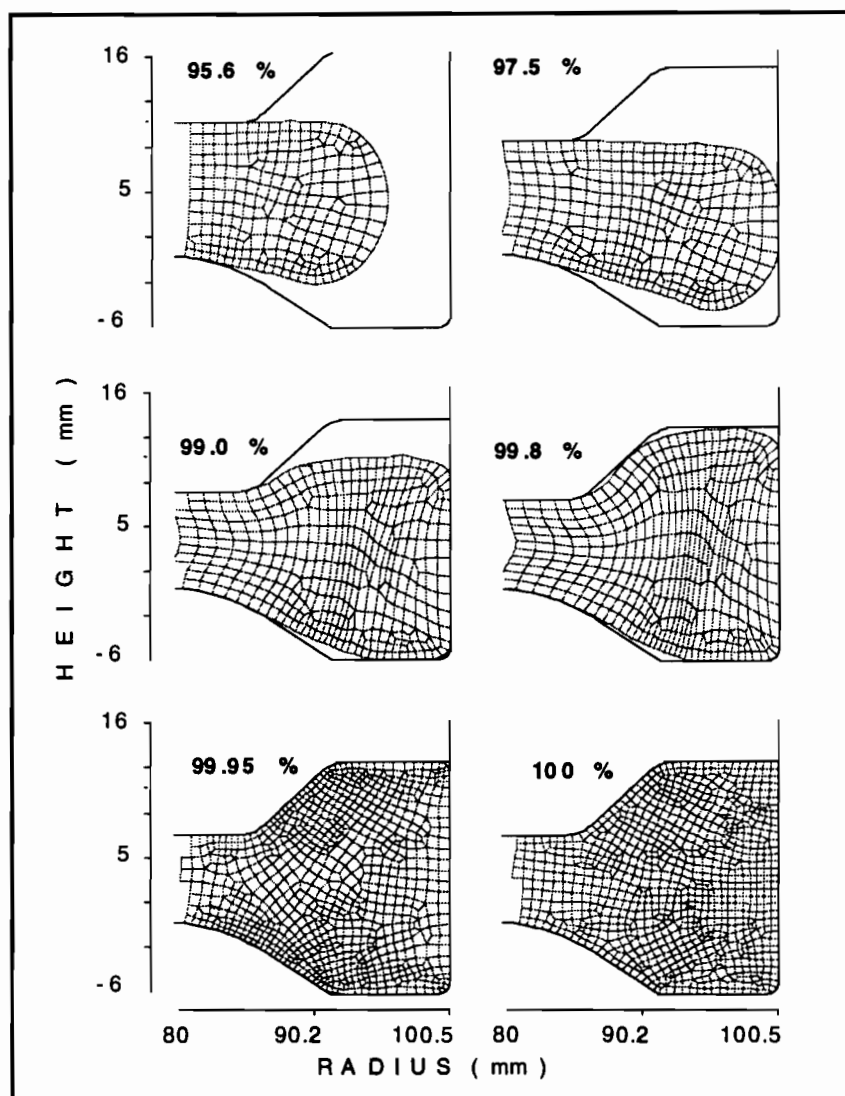
Figure 4.24: Deformation sequence of semi-solid A356 alloy under non-isothermal conditions for Disk 1 case with 7 mm final thickness (dimensions in mm)

**Load-Stroke Curve- Disk 1
Nonisothermal with t=7 mm**
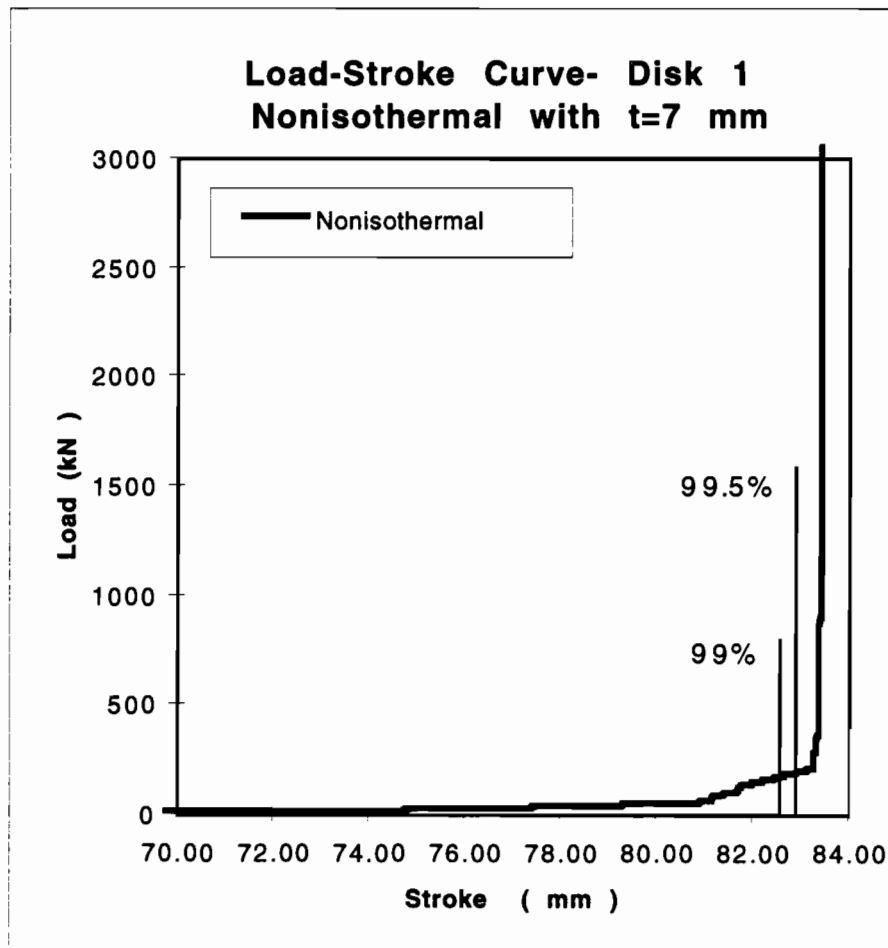
Figure 4.25: Load-stroke curve for Disk 1 case with 7 mm final thickness under non-isothermal conditions
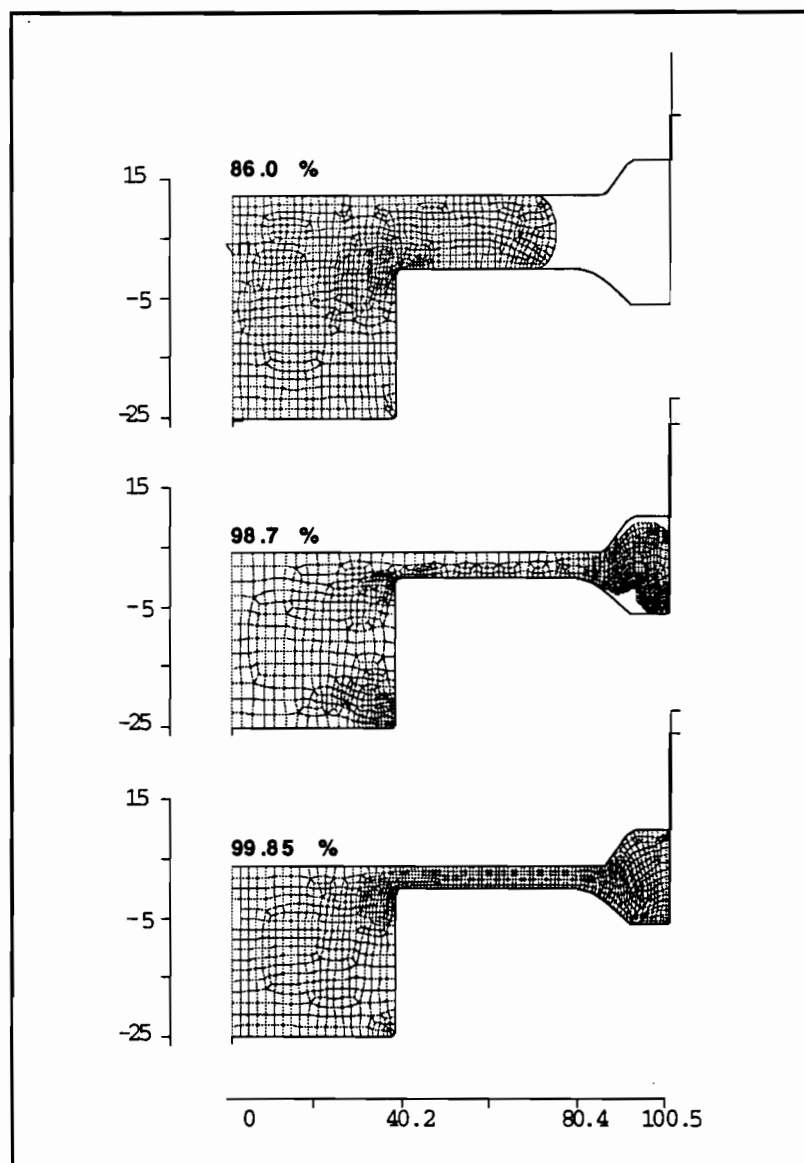
Figure 4.26: Deformation sequence of the semi-solid forging for Disk 2 case with 3.6 mm final thickness under non-isothermal conditions (dimensions in mm)
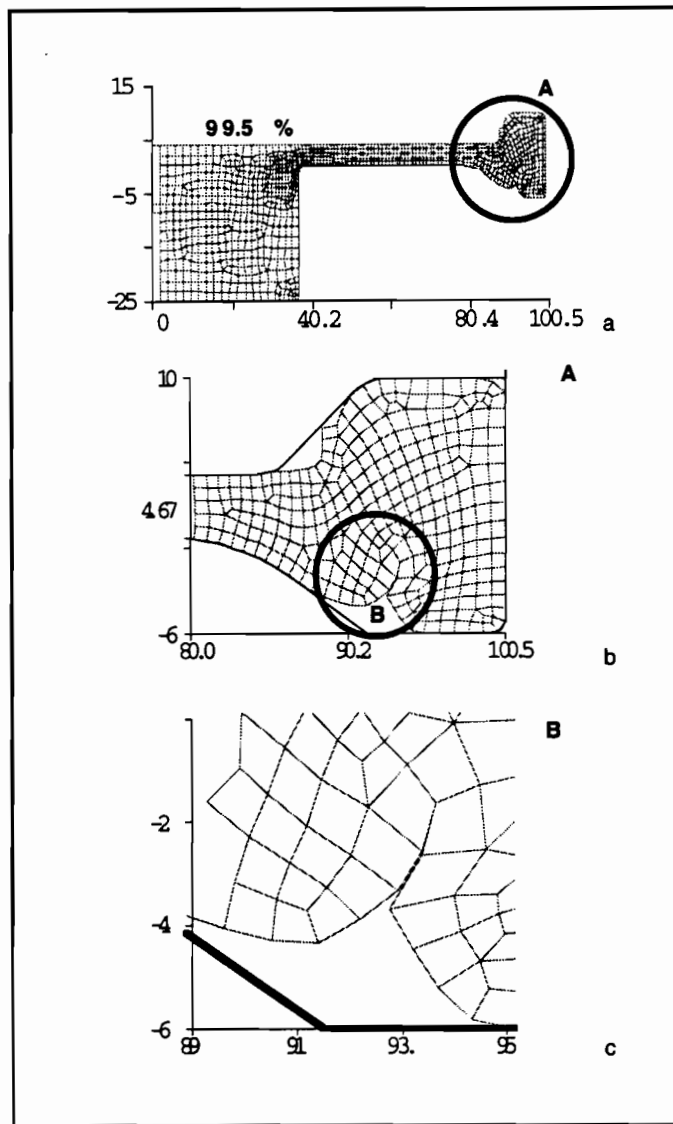
Figure 4.27: Beginning of the rewelding process in the Disk 2 case with a final thickness of 3.6 mm. A and B illustrates the detailed section of the flange region where rewelding of the folds occur (vertical axes indicate the Height (mm) and horizontal axes indicate the Radius (mm))
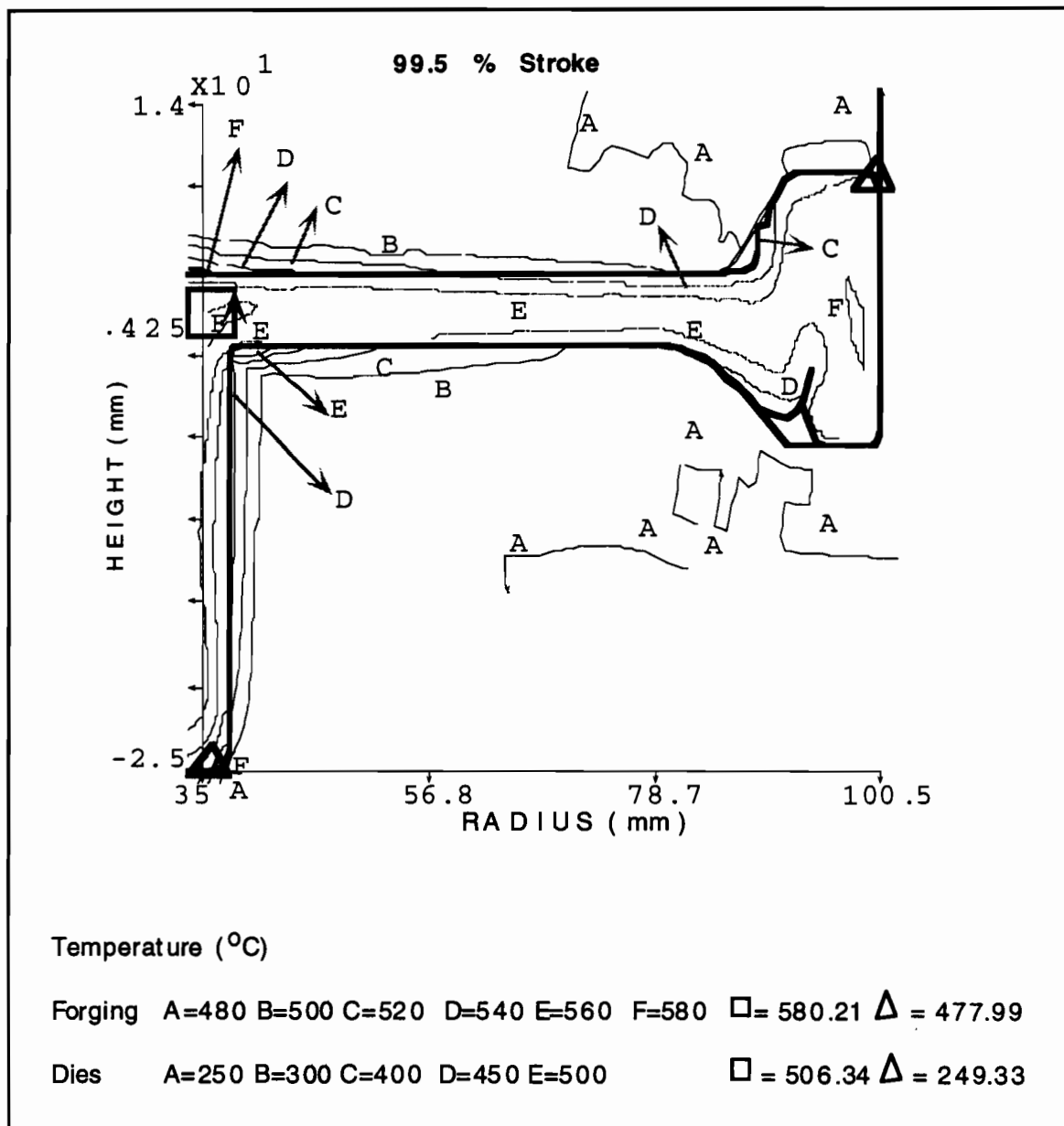
Figure 4.28: Temperature distribution (in °C) at the beginning of the rewelding process for Disk 2 case with 3.6 mm final thickness. Notice that the temperature is above 500 °C at the places where rewelding takes place
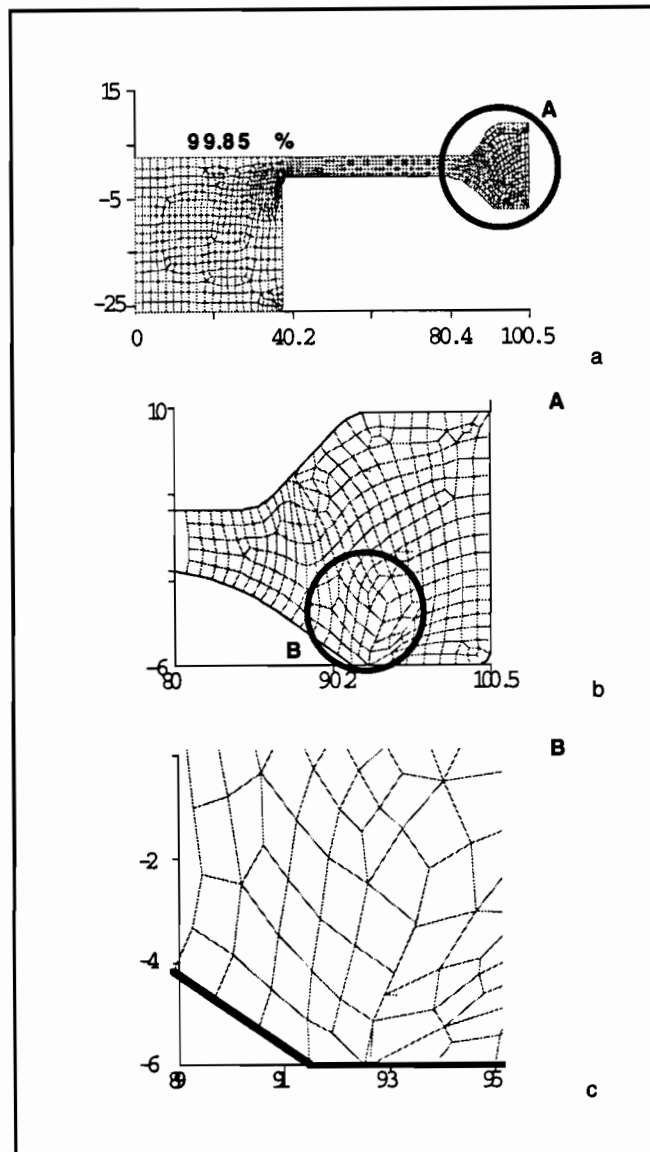
Figure 4.29: End of the rewelding process for Disk 2 case with a final thickness of 3.6 mm. A and B illustrates the detailed section of the flange region where rewelding of the folds takes place (dimensions in mm)
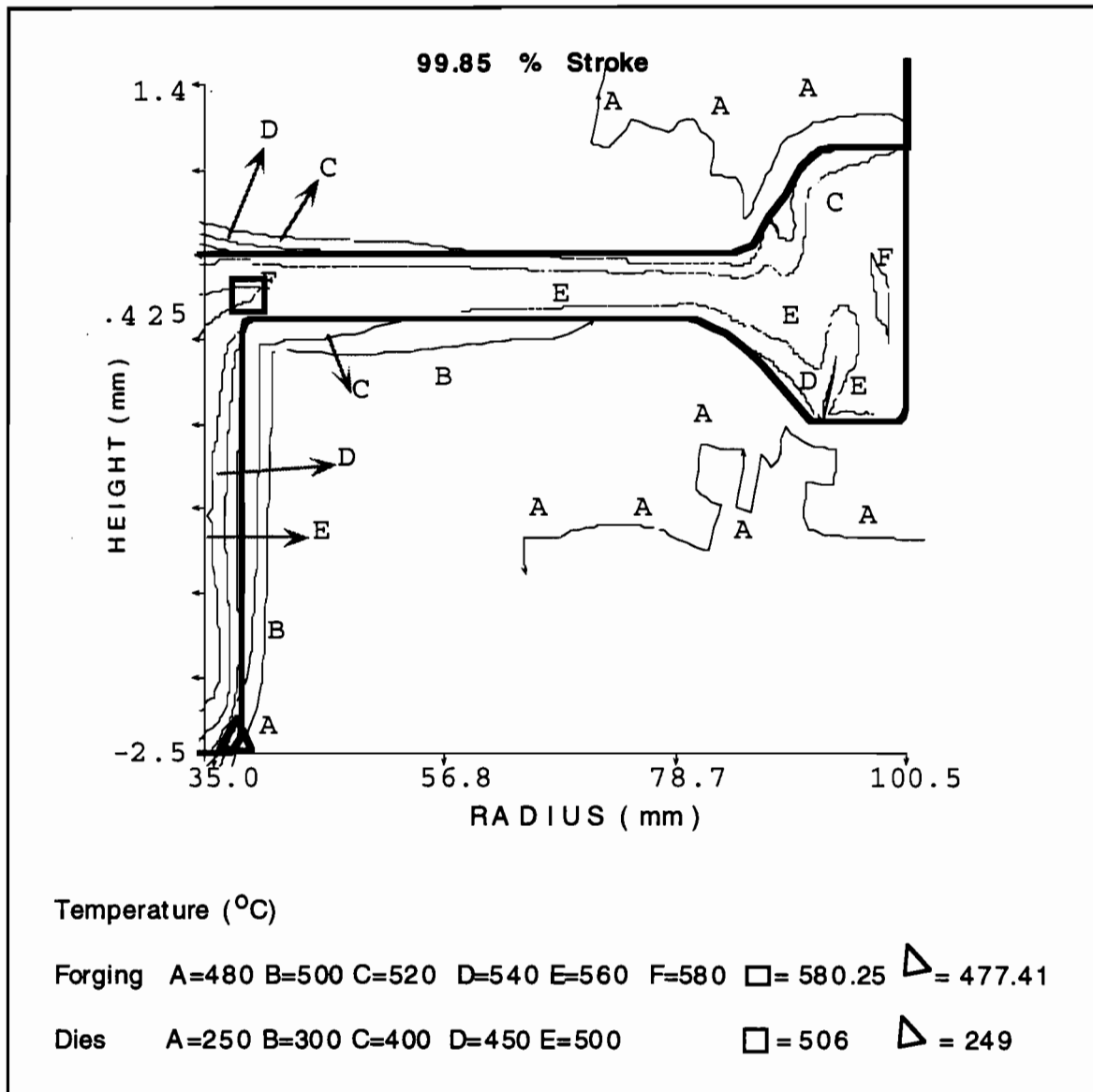
Figure 4.30: Temperature distribution (in °C) at the end of the rewelding process for Disk 2 case with 3.6 mm final thickness. Notice that the temperature is above 500 °C at the places where rewelding takes place
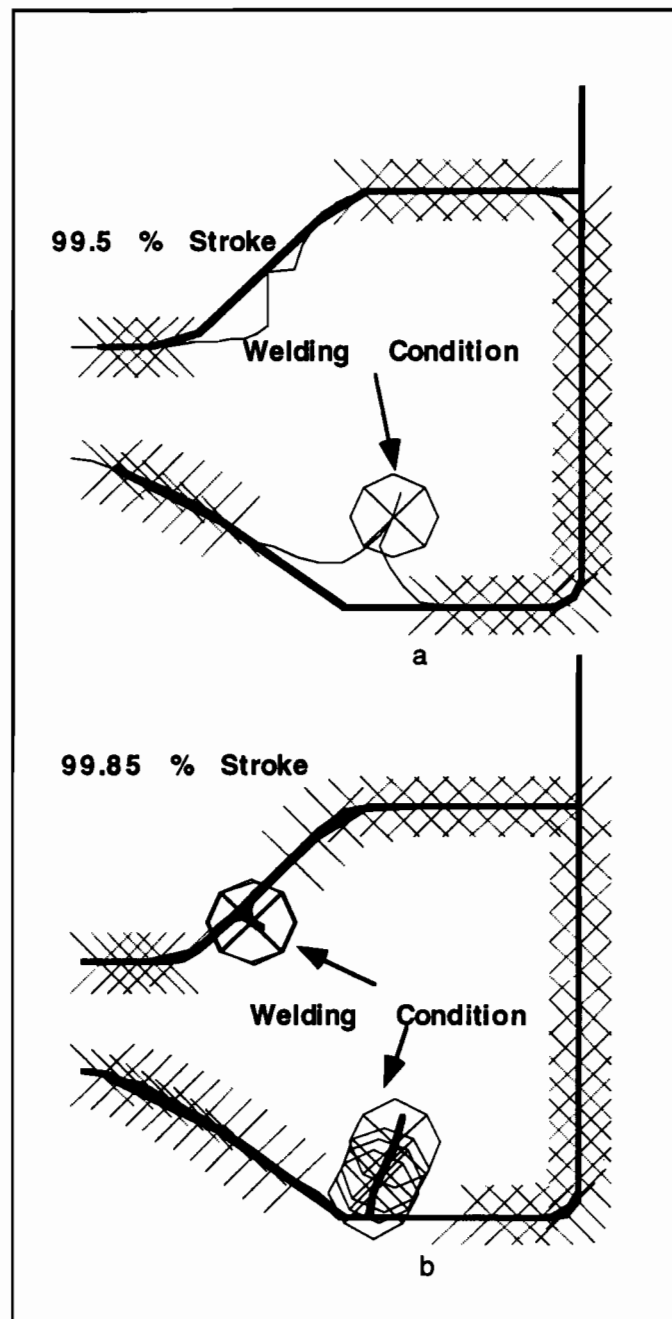
Figure 4.31: Welding condition at the beginning (99.5 % stroke) and at the end (99.85 % stroke) of the rewelding process for Disk 2 case with 3.6 mm final thickness
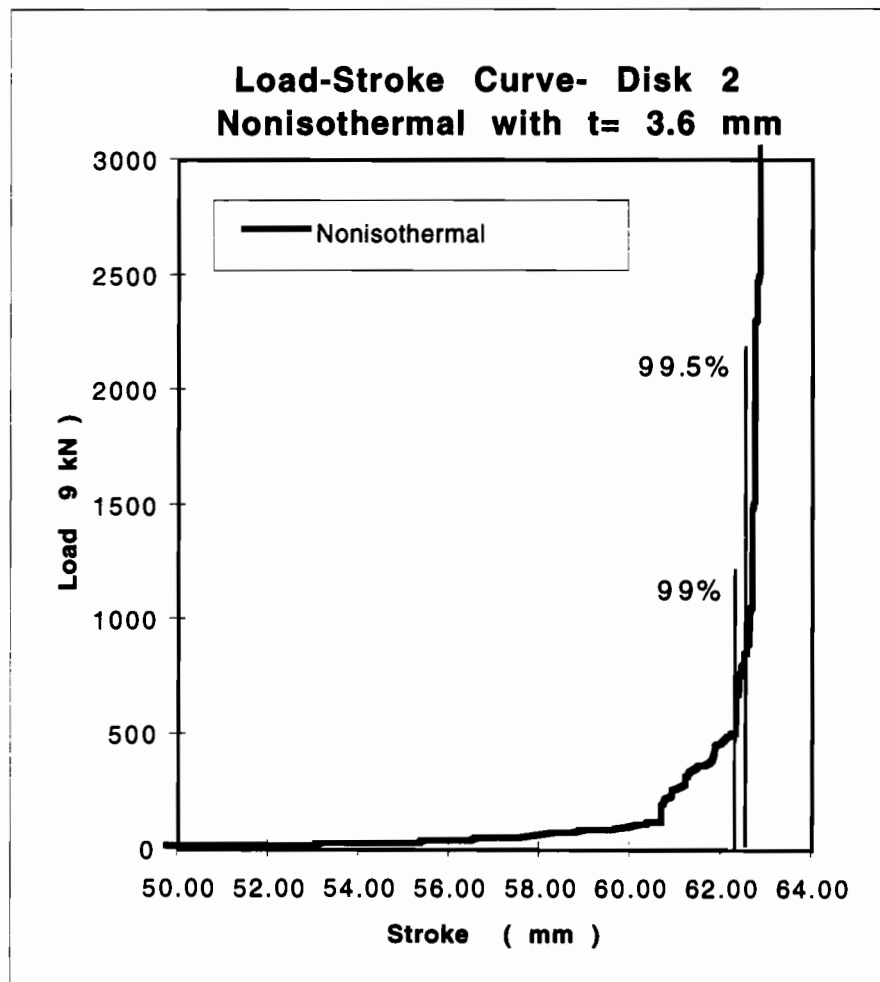
Figure 4.32: Load-stroke curve of the non-isothermal simulation for Disk 2 case with 3.6 mm final thickness
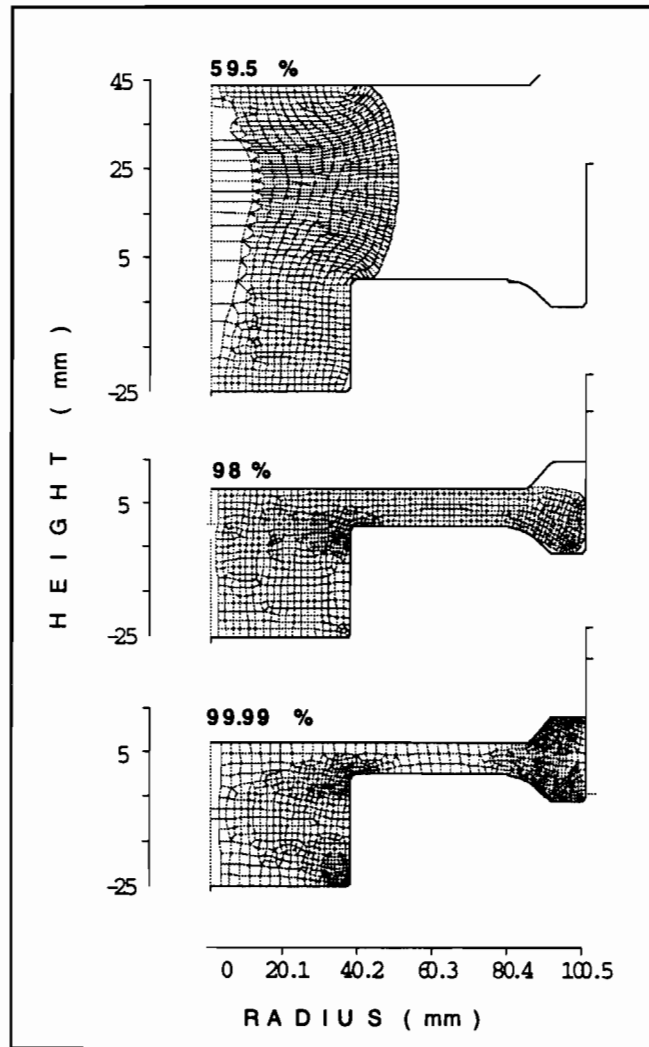
Figure 4.33: Deformation sequence of semi-solid billet for Disk 2 case with 7 mm final thickness under non-isothermal conditions (dimensions in mm)
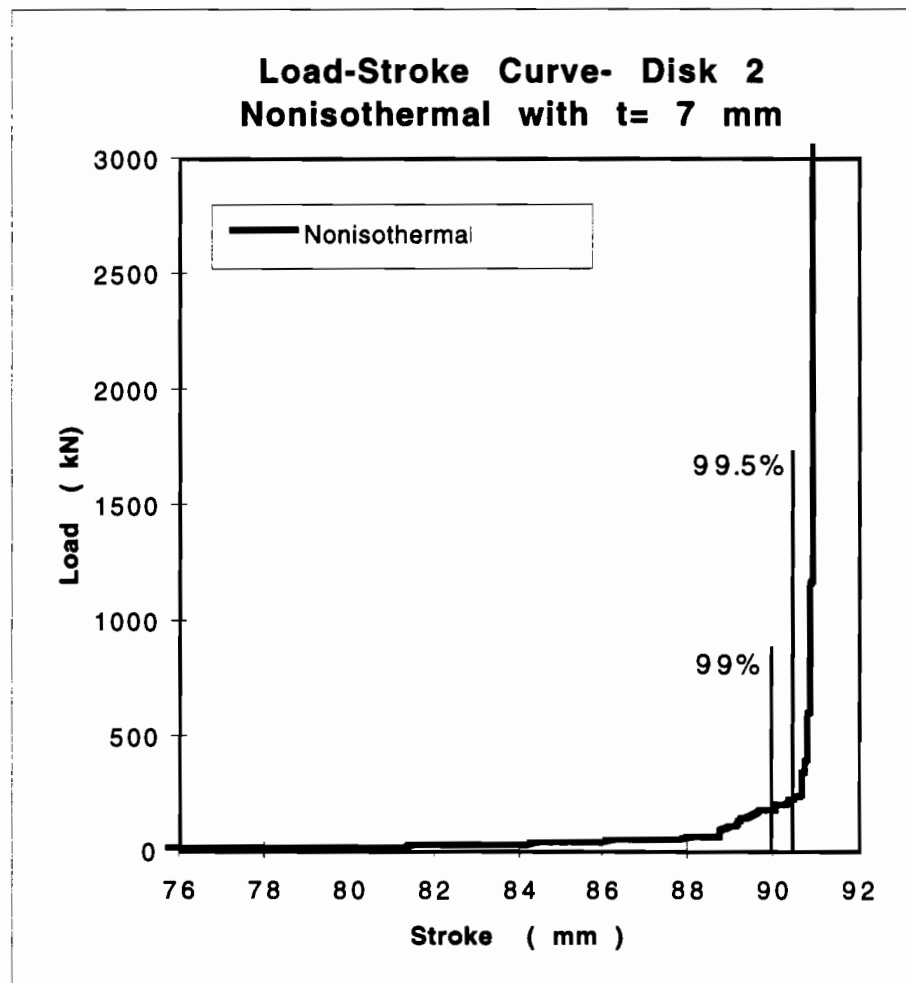
Figure 4.34: Load-stroke curve of non-isothermal simulation for Disk 2 case with a final thickness of 7 mm

4.5 Comparison of Predicted and Measured Load-Stroke Curves

While the FE simulations were conducted at the ERC/NSM as part of this project, the experiments were conducted by EFU in Germany [Hirt, G., 1995].

In the simulations, loads at the very end of the stroke were much higher than the loads when complete filling was obtained. The difference is due to the force caused by the hydrostatic pressure which builds up when the dies are completely filled [Witulski, T., 1995]. Therefore, comparison of loads were not made at 100 % stroke, but at 99% and 99.5%.

Simulations underestimated the loads when compared with experimental results. The underestimation is higher for isothermal simulations than non-isothermal simulations.

The comparison of the non-isothermal simulation and experimental loads is tabulated in Table 4.6. Figures 4.35 and 4.36 illustrate the difference between experimental and simulation load-stroke curves for both final web thickness cases. As seen from Figures 4.35 and 4.36 and Table 4.6, the difference between experimental and predicted loads is lessfor the part with 7 mm final web thickness than that with 3.6. In each case, the difference between experimental and simulation results is larger towards the end of the stroke.

One of the reasons for the difference between predicted and measured values is the inaccuracy in the estimation of the flow stress values. The flow stress, thus the forging load is strongly dependent on temperature. As temperature decreases, flow stress increases. Variation of flow stress with temperature is large when semi-solid alloys are cooled from liquid-solid region to solid region. The solidus temperature of A356 semi-solid alloy is 555°C. However, in the simulations, since linearly approximated flow stress curves were used, and since the FE code used performs linear interpolation when required, abrupt change of flow stress values could not be calculated close enough to the actual values when temperature decreases below 555°C. Therefore, in experiments, loads increase suddenly to high values towards the end of stroke whereas a linear increase is observed in simulation load-stoke curves until very end of the stroke where loads reach high values suddenly.

The value of the interface heat transfer coefficient used in simulations was the value between steel dies and conventional aluminum alloys, not semi-solid aluminum alloys because this value was not available in the literature. Therefore, the effect of die chilling might have not been well implemented. As a result, predicted loads deviate from experimental values.

4.6 Conclusions and Future Work

Metal flow behavior of semi-solid alloys is well simulated by DEFORM when compared with the experimental results. Folding and rewelding are also estimated within a reasonable accuracy. The loads are underestimated in both isothermal and non-isothermal simulations.

It could be concluded that non-isothermal simulations with proper input data would give results close to the experimental findings. In order to obtain accurate results in simulations, flow stress curves of semi-solid alloys need to be constructed at various temperatures using compression tests under a strictly controlled environment and at strain rates, comparable to that present in actual SSF. This would help us to simulate the sudden change in flow stress values when temperature decreases to a certain range (i.e. below solidus line).

In this study, instead of approximating the available flow stress curves in literature, flow stress curves using pseudoplastic behavior of the semi-solid alloys could be obtained, or they could be corrected to have a better approximation to the actual flow stress curves. However, available experimental data for this method was also limited.

Optimization of process variables such as die speed (i.e. shear rate), die temperature and solid fraction (i.e. temperature of the billet) is necessary for

soundness of the parts. Special tooling for SSF process is also crucial for achieving the same goal. Mechanical properties of the SSF parts must be determined and compared with conventional forging and casting components for verification of the SSF process.
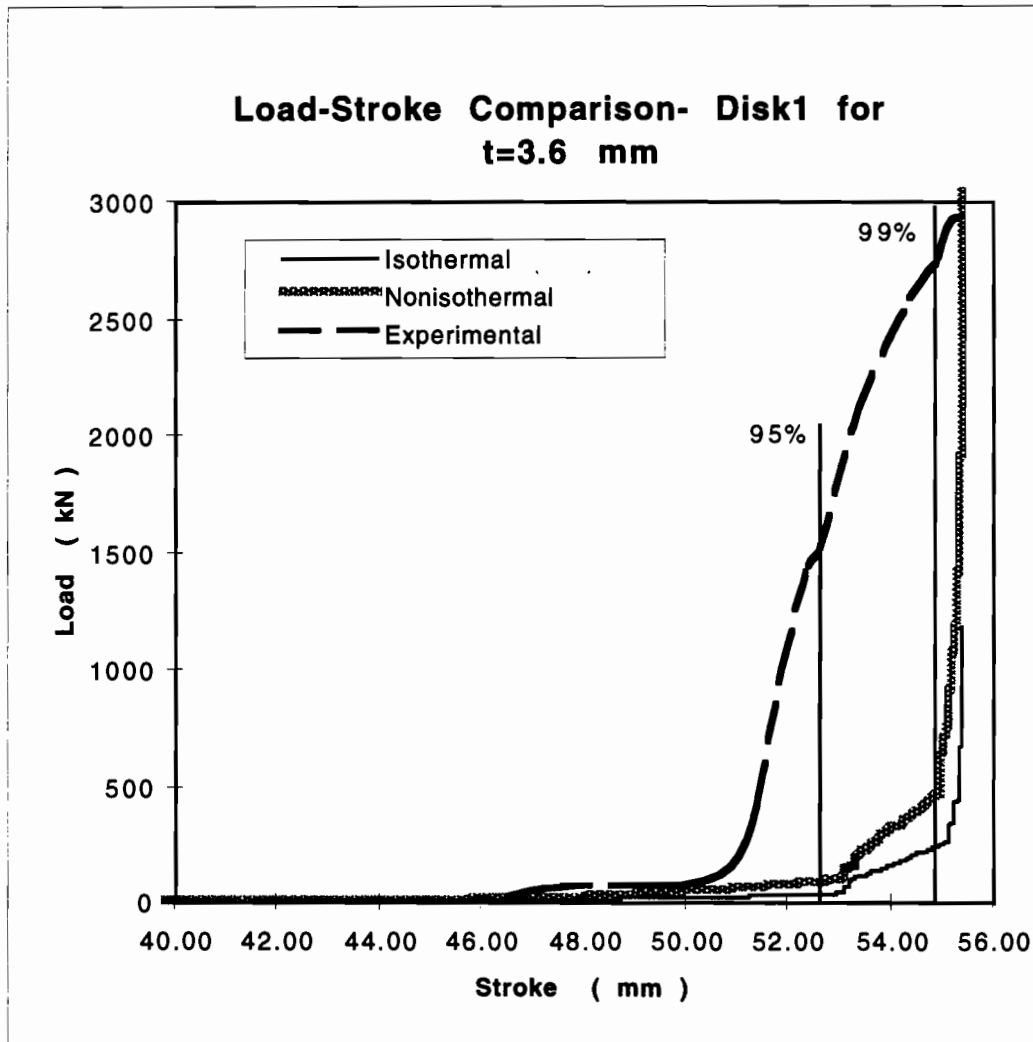
Figure 4.35: Comparison of load-stroke curves for Disk 1 case with a final web thickness of 3.6 mm

Determination of the actual friction conditions between semi-solid aluminum alloy and dies would also improve simulation results. In this study, a shear friction of m=0.2 was assumed.

Load-Stroke Comparison- Disk 1   t=7 mm
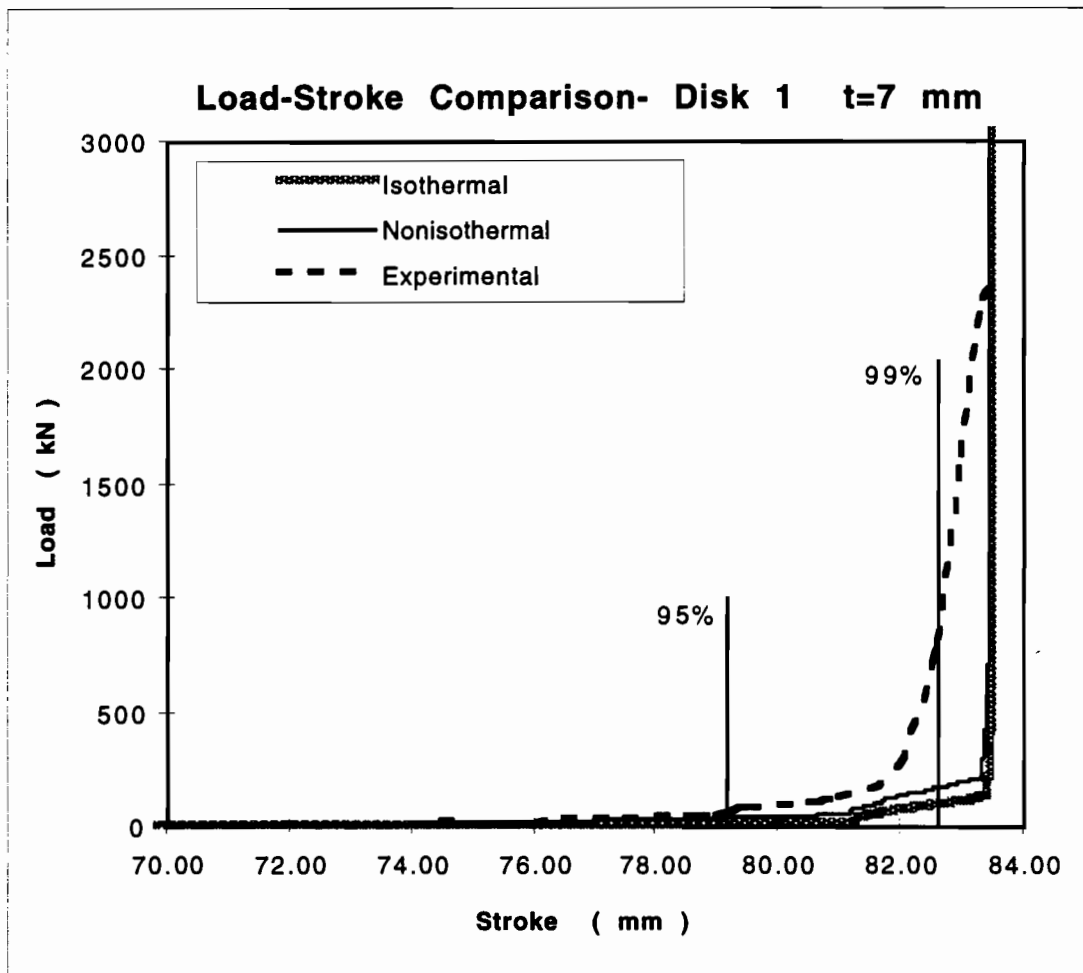
Figure 4.36: Comparison of load-stroke curves for Disk 1 case with a final thickness of 7 mm

Chapter V

DESIGN OF SHRINK RINGS FOR NON-AXISYMMETRIC FORGING DIES

5.1 Shrink Ring Design for Axisymmetric Dies

Catastrophic die failures are a consequence of the tangential (hoop) tensile stresses induced on the inner surface of the die during forming. In order to prevent failure, shrink rings (stress rings) are used to support the dies, Figure 5.1. Shrink rings improve the service life of the dies by inducing compressive stresses on the impression surfaces of the dies. The compressive prestressing is achieved by performing an interference fit between the die and shrink ring. An interference fit is obtained when the diameter of the mating surface of the shrink ring is smaller than outer diameter of the die. Through the use of shrink rings, the die is not subjected to extreme stresses that cause yielding. Furthermore, since prestressing the dies reduces the amplitude of the forming stresses induced on the die, it helps to increase the fatigue life of the die.

The yield strength (Y) of a tool steel should be higher than the maximum principal stress difference ($S_v = S_t - S_r$) occurring in the die, if the Tresca yield criterion is used, in order to remain in the elastic region.

$$Y \geq S_v = S_t - S_r$$

where

S_t = Tangential Stress

S_r = Radial Stress

If no shrink ring is used, the maximum stress that a monobloc die can withstand will be half its yield strength (Y) even if the die is infinitely thick. In practice, rough design guidelines and experience are used to determine the dimensions of the shrink rings for specific applications. Materials selection and die and shrink ring designs are chosen according to these basic guidelines such as Lamé equations. These guidelines are determined based on assumptions including steady-state stress conditions, uniform internal pressure along the whole length of the die, and no residual stresses in the die before assembly. Additional information on these guidelines is available through International Cold Forging Group (ICFG) publications [ICFG data sheet no: 6/72].
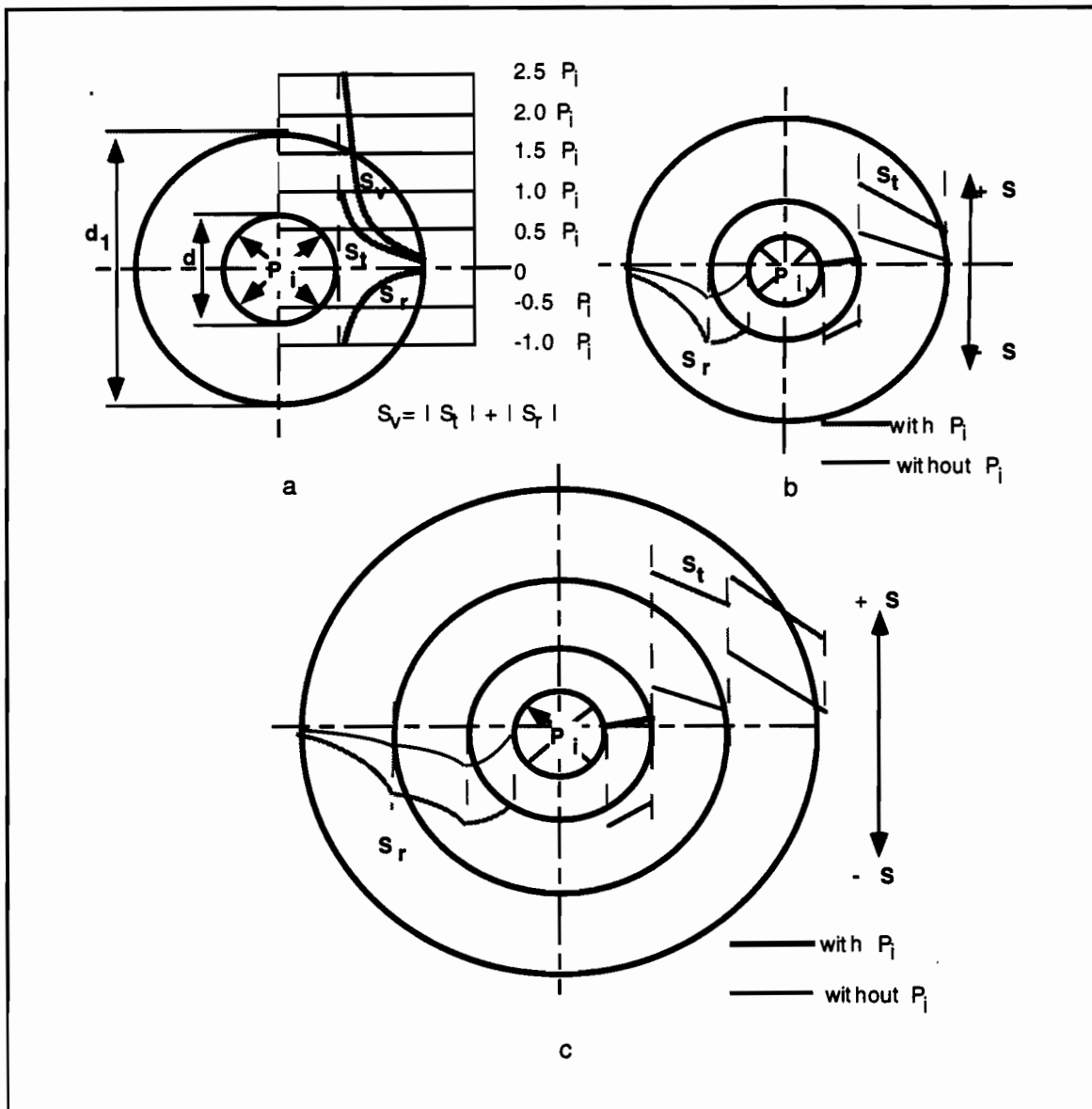
Figure 5.1: Three different die and shrink ring configurations a) monobloc, b)one die-one ring, and c) one die-two ring. Theoretical tensile stresses are lower in the designs with shrink rings than the monobloc design case.

5.2 Non-axisymmetric Shrink Ring Tool Design

In practice, guidelines used to design forging dies and shrink rings are applicable only to axisymmetric cases. In the case of non-axisymmetric parts, the tool stress distribution is totally different. Therefore, typical guidelines and the simple Lamé equations are not completely appropriate for use in non-axisymmetric forgings. In order to have accurate designs in non-axisymmetric cases, 3-D FEM elastic-plastic stress analysis of the dies and shrink rings is necessary.

In this study, an investigation on 2-D elastic-plastic stress analyses of a connecting rod die was performed using both analytical design guidelines and 2-D FE elastic-plastic stress analysis using the ABAQUS FE code. The 2-D models were used to simplify the 3-D problem and to define the preliminary tool design for 3-D simulations.

5.2.1 Forging of Connecting Rods

A connecting rod is an important functional component in an engine. During service, it is subjected to severe mechanical and thermal effects. Loads on the connecting rods are cyclic; therefore, connecting rods must have very good fatigue properties as well as good wear resistance. Connecting rods, used in internal combustion engines, are made from steel either by forging

(from billet or P/M preform) or by casting. The trend, however, is towards forging to increase the strength to weight ratio. For certain engines and compressors Al-Metal Matrix Composites (MMC) are being considered. In all these cases, the tendency is to reduce excess material, i.e., flash, and to forge near net. Thus, die design becomes increasingly important since dies are subjected to higher stresses.
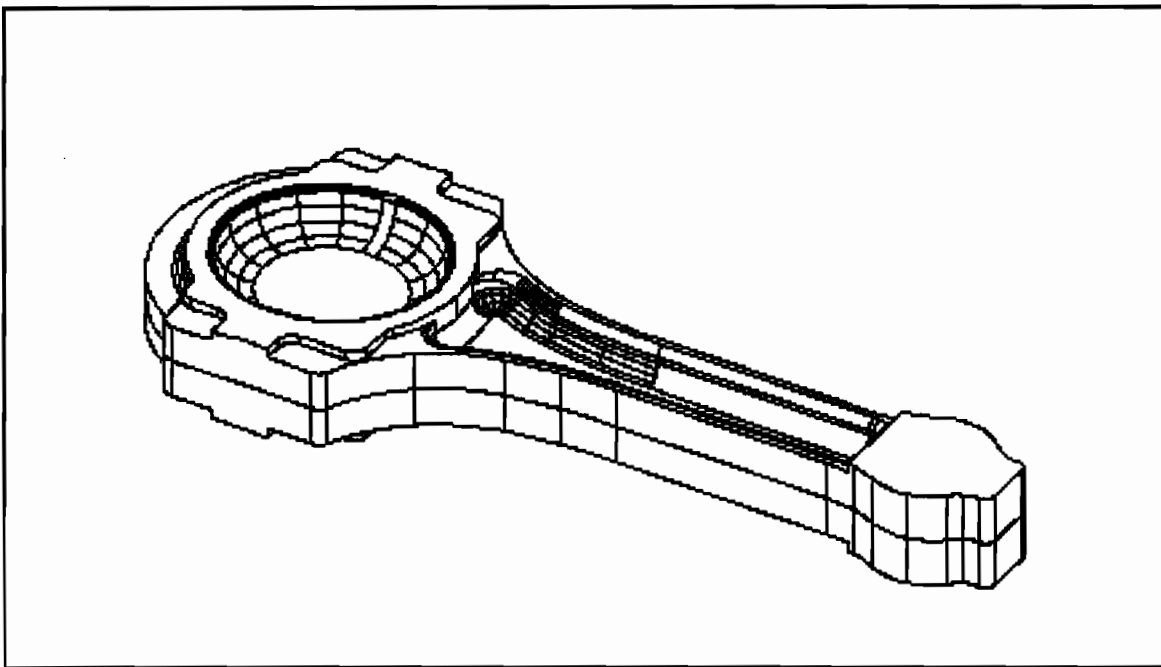
Figure 5.2:   Connecting rod designed at ERC/NSM

5.2.2 Research Objectives

It is desired to model connecting rod forging using 3-D FEM. Since the commercial DEFORM-3D FE is capable of 3-D simulations for complex parts, it

is used to model the metal forming simulation of a connecting rod. Flashless forging simulation of a connecting rod has been performed at the ERC/NSM [Takemasu, et al. 1995]. In that research, the design of the preform and the punches were designed using I-DEAS.

During these simulations, high contact stresses developed on the die surface in the closed forging of the connecting rod. These stresses are high particularly on the corners and fillets due to stress concentrations. To reduce the effect of the contact stresses, shrink rings are used to prestress the dies into compression .

For forging a connecting rod, shrink ring and die designs other than circular design need to be considered. Principally, if the stress distribution on the die is followed, a contoured design will be the optimum. But, due to manufacturability considerations, contoured shrink ring tooling would not be feasible. The elliptical shrink ring design seems to be more effective in counteracting the contact stresses than circular shrink ring.

Since the calculation of the die stresses due to forging were already estimated earlier at ERC/NSM, research on the design of shrink rings for non-axisymmetric parts assumed that internal die stresses are known, and concentrates mainly on the following steps:

1. Investigate current design methods and industrial applications and understand the principles of die and shrink ring design

2. (a) Simplify the non-axisymmetric tooling design into axisymmetric and plane strain sections

    (b) Perform 2-D Elastic-Plastic stress analysis of the simplified sections to verify the design to be used in the next phase

3. Perform 3-D FE Elastic-Plastic stress analysis of die and shrink ring for the following different designs based on results from step two:

    (a) elliptical die-elliptical shrink ring, (b) elliptical die-circular shrink ring, (c) tangential-circle die-elliptical shrink ring, (d) elliptical die-rectangular shrink ring, (see Figures 5.3 and 5.4, respectively)

4. Optimize the tooling design and develop a methodology to design shrink ring tooling for non-axisymmetric dies
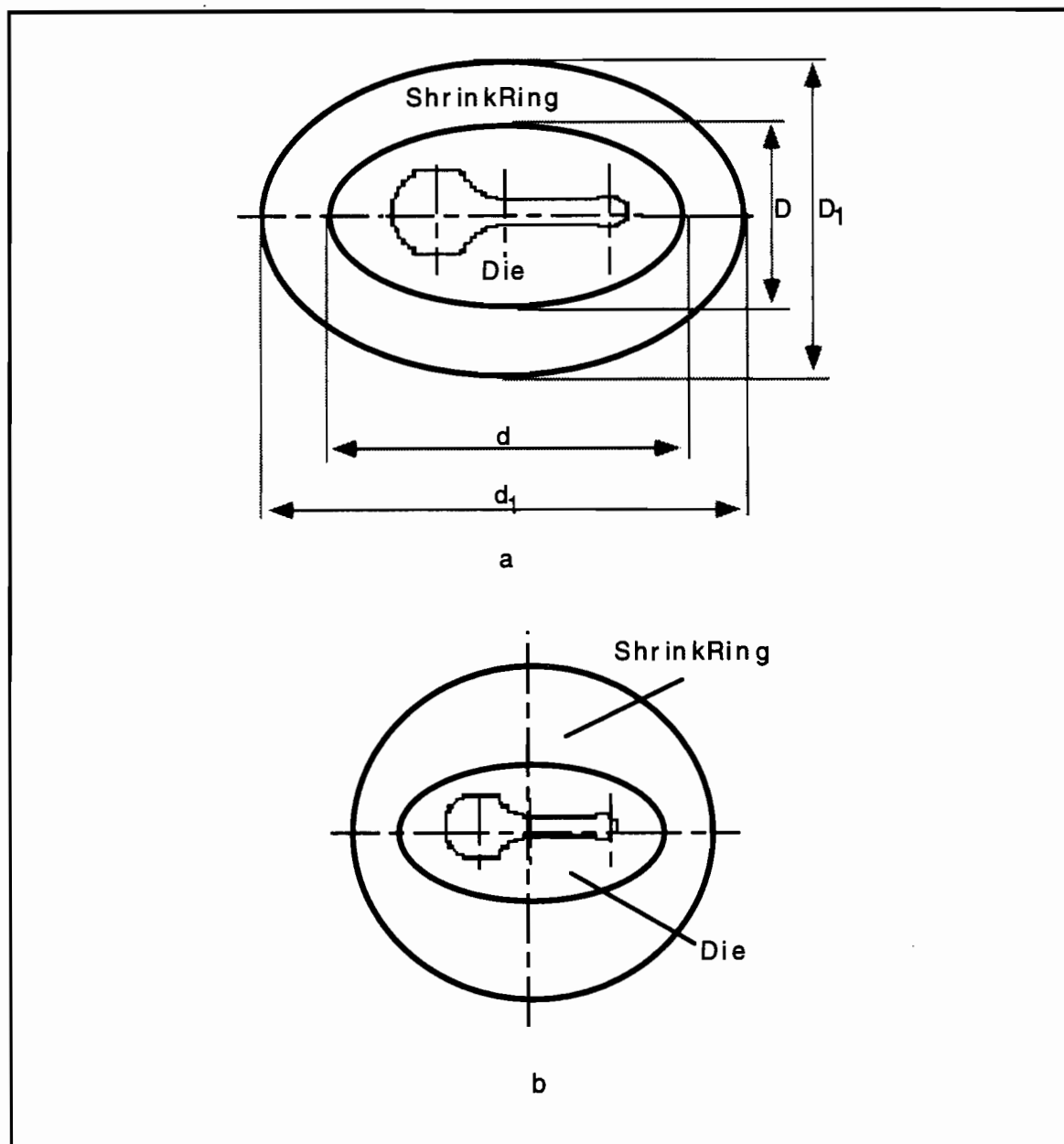
Figure 5.3: Proposed a) elliptical die- elliptical ring, b) elliptical die-circular ring designs for 3-D E-P simulations.
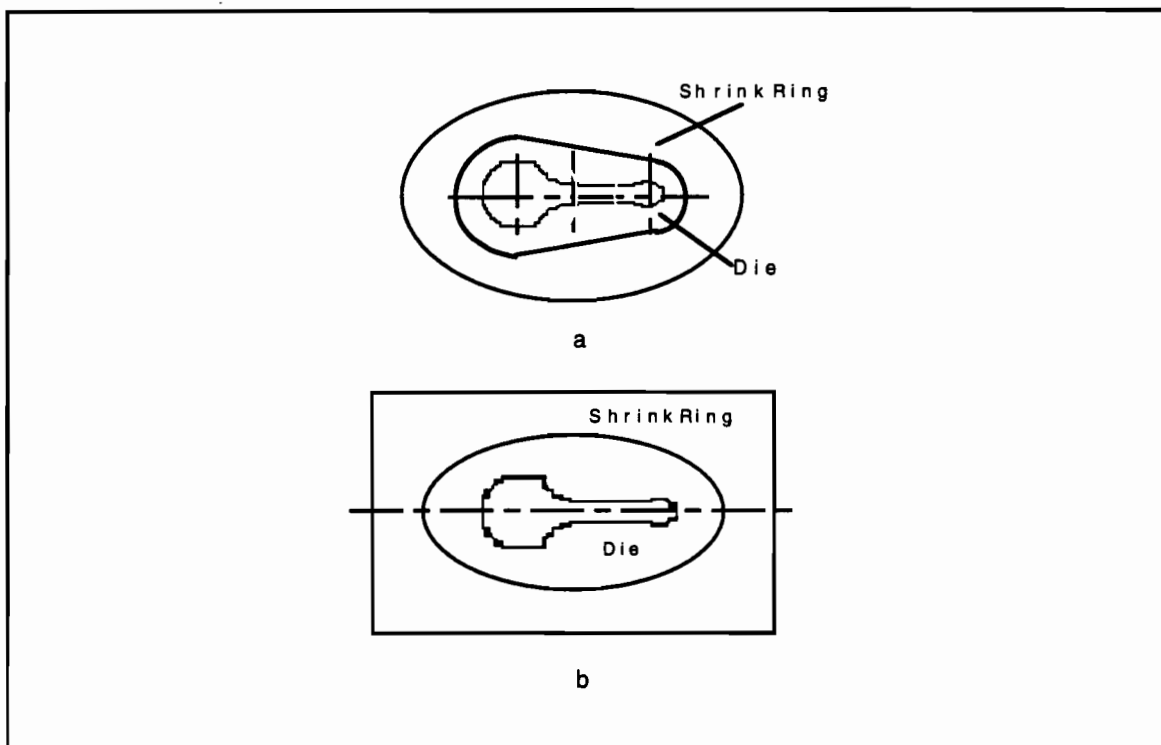
Figure 5.4: Proposed a)tangent-circle die-elliptical ring and b)elliptical die-rectangular ring designs for 3-D E-P simulations

5.2.3 Simplification of the Connecting Rod Die into Two Axisymmetric Sections

Figure 5.5 presents the connecting rod die divided into three sections (i.e. Big End (BE), Small End (SE) and I-Beam (IB) regions of a connecting rod). In order to define a preliminary die design, it is necessary to simplfy the complete design into simple 2-D models. Since the metal flow in sections BE

and SE is nearly axisymmetric, the loading of the dies can also be assumed as axisymmetric. The analysis to optimize the tool design consisted of two parts:

(a)   Conventional calculations of tool dimensions for BE and SE sections

(b)   FE stress analysis simulations of the design obtained from (a)
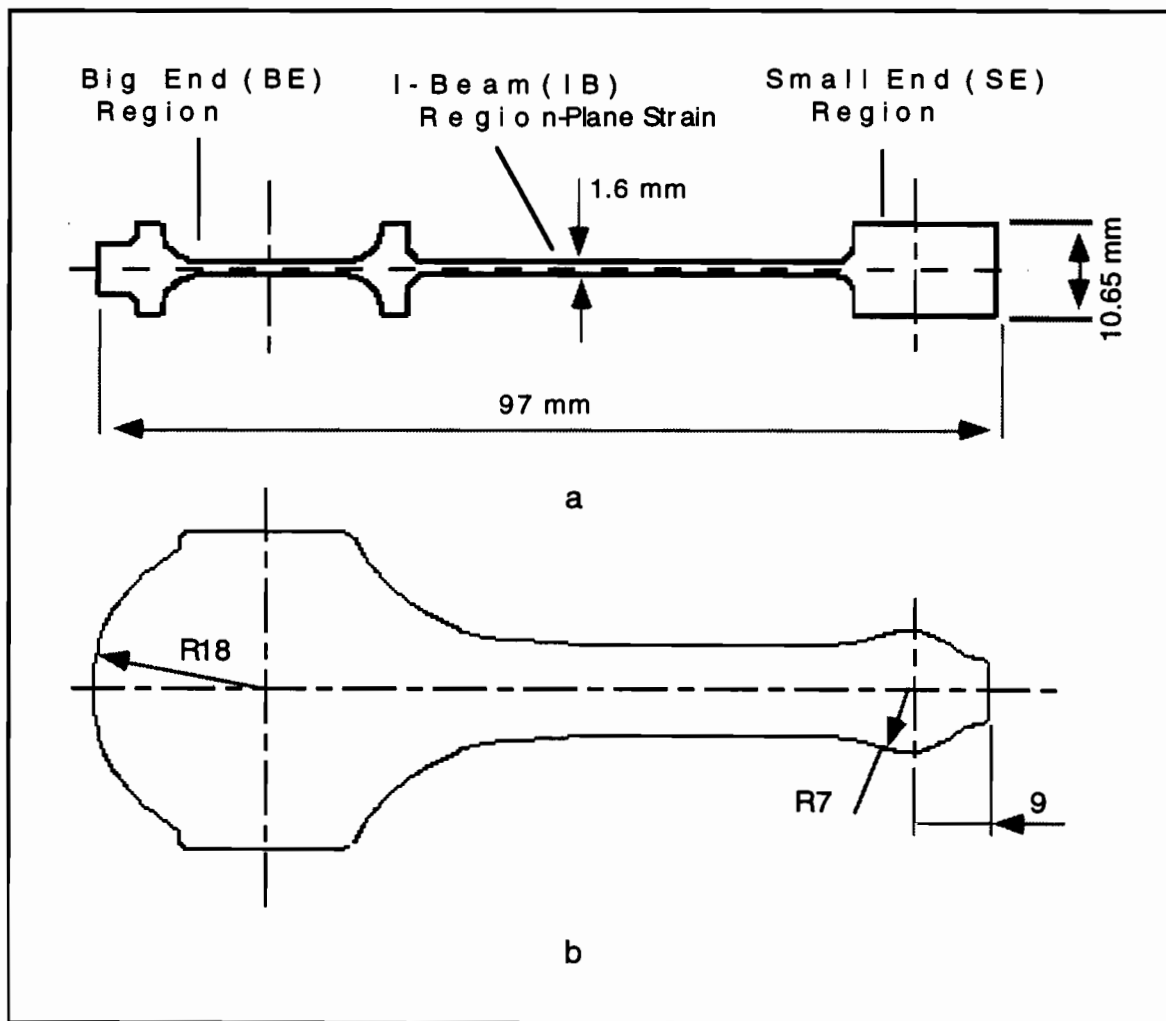
Figure 5.5:   a) Longitudinal cross-section b) top view of the connecting rod illustrating the regions used for simplification

5.2.4 Sample Conventional Calculations for Big End Section

The contact stresses obtained from previous 3-D metal forming simulations were found 1000 MPa (145 Kpsi) at big end (BE) section and 275 MPa (39.9 kpsi) at small end (SE) section. This may be due to the larger thickness reduction required in the BE section as can be seen from Figure 5.5.

Assuming that the contact stresses at each section are uniform along the die wall, conventional calculations were performed to obtain the initial dimensions (i.e. **D, d_1, d** and interference **ß**) for a one die-one shrink ring design. Below is the sample calculation procedure for the BE section [Laue, K. 1982] [ICFG, sheet no: 6/72]. Figure 5.6 presents the assumed circular inner die configuration and the calculated configuration of the shrink ring and die.

E = Elastic modulus of H13= **210 GPa** (30 Gpsi)

Y = Yield strength of H13 = **1300 MPa** (188.63 Kpsi)

ß = Interference = 0.4 %

d= inner diameter of the die = 36 mm

d_1= outer diameter of the die and inner diameter of the shrink ring

D= outer diameter of the shrink ring

Diameter ratios of the die and shrink ring

$$u = D / d = 4 \qquad u_1 = d_1 / d = 2 \qquad u_3 = D / d_1 = 2 \qquad (1)$$

Using the ICFG [ICFG, sheet no:6/72] recommendations for shrink ring design it is assumed that:

$$D = 4 * d = 144 \text{ mm} \qquad (2)$$

In order to determine diameter d_1, the following design rule from impact machining was used [Verson Allsteel Press Co, 1969]:

$$d_1 = [d * D]^{1/2} = 72 \text{ mm} \qquad (3)$$

First, the pressure between die and shrink ring developed during assembly is calculated as

$$P_s = (E * ß)/2 [u_3^2 - 1) (u_1^2 - 1) / (u^2 - 1)] = 252 \text{ MPa (36.5 Ksi)} \qquad (4)$$

P_{r_i} = Service stresses, i.e. contact stresses (MPa) = 1000 MPa (145 Ksi)

Radial stress on the inner surface of the die (MPa)

$$S_{dr} = - Pr = - 1000 \text{ MPa} < Sy \qquad (5)$$

Tangential stresses (hoop) on the inner surface of the die

$$S_{dt} = Pr [(u^2 + 1) / (u^2 - 1)] - [Ps [(2u_1^2 / (u_1^2 - 1)]$$

$$= 461 \text{ Mpa (66.9 Ksi)} < Y \qquad (6)$$
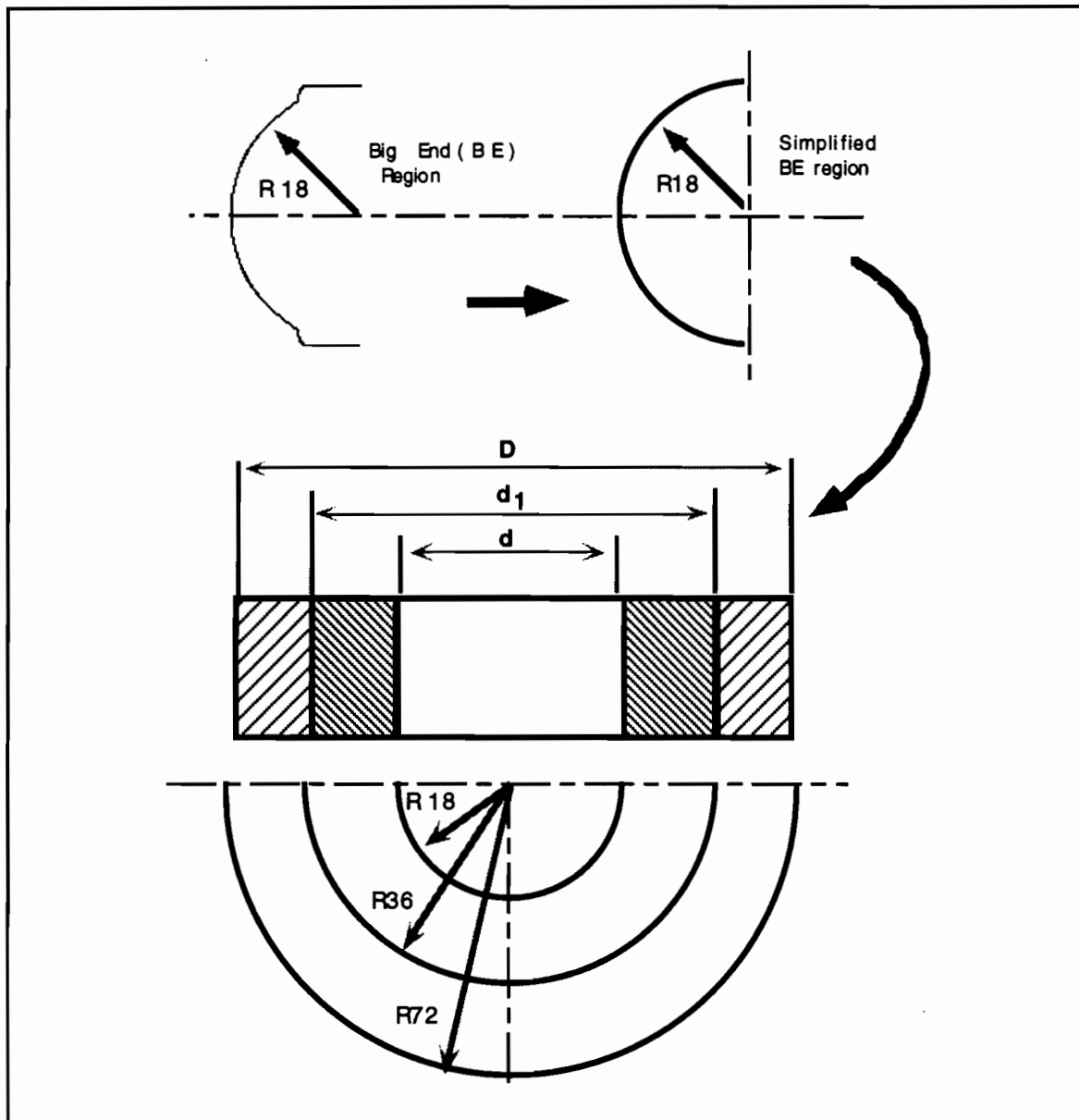
Figure 5.6: a) Assumed configuration of the big end section of the connecting rod, b) simplified configuration for the BE section with the calculated shrink ring design. Interference between the die and the shrink ring is assumed to be 0.278% and 0.556% in calculations

Tangential (hoop) stresses on the inner diameter of the shrink ring

$$S_{d1t} = Pr \left[\left(u_3^2 + 1 \right) / (u^2 - 1) \right] - Ps \left[(u_1^2 + 1) / (u_1^2 - 1) \right]$$

$$= 753 \text{ MPa (109.3 Ksi)} < Y \tag{7}$$

Therefore the design is found to be feasible

As seen from the above calculations, first using rough design guidelines, dimensions of the die and shrink ring were found. These values were then substituted into Lamé equations to check whether the induced die stresses were below the yield strength of the material. In this case, all stresses at the inner surface of the die and inner and outer surfaces of the shrink ring of the proposed design were acceptable, i.e. service stresses are lower than the yield strength of the tooling.

5.2.5 Elastic-Plastic 2-D FE Stress Analysis

For E-P stress analysis, ABAQUS FE code (version 5.3) was used. The FE model was generated using ABAQUS commands. The FE model for section BE is illustrated in Figure 5.7. Axisymmetric solid, four-node bilinear CAX4 elements were used to model the die and shrink ring whereas INTER2A interface elements were used to model the interference between the die and shrink ring as illustrated in Figure 5.7. Interface elements are easy to generate in a 2-D case, but is more time consuming for 3-D non-axisymmetric models.

In 3-D case, elements at the mating surfaces of the die and shrink ring must be grouped. These groups are used to generate the interface elements using special ABAQUS commands which are available only in version 5.4.

Calculation Conditions

The material used for both the die and shrink ring was H13 tool steel. The elastic and plastic properties were taken from DEFORM database and were verified with other sources [Harvey, P.D., 1982]. Figure 5.7 presents the model used for the BE section.

Using the maximum contact stress values, forces were calculated on the application area. Two different interferences, $ß = 0.278\%$ and $ß = 0.578\%$ were simulated for both sections. Each individual calculation consisted of two steps. First step was to simulate the assembly of the die and shrink ring. It provided the compressive stresses induced on the inner surface of the die and the stresses at the interface. The application of the contact forces to the inner surface of the die was calculated in Step two. Final resultant stresses were viewed after step two.

Calculation Results

The two dimensional, elastic-plastic FE calculations verified the design obtained through conventional calculations.
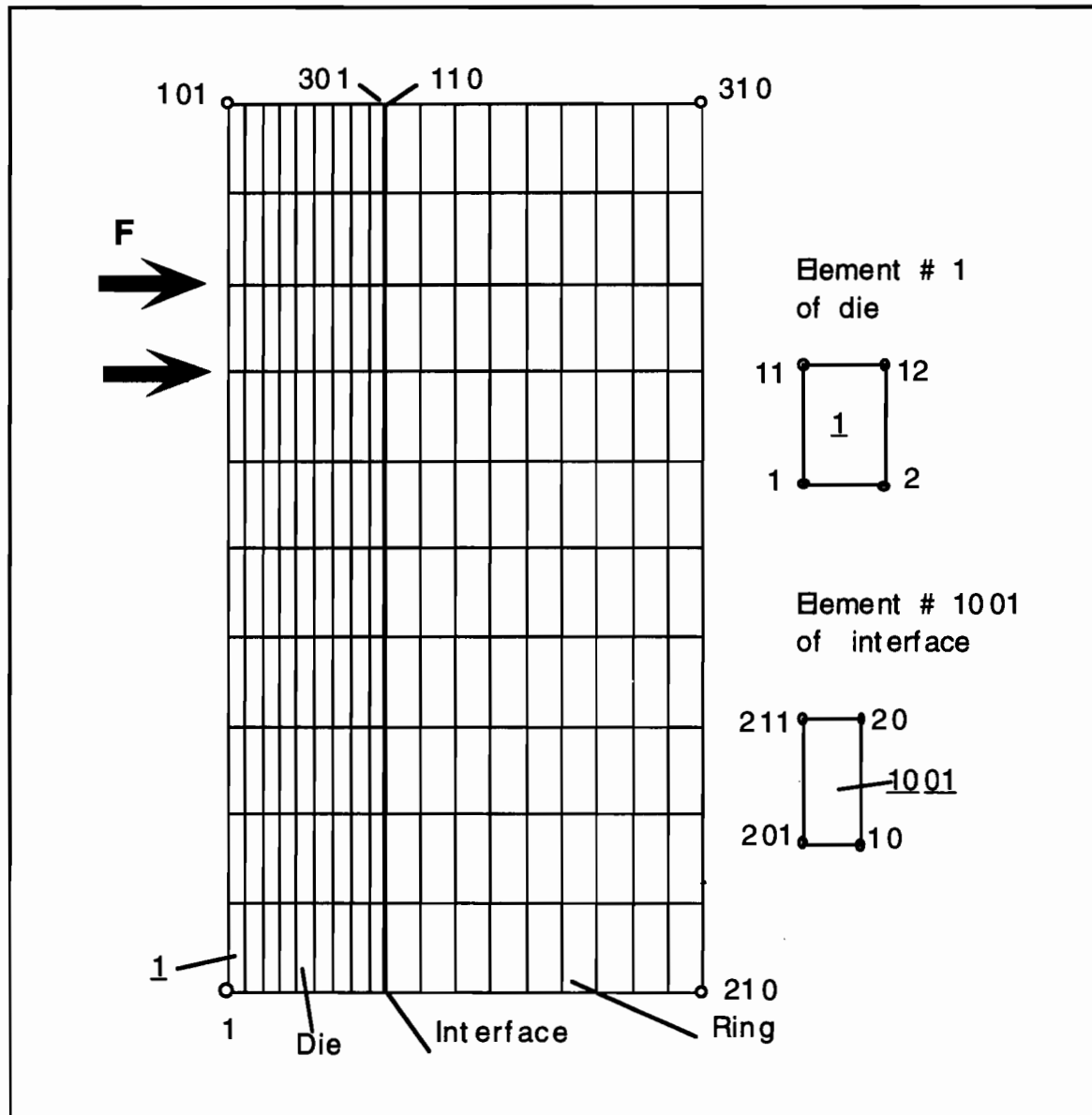
Figure 5.7: Two dimensional FE model for BE section

ABAQUS FE code provides the following parameters as a result for CAX4 elements:

S11:   Stresses in radial direction or in the local 1 (x) direction

S22:   Stresses in axial direction or in the local 2 (y) direction

S33:   Hoop stresses (tangential stresses)

S12:   Shear stresses

E11, E22, E33: Direct strains in x, y, z directions, respectively

E12:   Shear strain

Radial and tangential stresses are compared with calculation results for BE and SE sections. With an interference value of 0.556%, <u>assembly</u> of the die into shrink ring produced a radial stress of -206 MPa along the inner surface of the die. The radial stress magnitude at the contact surfaces of die and shrink ring was between -243 MPa and -169 MPa. Tangential or hoop stresses generated after assembly were also compressive along the inner surface of the die with a magnitude of 427 MPa. However, the distribution of stresses was not uniform as assumed theoretically.

When the stress distribution for STEP 2 (i.e. after loading) of the same BE section is viewed as in Figure 5.8 for radial stresses and Figure 5.9 for tangential stresses, it is found that the radial stresses at the region where the force is applied are -809 MPa while this value is 145 MPa at the outer surface of the shrink ring. The deflection of the die can be observed clearly. From the hoop stress distribution in Figure 5.9, it can be concluded that no permanent

yielding occurs on the die and shrink ring due to the maximum contact stresses on the inner die surface. The hoop stress is -438 MPa at the inner surface of the die, and the maximum tangential stress is at the interface and is -505 MPa. The maximum tensile hoop stress occurs at the inner upper corner of the die and outer upper corner of the shrink ring. Its magnitude is 368 MPa.
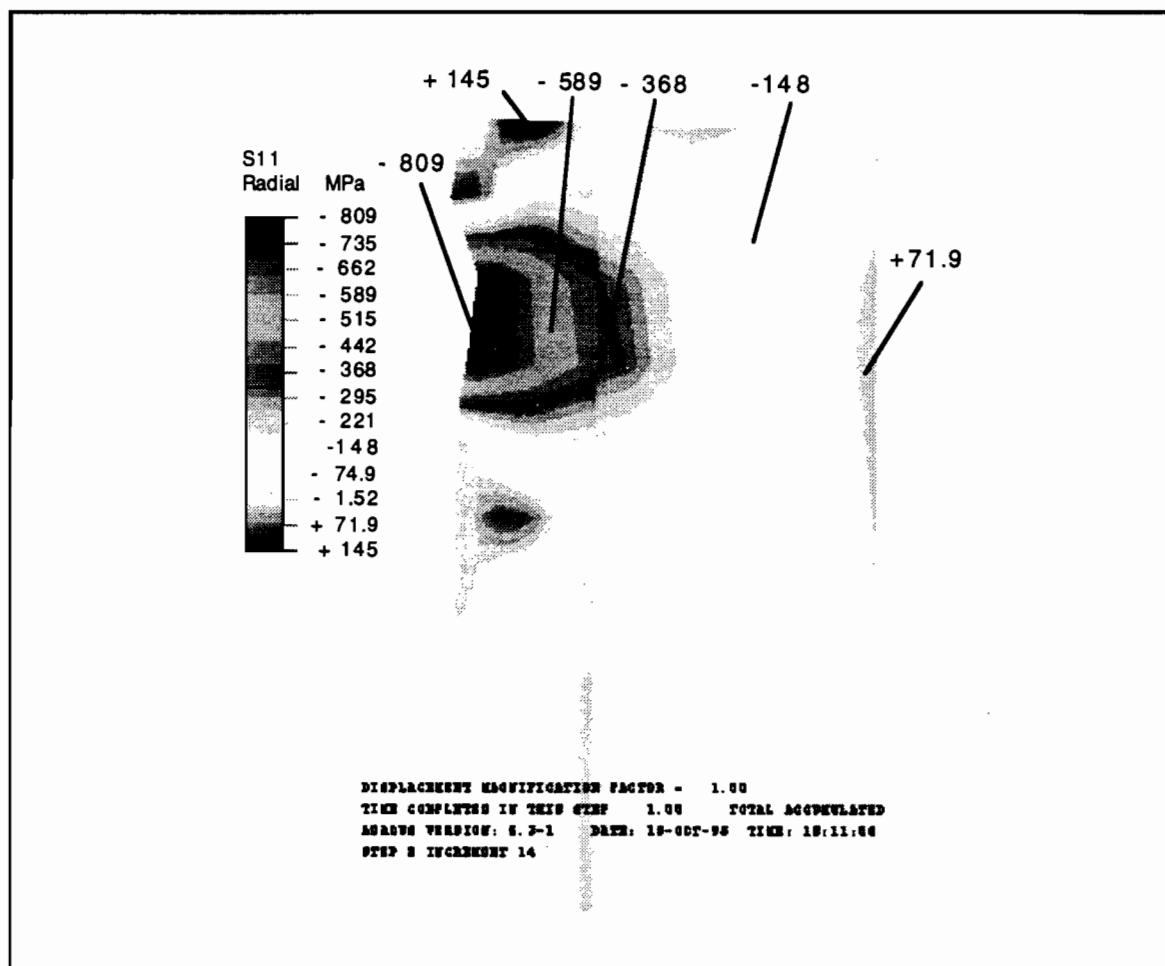
Figure 5.8: Radial stress distribution of the BE section under loading with an interference value of 0.556% (STEP 2) (100 MPa = 14.5 Ksi)
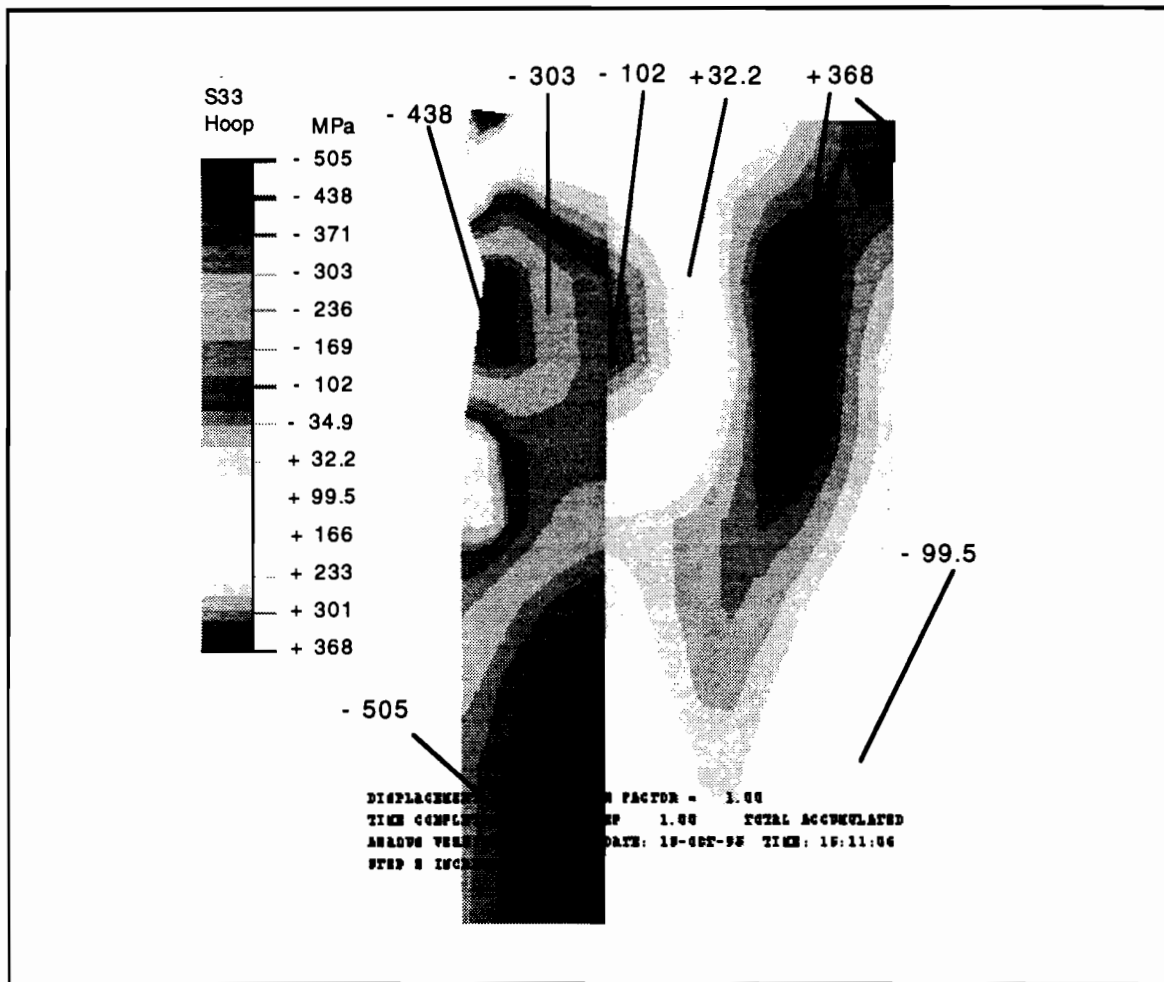
Figure 5.9:   Tangential stress distribution of the BE section under loading with an interference value of 0.556% (STEP 2) (100 MPa = 14.5 Ksi)

Similarly, stress distributions for SE section for an interference value of 0.278%, shown in Figures 5.10- 5.11, illustrate that with the design and materials used, there will be no permanent plastic deformation on the die

and shrink ring. The proposed designs for non-axisymmetric dies are presented in Figure 5.3 and Figure 5.4.
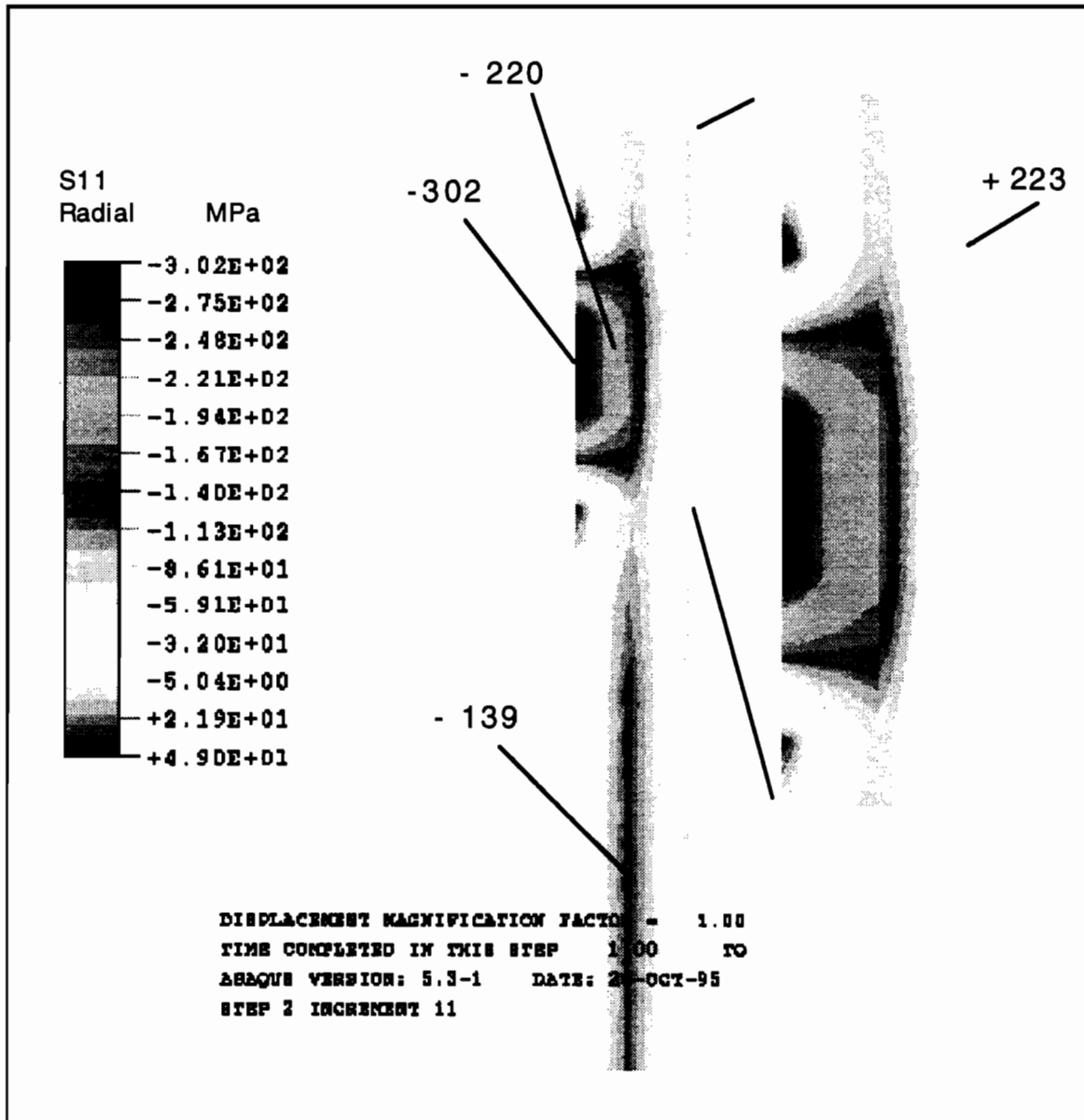
Figure 5.10: Radial stress distribution of the SE section under loading with an interference value of 0.278% (STEP 2) (100 MPa = 14.5 Ksi)
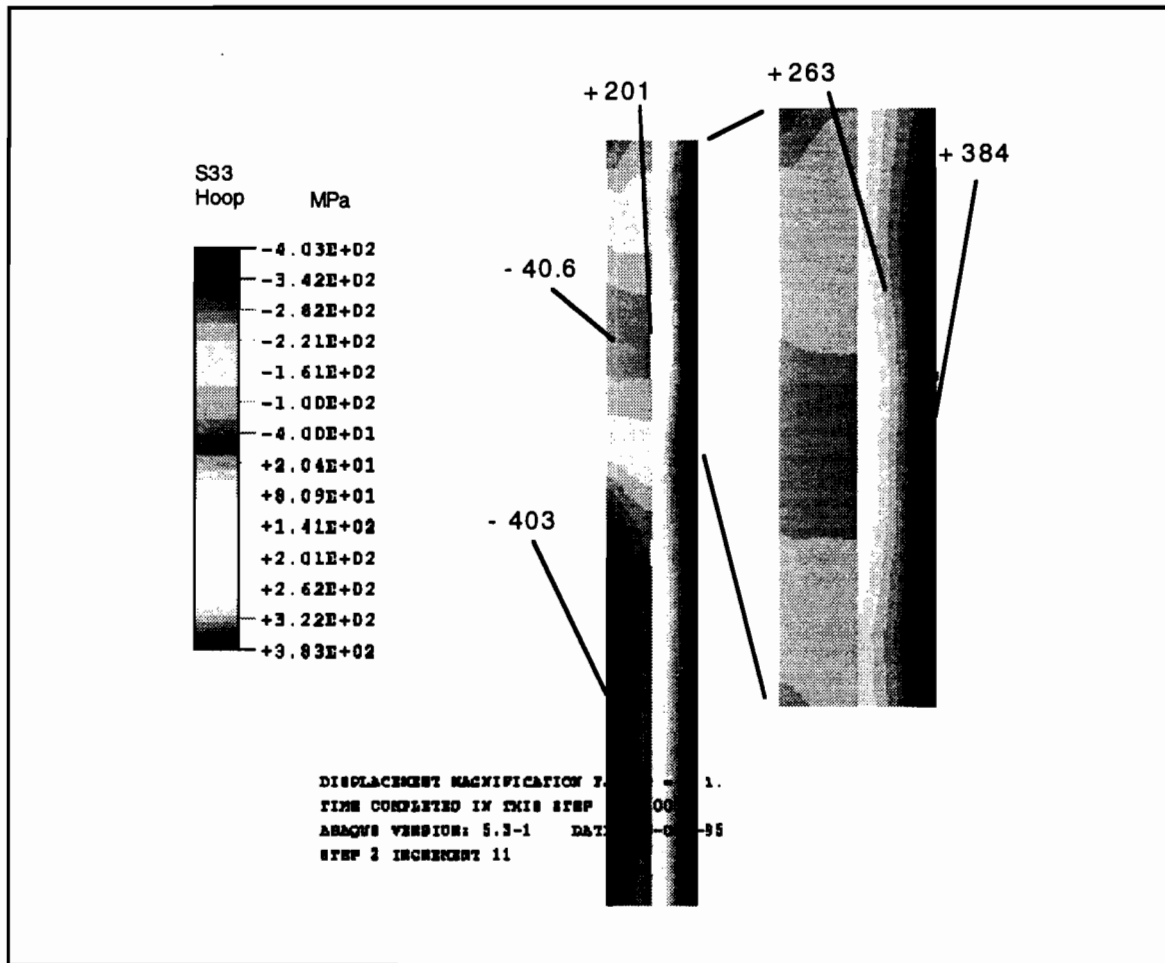
Figure 5.11: Tangential stress distribution of the SE section under loading with an interference value of 0.278% (STEP 2) (100 MPa = 14.5 Ksi)

5.3 Conclusions and Future Work

Design of the dies and shrink rings for non-axisymmetric parts was performed by simplifying the non-axisymmetric design into axisymmetric conditions. Design was first carried out using design guidelines and Lamé

equations. It was verified by the SHRINKAX. EXE program available at ERC/NSM for axisymmetric shrink ring calculations. Finally, verification and optimization of the design were performed in 2-D elastic-plastic stress analysis simulations using ABAQUS 5.3 FE code. The design obtained is shown to be safe when the maximum but constant contact stresses are applied to the die. Elliptical design of the dies and shrink rings with different aspect ratios was proposed for 3-D simulations. Figure 5.3 and Figure 5.4 illustrate these proposed designs.

In the next phase of this research, 3-D elastic-plastic FE stress analysis of the elliptical simulations will be performed. FE models will be prepared in I-DEAS. Generation of the interface elements is crucial in 3-D simulations. For this reason ABAQUS 5.4 will be used since it provides easy generation of interface elements using the element and node groups prepared in I-DEAS [Rebello, N., 1995]. Different designs will be investigated using 3-D elastic-plastic simulations to obtain the optimum design for non-axisymmetric parts. A methodology will be developed to facilitate the use of the design guidelines found. Finally, experiments for Al-MMC connecting rods will be performed using the die and shrink ring designs at ERC/NSM labs to verify the 3-D metal forming and stress analysis simulations.

BIBLIOGRAPHY

Altan, T., Oh, S.I., and Gegel, H.L. (1983). <u>Metal Forming Fundamentals and Applications</u>. Metals Park, OH. ASM. pp. 83-88.

Antona, R. and Moschini, R. (Aug. 1986). New Foundry Process for the Production of Light Metals in the Semi-Solid, Doughy State. <u>Metallurgical Science Technology, vol. 4, n. 2,</u> pp. 49-59.

<u>Atlas of Hot Working Properties of Non-Ferrous Metals, Aluminum and Al Alloys.</u> (1978). German Society of Materials Science. vol.2. Section for AlSiMg Alloys.

Avitzur, B. (1984). <u>Handbook of Metal Forming Processes.</u> New York. John-Wiley&Sons, Inc. pp.179-181.

Brown, S. B., Kumar, P. and Martin, C.L. (1992). Exploiting and Characterizing the Fundamental Rheology of Semi-Solid Materials. <u>Proceedings of the Second International Conference on the Processing of Semi-Solid Alloys and Composites,</u> pp. 183-192.

Brown, S.B., and Flemings, M.C. (Jan. 1993). Net-Shape Forming via Semi-Solid Processing. <u>Advanced Materials and Processes, vol. 143, n. 1,</u> pp. 36-40.

125

Burte, P., Semiatin, S.L., and Altan, T. (1989). Measurement and Analysis of Heat Transfer and Friction During Hot Forging. ERC/NSM Report-B-89-20. pp. 50-60.

Charreyron, P. O. and Flemings, M. C. (1985). Rheology of Semi-Solid Dentritic Sn-Pb Alloys of Low Strain Rates; Application to Forming Press. International Journal of Mechanical Science, vol. 27, n. 11-12, pp. 781-791.

Chen, C. Y., Sekhar, J. A., Backman, D. and Mehrabian, R. (1979). Thixoforging of Al-Alloys. Journal of Materials Science and Engineering, vol. 40, pp. 265-272.

Cheng, J., Apelian, D. and Doherty, R.D. (Nov. 1986). Processing-Structure Characterization Rheocast IN-Superalloy. Metallurgical Transactions A, vol. 17A, no. 9, pp. 2049-2062.

Chu, Y.L., Cheng, P.S., Brevick, J. R. and Altan, T. (1994). A Review of the Development of Semi-Solid Metal Forming Processes, ERC/NSM Report.

Collot J., Shen, J. Y., Levaillant, C., Bisson, C. and Yiasemides, G. P. (1992). Semi-Solid Processing of Magnesium Alloys. Proceedings of the Second International Conference on the Processing of Semi-Solid Alloys and Composites, pp. 11- 21.

Dendo, T., Shirota, T. and Kiuchi, M. (1993). Pressure Infiltration Under Semi-Molten State For Making Composite Layer Structure. Advanced Technology of Plasticity, Proceedings of the Fourth

International Conference on Technology of Plasticity, vol. 1, pp. 194-199.

Davis, J.K. (1993). Specialty Handbook for Aluminum and Al Alloys. ASM. Metals Park, Ohio. pp. 718-719.

EFU (Endabmessungsnahe Fertigung-Ur-/Umformtechnik GmbH. Postfach 11 80, 52147 Simmerath, Germany) Brochures. (1994-1995).

Flemings, M. C. and Mehrabian, R. (1973). Casting Semi-Solid Metals. AFS Transactions, vol. 81, pp. 81-88.

Flemings, M.C. (1974). Solidification Processing , McGraw Hill, New York.

Flemings, M.C., Riek, R.G. and Young, K.P. (1976). Rheocasting Processes. AFS International Cast Metals Journal, pp. 11-22.

Flemings, M.C. (1991). Behavior of Metal Alloys in the Semi-Solid State. Metallurgical Transactions A, ASM International, vol. 22A, pp. 957-981.

Gabathuler, J.P., Barras, D., Krahenbuhl, Y. and Weber, J.C. (1992). Evaluation of Various Processes for the Production of Billets with Thixotropic Properties. Proceedings of the Second International Conference on the Processing of Semi-Solid Alloys and Composites, pp. 33-45.

Harvey, P. (1982). Engineering Properties of Steel. ASM. Metals Park, Ohio. pp. 457-512.

Hirai, M., Takebayashi, K., Yoshikawa, Y., Furukawa, M., Fujikawa, Y. and Nanba, A. (1990). Viscosity of Semi-Solid Metals. International Conference on Semi-Solid Processing, Ecole Nationale Superieure des Mines de Paris, Sophia - Antipolis, France, April 4-5.

Hirt, G., Witulski, T., Kopp, R., Bremer, T. and Tietmann, A. (1993). Thixoforming: Welche Moglichkeiten bietet die Formgebung im Solidus/Liquidus Interval. EFU Mitteilungen 1-1994.

Hirt, G., Cremer, R.A., Winkelmann, T., Witulski, T., and Zillgen., M. (1994). SSM Forming of Usually Wrought Aluminum Alloys. Proceedings of the 3rd International Conference on SS Processing of Alloys and Composites, pp.11.1-11.10.

Hirt, G., Cremer, R.A., Winkelmann, T., Witulski, T., and Zillgen., M. (1994). SS Forming of Aluminum Alloys by Direct Forging and Lateral Extrusion. EFU Mitteilungen, 1-1994.

Hirt, G. (1995). Personal Communication with Dr. G. Hirt, President of EFU.

Hosford, W. and Caddell, R. (1993) Metal Forming Mechanics and Metallurgy. 2nd Edition. pp. 84. Prentice Hall, Cliffs, NJ.

Im, Y.T., and Altan, T. (1987). Applications of FEM to Simulations of Non-isothermal Forging Processes. ERC/NSM Report-B-87-15. pp. 76.

International Cold Forging Group (ICFG). Die (die assemblies) for cold extrusion of steel. Data Sheet n: 6/72. Source Book on Cold Forming. pp. 311-320. ASM, Metals Park, OH

Joly, P.A. and Mehrabian, R. (1976). The Rheology of a Partially Solid Alloy. Journal of Material Science, vol. 11, pp. 1393-1418.

Kapranos, P., Kirkwood, D.H. and Sellars, C.M. (1992). Semi-Solid Forging of High Temperature Alloys. Proceedings of the Second International Conference on the Processing of Semi-Solid Alloys and Composites, pp. 119-129.

Kattamis, T. Z. and Piccone, T. J. (Jan. 1991). Rheology of Semi- Solid Al-4.5% Cu-1.5% Mg Alloy. Materials Science and Engineering A: Structural Materials, Properties, Microstructure and Processing, vol. A131, n. 2, pp. 265-272.

Kattamis, T. Z. and Nakhla, A. I. (1992). Rheological, Microstructural and Constitutional Studies of Semi-Solid Al- 4.5% Cu-1.5% Mg Alloy. Proceedings of the Second International Conference on the Processing of Semi-Solid Alloys and Composites, pp. 237-247.

Kenney, Malachi. (1994). Personal contact, President of Alumax Auto Parts Plant, TN.

Kiuchi, M., Sugiyama, S. and Endo, N. (1983). Production and Working of Particle Reinforced Clad-Metals by Mashy-State Processes. Journal of Japan Society for Technology of Plasticity (JSTP) , 24- 274, pp. 1113.-1119.

Kiuchi, M. and Sugiyama, S. (1987). Mashy State Rolling of Composite Sheets. Advanced Technology of Plasticity, Proceedings of the Second

International Conference on Technology of Plasticity, vol. 2, pp.753-758.

Kiuchi, M. (1987). Application of Mashy-State Working Processes for Production of Metal-Ceramics Composites. Annals of the CIRP, vol. 36/ 1, pp. 173-175.

Kiuchi, M., Sugiyama, S. (1989). Mashy-State Rolling of Cast Iron -1. Proceedings of 1989 Japanese Spring Conference for Technology of Plasticity, pp. 57-60.

Kiuchi, M., Sugiyama, S. (1989). Semi- Solid Forging of Cast Irons -1. Proceedings of the 40th Japanese Joint Conference for Technology of Plasticity vol. 2, pp. 631-634.

Kiuchi, M., Sugiyama, S., Kuwasaki, N. and Hoshino, Y. (1989). Mashy-State Processing of Al Alloy Composite Reinforced with SiC Short Fibers. Journal of Japan Society For Technology of Plasticity (JSTP), 30- 346, pp. 1524-1531.

Kiuchi, M., Sugiyama, S. and Arai, M. (1990). Mushy-State Forging of Cast Irons-2. Proceedings of the 1990 Japanese Spring Conference for the Technology of Plasticity, vol.1, pp. 371-374.

Kiuchi, M. and Sugiyama, S. (1991). Production of Semi-Solid Metals by SCR-Process, 1st Report. Proceedings of 1991 Japanese Spring Conference for the Technology of Plasticity (JSTP), vol.1, pp. 1-4.

Kiuchi, M. and Sugiyama, S. (1991). Production of Semi-Solid Metals by SCR-Process, 2nd Report. _Proceedings of 1991 Japanese Spring Conference for the Technology of Plasticity (JSTP), vol. 1,_ pp. 5-8

Kiuchi, M. and Sugiyama, S. (1991). A New Method to Detect Solid Fraction of Mushy/ Semi -Solid Metal - 1. _Proceedings of 42nd Japanese Joint Conference for the Technology of Plasticity, vol. 2,_ pp. 647-650.

Kiuchi, M., Morimoto, Y., and Yanagimoto, Y. (1991). Computer Aided Simulation Techniques for Mushy-State Metal-1. _Proceedings of the 42nd Japanese Joint Conference for the Technology of Plasticity, vol. 2,_ pp. 643-645.

Kiuchi, M. and Sugiyama, S. (Aug. 1991). Mushy State Rolling of Aluminum and Cast Irons. _Manufacturing Technology CIRP Annals, vol. 40, n .1,_ pp. 259-262.

Kiuchi, M. and Sugiyama, S. (1992). A New Method to Detect Solid Fraction of Mushy/ Semi -Solid Metal-2. _Proceedings of the 1992 Japanese Spring Conference for the Technology of Plasticity, vol. 1,_ pp. 295-298.

Kiuchi, M., Morimoto, Y., and Yanagimoto, Y. (1992). Computer Aided Simulation Techniques for Mushy-State Metal-2. _Proceedings of 1992 Japanese Spring Conference for the Technology of Plasticity, vol. 1,_ pp. 299-302.

Kiuchi, M. and Sugiyama, S. (1992). Application of Mushy Metal Processing and Forming Technologies to Manufacture Fiber Reinforced Metals.

Proceedings of the Second International Conference on the Processing of Semi-Solid Alloys and Composites, pp. 382-389.

Kiuchi, M. and Sugiyama, S. (1992). A New Process To Manufacture Semi-Solid Metals. Proceedings of the Second International Conference on the Processing of Semi-Solid Alloys and Composites, pp. 47-55.

Kiuchi, M., Sugiyama, S., Yanagimoto, J., et al. (1993). Production of Semi-Solid Steel Alloys by SCR-2. The Proceedings of the 44th Japanese Joint Conference for the Technology of Plasticity, vol. 1, pp. 667-670.

Kiuchi, M., Sugiyama, S. and Yanagimoto, J. (1993). Production of Semi-Soid Steel Alloys-3. The Proceedings of the 1993 Japanese Spring Conference for the Technology of Plasticity, vol. 1, pp. 269-272.

Kiuchi, M. (1993). Mashy-State Processing of Metals, Alloys and Composites. Advanced Technology of Plasticity, Proceedings of the Fourth International Conference on Technology of Plasticity, vol. 1, pp. 122-133.

Koç, M., Sweeney, K., and Altan, T. (1994). A Review of the Semi-Solid Forging Process. ERC/NSM Report-B-94-53.

Knoerr, M., Kruger, H., Rentsch, C. and Altan, T. (1992) A Technique to Avoid Failure of Forging Dies- Integrating Proc. Simulations and Die Stress Analysis and Devloping a Fatigue Test for Hot Forging Die Material- Progress Report. ERC/NSM Report-B-D-92-18. pp. 40-78

Kumar, P., Martin, C. L. and Brown, S. (1992). Flow Behavior of Semi-Solid Alloy Slurries. Proceedings of the Second International Conference on the Processing of Semi-Solid Alloys and Composites, pp. 248-262.

Kumar, P., Martin, C. L. and Brown, S. (1993). Constitutive Behavior of Semi-Solid Metal Alloy Slurries. Proceedings of the Symposium on Flow and Microstructure of Dense Suspensions, Materials Research Society Symposium Proceedings, vol. 289, pp. 213-219.

Lalli, L. A. (1985). A Model for Deformation and Segregation of Solid-Liquid Mixtures. Metallurgical Transactions A, vol. 16A, pp. 1393.

Lalli, L. A. (1992). A Deformation Model For Semi-Solids. Proceedings of the Second International Conference on the Processing of Semi-Solid Alloys and Composites, pp. 263-265.

Laxmanan, V. and Flemings, M. C. (1980). Deformation of Semi-Solid Sn-15% Alloy. Metallurgical Transactions A, vol. 11, pp. 1927-1937.

Laue, K. and Stenger, H. (1982). Extrusion, Process, Machinery and Tooling. ASM. Metals Park, Ohio. pp. 72-146.

Loue, W. R., Landkroon, S. and Kool, W. H. (1992). Rheology of Partially Solidified Al Si7 Mg 0.3 and Influence of Si C Additions. Material Science and Engineering vol. A151, n. 2, pp. 255-262.

Loue, W. R., Suery, M. and Querbes, J. L. (1992). Microstructure and Rheology of Partially Remelted Al Si-Alloy. Proceedings of the Second

International Conference on the Processing of Semi-Solid Alloys and Composites, pp. 266-275.

Lux, A. L. and Flemings, M. C. (1979). Refining by Fractional Solidification. Metallurgical Transactions B, Vol. 10 B, pp. 71-78.

Lux, A. L. and Flemings, M. C. (1979). Refining by Fractional Melting. Metallurgical Transactions B, Vol. 10 B, pp. 79-84.

May, W. A., Midson, S.P. and Young, K.P. (1992). Semi-Solid Metal Forming of Highly Loaded XD Aluminum Alloy Composites. Proceedings of the Second International Conference on the Processing of Semi-Solid Alloys and Composites, pp. 390-397.

McLelland, A. R. A., Henderson, N. G., Atkinson, H. V. and Kirkwood, D. H. (1992). Evaluation of Rheological Measurements on Semi-Solid Metal Slurries. Proceedings of the Second International Conference on the Processing of Semi-Solid Alloys and Composites, pp. 290-295.

Mehrabian, R., Riek, R. G. and Flemings, M. C. (1974). Preparation and Casting of Metal-Particulate Non-Metal Composites. Metallurgical Transactions, vol. 5, pp. 1899-1905.

Moschini, R.,-Weber (1992). Manufacture of Automotive Components by Semi-Liquid Forming Process. Proceedings of the Second International Conference on the Processing of Semi-Solid Alloys and Composites, pp. 149-158.

Murakami, H., Yoshikawa, Y., Takebayashi, K., Moriya, T., Hirai, M. and Nanba, A. (1992). Semi-Solid Metal Making of High Melting Point Alloys by Electromagnetic Stirring. Proceedings of the Second International Conference on the Processing of Semi-Solid Alloys and Composites, pp. 67-75.

NCEMT. (1993). Semi-Solid Metalworking Program Definitions Workshop Minutes. National Center for Excellence in Metalworking Technology.

NCEMT. (1994). Semi-Solid Metal Forming Users' Group Meeting Minutes, CTC.

Pinsky, D. A., Charreyron, P. O. and Flemings, M. C. (1984). Compression of Semi-Solid Dentritic Sn-Pb Alloys at low Strain Rates. Metallurgical Transactions B, vol. 15B, pp. 173-181.

Rebello, Nuno. (1995) Personal Communication with Dr. Nono Rebello, Hibbitt, Karlsson and Sorenson, Inc. CA.

Salvo, L., Loue, W.R. and Suery, M. (1994). Influence of Thermomechanical History on the Structure and Rheological Behavior of Semi-Solid Al-Alloys. Proceedings of the 3rd International Conference on SS Processing of Alloys and Composites, pp.24.1-24.10.

Seconde, J. F. and Suery, M. (1984). Effect of Solidification Conditions on Deformation Behavior of Semi-Solid Pb-Sn Alloys. Journal of Material Science, vol. 19, pp. 3995-4005.

Spencer, D. B., Mehrabian, R. and Flemings, M. C. (1972). Rheological Behavior of Sn-15% Pb in the Crystallization Range. Metallurgical Transactions, vol. 3, pp. 1925-1932.

Suery, M. and Flemings, M.C. (1982). Effect of Strain Rate on Deformation Behavior of Semi-Solid Dentritic Alloy. Metallurgical Transactions A, vol. 13A, pp. 1809-1819.

Takemasu, T., Vazquez, V. and Altan, T. (1995). Flashless Forgin of an Aluminum Connecting Rod- Preform Optimization by 3-d FEM Process Simulations. ERC/NSM Report-B-95-55.

Tietmann, A., Bremer, T., Hirt, G. and Kopp, R. (1992). Preliminary Results in Thixoforging Aluminum Wrought Alloys. Proceedings of the Second International Conference on the Processing of Semi-Solid Alloys and Composites, pp. 170-179.

Tietmann, A., Baldner, K. and Kopp, R. (1993). Squeeze Forging-A Net Shape Technique for High Strength Applications. Institute for Bildsame Formgebung, Aachen, Germany.

Tijunelis, D. and McKee, K. E. (1990). Manufacturing High Technology Handbook, pp. 462-463.

Toyoshima, S. and Takahashi, Y. (1989). Numerical Simulation for Semi-Solid Materials. The Procedings of the 40th Japanese Joint Conference for the Technolgy of Plasticity, vol. 2, pp. 635-638.

Toyoshima, S. (1992). Numerical Simulation of Semi-Solid Deformation: Effect of Segragated Liquid Phase and Velocity on Deformation. The Proceedings of the 43rd Japanese Joint Conference for the Technology of Plasticity, vol. 1, pp. 337-340.

Toyoshima, S. (1993). Numerical Analysis for Extrusion of Semi-Solid Materials. The Proceedings of the 44th Japanese Joint Conference for the Technology of Plasticity, vol. 2, pp. 663-665.

Toyoshima, S. (1994). A FEM Simulation of Densification in Forming Processes for Semi-Solid Materials. Proceedings of the 3rd International Conference on SS Processing of Alloys and Composites, pp.47.

Turng, L.S. (1991). Rheological Behavior and Modeling of Semi-Solid Sn-15%Pb Alloy. Journal of Materials Science, vol. 26, pp. 2173-2183.

Verson Allsteel Press Company. (1969). Impact Machining. pp. 311-315. Chicago, IL.

Vives, C. (1992). Production of Metal Matrix Composites by Means of New MHD Rheocaster. Proceedings of the Second International Conference on the Processing of Semi-Solid Alloys and Composites, pp. 435.

Yoshida, C., Morittaka, M., et. al. (1992). Semi-Solid Forging of Aluminum Alloy. Proceedings of the Second International Conference on the Processing of Semi-Solid Alloys and Composites, pp. 95.

Young, K. P., Riek, R. G., Boylan, J. F., Bye, R. L., Bond, B. E. and Flemings, M.C. (1976). Machine Casting of Cu-Based Alloys by Thixocasting. Transactions AFS, vol. 84, pp. 169-174.

Young, K. M. R. and Clyne, T. W. (1986). A Powder Mixing and Preheating Route to Slurry Producyion for Semi-Solid Diecasting. Powder Metallugy, vol. 29, n. 3, pp. 195-199.

Wan, G., Witulski, T. and Hirt, G. (1994). Thixoforming of Al Alloys using Modified Chemical Grain Refinement for Billet Production. EFU, Mitteilungen 1-1994.

Witulski, T., HeuBen, J.M.M., Winkelmann, A., Hirt, G. and Kopp, R. (1994). Near Net Shape Forming of Particulate Reinforced Al Alloys by Isothermal Forming Compared to Semi-Solid Forming. EFU, Mitteilungen 1-1994.

APPENDIX A

Properties of Semi-Solid and Solid A356 Aluminum Alloy

Table A.1: Thermal conductivity of A356 semi-solid alloy [EFU, 1994].

Temperature °C	Thermal Conductivity (W/mK)	Temperature °C	Thermal Conductivity (W/mK)
1	160	582	149
100	172	587	150
300	175	592	150
400	180	597	150
500	170	602	150
549	167	607	150
550	167	611	150
576	165	612	150
577	165	613	150
581	149	800	300

Table A.2:   Heat capacity (specific heat * density) of A356 semi-solid alloy (including latent heat) [EFU, 1994].

Temperature °C	Heat Capacity J/m³K	Temperature °C	Heat Capacity J/m³K
1	2.58	566	56.8
100	2.72	567	22.3
200	2.85	570	22.2
300	2.98	571	12.2
400	3.11	593	12.0
500	3.21	594	10.5
542	3.28	608	10.4
543	6.25	609	46.9
552	6.17	614	26.6
553	2.45	618	26.6
561	2.38	700	26.2
562	56.9	800	25.8

Table A.3: Thermal conductivity of DIN 1.2312 [EFU, 1994]

Temperature, °C	Thermal Conductivity, W/mK
20	0.345
350	0.335
700	0.320

Table A.4: Heat capacity of H13 tool steels [Burte, P., 1989] [Im, Y.T., 1980]

T (°C)	Heat Capacity (J/m^3K)	T (°C)	Heat Capacity (J/m^3K)	T (°C)	Heat Capacity (J/m^3K)
25	3.5	350	3.65	871	4.2
100	3.53	538	3.73	982	4.54
215	3.56	650	3.9	1093	4.7

APPENDIX B

The INPUT FILE of the ABAQUS simulation for Big End (BE) region of the Connecting Rod

```
**********************************************
**                           **
**   <<< Shrink Ring Design  >>>      **
**                           **
**      Axisymmetric Model           **
**                           **
**      10/13/95 Muammer KOC         **
**                           **
**********************************************
*PREPRINT,ECHO=NO,MODEL=YES,HISTORY=YES
*HEADING
Shrink Ring Big End (BE)(Axisymmetric Model) Interference=0.556%=0.2mm
* *
**_____**
**   NODES (DIE & RING)               **
**_____**
*NODE
  1, 18.0, 0.0
  10, 36.0, 0.0
  101,  18.0, 100
  110, 36.0, 100
*NGEN,NSET=NDIELOW
  1,10,1
*NGEN,NSET=NDIEUP
  101,110,1
*NFILL,NSET=NDIE
  NDIELOW,NDIEUP,10,10
*NSET,GEN,NSET=INNER
  1,101,10
* *
*NODE
 201, 35.8, 0.0
 210, 72.0, 0.0
 301, 35.8, 100.0
 310, 72.0, 100.0
*NGEN,NSET=NRINGLOW
 201,210,1
*NGEN,NSET=NRINGUP
 301,310,1
*NFILL,NSET=NRING
```

```
    NRINGLOW,NRINGUP,10,10
**
**_____**
**   ELEMENTS (DIE & RING)          **
**_____**
*ELEMENT,TYPE=CAX4
 1,1,2,12,11
*ELGEN,ELSET=DIE
 1,9,1,1,10,10,10
*SOLID SECTION,ELSET=DIE,MATERIAL=MAT1
**
*ELEMENT,TYPE=CAX4
 201,201,202,212,211
*ELGEN,ELSET=RING
 201,9,1,1,10,10,10
*SOLID SECTION,ELSET=RING,MATERIAL=MAT1
**
**_____**
**   CONTACT (BETWEEN DIE & RING)      **
**_____**
*ELEMENT,TYPE=INTER2A
 1001,201,211,10,20
*ELGEN,ELSET=CONTACT
 1001,10,10,10
*INTERFACE,ELSET=CONTACT
*FRICTION,ROUGH
 1.0,
**_____**
**   MATERIAL                        **
**_____**
**   Material   : H13               **
**   Young's mod. : 210000  (MPa)      **
**_____**
*ELASTIC,TYPE=ISOTROPIC
 210E3, 0.3,   20.0
 180E3,      0.3,    260.0
 345E3,      0.3,    345.0
*PLASTIC
 343.0000000,          .0000000
 396.5190000,      .1000000
 449.2750000,      .2000000
```

```
467.8910000,      .3000000
451.7980000,      .4000000
*EXPANSION
12.2E-6
*CONDUCTIVITY
24.6,  215.0
24.4,  350.0
*SPECIFIC HEAT
460,   100.0
*DENSITY
7.865E-6
**_____**
**   BOUNDARY CONDITION              **
**_____**
*BOUNDARY
  NDIELOW,2,2
  NRINGLOW,2,2
**_____**
**   HISTORY                   **
**_____**
* *
**    Shrink Fitting of the Ring
* *
*STEP,NLGEOM,INC=50
*STATIC
 1E-2,1.0
*RESTART,WRITE,FREQ=50
*VALUE
 CONTACT,-0.2, -1.,0.,0.
*MONITOR,NODE=10,DOF=1
*PRINT,CONTACT=YES,RESIDUAL=NO
*EL PRINT,FREQ=10
S,E,
*NODE PRINT,FREQ=10
U,
*END STEP
* *
**    Pressurize the die
* *
*STEP,NLGEOM,INC=50
*STATIC
```

```
 1E-2,1.0
*RESTART,WRITE,FREQ=50
*CLOAD
 71,1,1130973.4
 81,1,1130973.4
*MONITOR,NODE=10,DOF=1
*PRINT,CONTACT=YES,RESIDUAL=NO
*EL PRINT,FREQ=10
S,E
*NODE PRINT,FREQ=10
U
*END STEP
```